UFRJ

UNIVERSIDADE FEDERAL DO RIO DE JANEIRO

OBSERVATÓRIO DO VALONGO

TESE DE DOUTORADO

Accuracy of effective temperature scales for FGK stars

Author:
Riano ESCATE GIRIBALDI

Supervisor:
Dr. Gustavo Frederico PORTO DE MELLO (OV/UFRJ)

Co-supervisor:
Dr. Luca PASQUINI (ESO)

Tese de Doutorado apresentada ao Prgrama de Pósgraduação em Astronomia da Universidade Federal do Rio de Janeiro - UFRJ, como parte dos requisitos necessários à obtenção do título de Doutor em Ciências (Astronomia)

May 16, 2019

"I fear not the man who has practiced 10 000 kicks once, but I fear the man who has practiced one kick 10 000 times."

Bruce Lee

Abstract

The accurate determination of effective temperature ($T_{\rm eff}$) is a classical astrophysical problem that got more interest with the discrepancy of the primordial lithium –measured by the Cosmic Microwave Background compared with that measured in the oldest stars of the Galaxy–, and with the discovery of exoplanets. Both the abundance measurement of Li in stellar atmospheres and the exoplanet characterization are based on stellar $T_{\rm eff}$, and are largely sensitive to it. Furthermore, the extremely precise and accurate parallaxes provided by Gaia are addressed to access with high precision the evolutionary stellar parameters mass (M), radius (R), and luminosity (L), which are required for reconstructing the Galaxy population. However, the accuracy of these parameters is necessarily tied to the accuracy of $T_{\rm eff}$. The improvement of interferometric measurements of stellar radius in the last decade allows now to obtain quasi-direct $T_{\rm eff}$ for the nearest dwarfs, with which predictions of theoretical models can be evaluated. This thesis presents a diagnostic of accuracy of the most used model-dependent techniques for deriving $T_{\rm eff}$ for F-, G-, and K-type stars, based on interferometric $T_{\rm eff}$ as the reference scale. The techniques analysed are: the excitation & ionization equilibrium of iron lines (spectroscopy), the InfraRed Flux Method (IRFM), and Hα profile fitting. This work enables the Hα profile fitting as a technique by which accurate $T_{\rm eff}$ can be derived for stars more distant than those resolved by interferometry. $T_{\rm eff}$ from Hα are non metallicity-degenerated and non-reddening affected, unlike other techniques. The problem for the application of the Hα profile fitting, which so far prevented the reliable verification of the accuracy of theoretical models, was solved here. This is the normalization of observational wide line profiles, which are affected by artificial features imprinted by the instruments of acquisition, and by custom data reduction procedures. Undistorted normalized profiles of the Sun and stars with the best interferometric $T_{\rm eff}$ (Gaia Benchmark stars) allowed to determine the accuracy of the Hα model synthesized by 1D LTE model atmospheres, which was used as an empirical correction for precise Hα $T_{\rm eff}$ (± 20 K) of many other FGK stars with well spread atmospheric parameters. Hence, I established a sample of 43 stars with interferometric-based $T_{\rm eff}$ that complements the Gaia Benchmarks, that was used to determine the accuracy of other techniques preventing selection biases. Hα profiles synthesized from 1D LTE models were found to underestimate $T_{\rm eff}$ by 28 K at solar parameters, and to underestimate $T_{\rm eff}$ progressively as a function of metallicity according to the relation: $T_{\rm eff} = T_{\rm eff}^{\rm H\alpha} - 159[{\rm Fe/H}] + 28$ K. Such underestimates are found to be removed when Hα is synthesized from 3D models. Temperatures derived by IRFM are confirmed to be accurate and equivalent to interferometric $T_{\rm eff}$. Spectroscopy from 1D models is found to produce biased $T_{\rm eff}$ as a function of [Fe/H], namely to underestimate/overestimate $T_{\rm eff}$ by 100 K for $-0.6/+0.4$ dex; this result is independent to the line-list selection and even to non-LTE corrections. An application to stars in M67 is presented: the study aims to trace the evolutionary path of Li on stars with solar age and solar metallicity. The comparison of IRFM-, and Hα-based $T_{\rm eff}$ asserts the precise and approximately even reddening estimated for the cluster.

Resumo

A determinação de temperatura efetiva acurada (T_{eff}) é um problema clássico da Astrofísica que ganhou interesse com a da discrepância do lítio primordial –medida pela radiação micro-ondas do fundo cósmico comparada com aquela medida nas estrelas mas velhas da Galaxia– e com a descoberta dos exoplanetas. A medição das abundancias de Li nas atmosferas estelares e a caracterização de exoplanetas são baseadas na T_{eff} estelar e são altamente sensitivas a ela. Além disso, as paralaxes extremadamente precisas e acuradas do Gaia são dirigidas a obter com alta precisão os parâmetros evolutivos massa (M), raio (R) e luminosidade (L), que são necessários para reconstruir a população da Galaxia. No entanto, a acurácia destes parâmetros é necessariamente ancorada na acurácia da T_{eff}. O aprimoramento das mediçoes interferométricas do raio estelar na década anterior permite obter T_{eff} quase-direta para as estrelas anás mais próximas, com as que as predições pelos modelos teóricos podem ser avaliadas. Esta tese apresenta um diagnóstico de acurácia das técnicas modelo-dependentes mais usadas para derivar T_{eff} para estrelas do tipo F, G e K, baseado na T_{eff} interferométrica como referência. As técnicas revisadas são: o equilíbrio de excitação & ionização das linhas de ferro (espectroscopia), o método do fluxo infravermelho (IRFM) e o ajuste do perfil Hα. Este trabalho habilita o ajuste do perfil Hα como uma técnica com que T_{eff} acurada pode derivar-se para estrelas ainda mais distantes que aquelas resolvidas pala interferometria. T_{eff} obtida pelos perfis Hα é não degenerada com a metalicidade e não é afetada pelo ao avermelhamento, a contrário de outras técnicas. O problema da aplicação desta técnica, que ate o presente evitou o diagnostico confiável da acurácia dos modelos teóricos, foi resolvido neste trabalho. Este é a normalização dos perfis de linha largos observacionais, que são afetados por características artificiais introduzidas pelos instrumentos de aquisição e pelos procedimentos padrão de normalização. Perfis de linha não distortos do Sol e de estrelas com as melhores T_{eff} interferométricas (Gaia Benchmark stars) permitiram determinar a acurácia do modelo de Hα sintetizado por modelos de atmosfera 1D LTE, o que foi usado como uma correção empírica para Hα T_{eff} precisa (± 20 K) de varias outras estrelas FGK com parâmetros atmosféricos bem distribuídos. A partir disto eu estabeleci uma amostra de 43 estrelas com T_{eff} baseada na interferometria que complementa a amostra das Gaia Benchmarks, que foi usada para determinar a acurácia de outras técnicas evitando vieses de seleção. Encontra-se que perfis de Hα sintetizados por modelos atmosféricos 1D LTE subestimam T_{eff} por 28 K para parâmetros solares, e subestimam T_{eff} progressivamente em função da metalicidade segundo a relação: $T_{\text{eff}} = T_{\text{eff}}^{\text{H}\alpha} - 159[\text{Fe/H}] + 28$ K. Encontra-se que estas subestimações são removidas quando Hα é sintetizado pelos modelos de atmosfera 3D. Confirma-se que T_{eff} derivada pelo IRFM são acuradas e equivalentes a T_{eff} interferométrica. Encontra-se que o equilíbrio de excitação e ionização de linhas de ferro usando modelos de atmosfera 1D produz T_{eff} viesados em função de [Fe/H], isto é ele subestima/superestima T_{eff} por 100 K para $-0.6/+0.4$ dex; este resultado é indiferente à seleção de linhas e ainda à correções não-LTE. Uma aplicaçao para estrelas no aglomerado M67 é apresentada como parte de um estudo com o objetivo de tracejar o caminho evolutivo do Li nas estrelas com idade e matalicidade solar. A comparação das T_{eff} baseadas no IRFM e Hα comfirma a precisa e aproximadamente uniforme estimativa do avermelhamento para o aglomerado.

Acknowledgements

I acknowledge the people and institutions that promoted this work. These are my parents, my supervisor in my home institution Gustavo Porto de Mello, my supervisor in my visiting institution Luca Pasquini, the Observatório do Valongo, the European Southern Observatory (ESO), and the Observatório do Pico dos Dias. I acknowledge the institutions that funded this project, these are CAPES, and ESO. I also acknowledge the colleagues that collaborated to make this work possible, these are Maria L. Ubaldo-Melo, Hans G. Ludwig, Diego Lorenzo-Oliveira, and Sòllene Ulmer-Moll. I aknowledge Claudia Fortes for being extremely helpful. An especial acknowledge to a dear person who recently passed away, great part of the work in this thesis was supported and promoted by her.

Contents

List of Figures

List of Tables

List of Abbreviations

BBN	**B**ig **B**ang **N**ucleosynthesis
ESO	**E**uropean **S**outhern **O**bservatory
HARPS	**H**igh **A**ccuracy **R**adial velocity **P**lanet **S**earcher
IRFM	**I**nfra**R**ed **F**lux **M**ethod
KPNO	**K**itt **P**eak **N**ational **O**bservatory
LNA	**L**aboratório **N**acional de **A**strofísica
LTE	**L**ocal **T**hermodynamic **E**quilibrium
MS	**M**ain **S**equence
OC	**O**pen **C**luster
OPD	**O**bservatório do **P**ico dos Dias
PM	**P**roper **M**otion
PWV	**P**recipitable **W**ater **V**apor
RV	**R**adial **V**elocity
VLT	**V**ery **L**arge **T**elescope
WMAP	**W**ilkinson **M**icrowave **A**nisotropy **P**robe

List of Symbols

L	luminosity
R	radius
M	mass
D	distance
T_{eff}	effective temperature
[Fe/H]	metallicty
$\log g$	surface gravity
$\log gf$	oscillator strength
θ_{LD}	limb-darkened angular diameter
σ	Stefan-Boltzmann constant
F_{bol}	bolometric flux

Dedicated to my parents, my aunt, and my grandma.

Chapter 1

Introduction

A significant fraction of the observing time in large telescopes is dedicated to the understanding of the stellar content of galaxies at high and low redshift. Studying galaxy formation and evolution requires the use of stellar population models, which are built according to the deepest knowledge of stellar evolution mainly learned from stars of our own Galaxy. Stars, specially main sequence stars, are basic elements for modeling stellar populations because, thanks to their long lifetimes, they store in the chemical composition of their atmospheres the information to trace the evolution of the populations.

Stellar characterization should be simple, in the sense of obtaining their physically modeled parameters (e.g. chemical abundances) from observable parameters (e.g. spectra and photometric colors) and their direct measurable physical properties: luminosity (L), radius (R), and mass (M). However, it is not simple at all: models link chemical abundances with the star's physical properties through the atmospheric parameters effective temperature ($T_{\rm eff}$) and surface gravity ($\log g$). Although R and M are first order observables from which $T_{\rm eff}$ and $\log g$ can be accurately derived by fundamental relations, they are 'directly'[1] measurable only for nearby spectroscopic eclipsing binaries (e.g., Andersen, 1991) with well known distances (D). Therefore, for practically all stars, the reverse process has to be applied: R and M are derived from $T_{\rm eff}$ and $\log g$ accepting their accuracy as given by model atmospheres. It is in this context where $T_{\rm eff}$ becomes the most important parameter, because minor variations in it easily change all other stellar parameters, especially in main sequence stars.

In model atmospheres the interdependence of $T_{\rm eff}$ with the total iron content (or metallicity [Fe/H][2]) is strong, while in evolutionary models the interdependence expands to M and stellar age. This is a complex problem because it generates high parameters degeneracy, and may possibly lead to biased results and wrong interpretations of the natural phenomena. Another problem is the accuracy of the models, for which generalizations are assumed such as the local thermodynamic equilibrium (LTE) and the one dimensional or plane parallel geometry (1D). Several model-dependent techniques have been developed for deriving atmospheric parameters with high or low degree of degeneracy, and high or low model dependence. There are no good or bad techniques, but rather various techniques with different characteristics that can be used in combination as a strategy to access accurate $T_{\rm eff}$ as a first step to recover accurate star physical properties and chemical abundances; see for example Cayrel de Strobel (1992), and Ramírez, Allende Prieto, and Lambert (2013)
.

[1] Stellar radius are directly measured by interferometric measurements of the angular diameter, the limb-darkening of which is typically fit and corrected by model atmospheres.

[2] $[A/B] = \log N(A)/N(B)_{\rm star} - \log N(A)/N(B)_{\rm Sun}$, where N denotes the number abundance of a given element.

Theoretical model atmospheres could not be tested against direct T_{eff} measurements because of the lack of standard stars, except for the Sun. The Sun have always been, and will continue to be the prime referential object for this task: due to its proximity, it is the only star that has accurate and extremely precise fundamental parameters inferred by direct measurements and fundamental relations: T_{eff} from observed irradiance and radius (e.g., Neckel, 1986), age from nucleochronology and undisturbed meteorite differentiates (e.g., Guenther, 1989), and mass from planetary motion. On the other hand, its proximity prevents to directly measure its observational characteristics in the same way its is done for distant stars, which represents an additional difficulty for evaluating the accuracy of model atmospheres. For example, its photometric colors, must be inferred by interpolating a T_{eff}–color relation with stars with identical solar [Fe/H]; see for example Pasquini, Biazzo, Bonifacio, et al. (2008). Former theoretical models of main sequence stars (e.g., Peytremann, 1974; Bell et al., 1976; Kurucz, 1979) were tested to recover the observed solar flux distribution without success (e.g., Gehren, 1979; Holweger, 1979). These models also produced from solar parameters synthetic colors that were significantly bluer than those inferred by other indirect methods. This meant substantial errors in element abundance determinations, when T_{eff}–color relations based in synthetic colors were applied. The synthetic $(B-V)_{\odot}$, for example, was determined between 0.59 and 0.60 mag, which is very far from the currently accepted value $(B-V)_{\odot} = 0.68$ mag. This translated to dramatic changes in [Fe/H] for solar-type stars, For example, for the Hyades, Parker et al. (1961) found [Fe/H] = 0.11 dex by using $(B-V)_{\odot} = 0.63$ mag, while Nissen (1970) found [Fe/H] = 0.38 dex by using $(B-V)_{\odot} = 0.66$ mag. Furthermore, an additional source of error that contributed to the solar colors discrepancy is the absolute flux calibration of the photometric system, which persisted until not too many years ago (Casagrande et al., 2010; Casagrande et al., 2014).

The problem of the solar colors was solved by Hardorp (1978), Hardorp (1980a), and Hardorp (1980b), who placed the Sun photometrically among G-type stars by comparing their spectral features in the ultraviolet region, obtaining $(B-V)_{\odot} = 0.67$ mag, thus making an important contribution to the diagnostic of accuracy of model atmospheres. However, due to its relevance, the precision of this determination have been continuously revised, for example: Tueg and Schmidt-Kaler (1982a), Tueg and Schmidt-Kaler (1982b), Saxner and Hammarback (1985), Neckel (1986), Gray (1992), Porto de Mello and da Silva (1997), Ramírez and Meléndez (2005), Holmberg, Flynn, and Portinari (2006), Pasquini, Biazzo, Bonifacio, et al. (2008), and Meléndez et al. (2010a), among others. Practically the same result as Hardorp's was found by Gehren (1981), $(B-V)_{\odot} = 0.68$ mag, who calibrated temperatures derived from Balmer lines fitting against photometric colors. They convincingly demonstrated that temperature calibrations from synthetic colors were biased by around 300 K to cooler values for stars with solar parameters. Due to the advantage of Balmer profiles being almost exclusively dependent on T_{eff}, their use became more frequent in subsequent years (e.g., Cayrel de Strobel et al., 1981; Gehren et al., 1985; Cayrel, Cayrel de Strobel, and Campbell, 1985; Cayrel de Strobel, 1985; Cayrel de Strobel and Bentolila, 1989a; Cayrel de Strobel, 1992; Fuhrmann, 1998; Mishenina and Kovtyukh, 2001), while the accuracy of empirical and theoretical atmosphere models for synthesizing the solar Balmer profiles was also periodically examined without achieving complete success (e.g., Praderie, 1967; Fuhrmann, Axer, and Gehren, 1993; Fuhrmann, Axer, and Gehren, 1994; Fuhrmann et al., 1997; Barklem, Piskunov, and O'Mara, 2000; Barklem et al., 2002; Cayrel et al., 2011; Pereira et al., 2013). This changed the present year as the results of Amarsi et al. (2018), Giribaldi et al. (2019) and those presented in this thesis show complete consistence between

Hα from 3D non-LTE models and interferometry.

In parallel, a technique called InfraRed Flux Method (IRFM) was introduced by (Blackwell and Shallis, 1977; Blackwell, Shallis, and Selby, 1979; Blackwell, Petford, and Shallis, 1980), the dependence of which on models is marginal. Briefly, it consist on comparing the bolometric flux measured by spectrophotometry with fluxes measured in infrared bands. Since the former is proportional to $T_{\rm eff}^4$, it is only required to reproduce the latter by modeling. The influence of models in this technique is negligible because the infrared part of the spectrum for main sequence stars (with $T_{\rm eff} \gtrsim 4200$ K) is mostly governed by the Rayleigh-Jeans law. The first results on the Sun showed acceptable agreement, as the solar radius was recovered within 1% of accuracy from its determined temperature. Also, the temperature of Arcturus derived in the first work of the series of papers above was within 1.5σ error when compared with the latest quasi-direct measurements by interferometry. This technique is very sensitive to small changes in the absolute flux calibration of the photometric system of use, and this have been responsible for large temperature biases of several subsequent IRFM implementations, such as those of Alonso, Arribas, and Martinez-Roger (1996) and Ramírez and Meléndez (2005) which were of broad use, and continue being considered; see for example Heiter et al. (2015).

On the side of the spectroscopic techniques, the excitation & ionization equilibrium of metal lines became of broad use with the implementation of the program MOOG[3] by Sneden (1973). It uses model atmospheres, line parameters (oscillator strength, excitation potential, and equivalent widths or line depths), and atmospheric parameters to compute synthetic spectra. The determination of element abundances, and the atmospheric parameters $T_{\rm eff}$ and $\log g$ is performed by matching observed line measurements with synthetic ones, and by forcing the abundances of the ionized and non-ionized species to be consistent and independent of the excitation potential. A long list of authors that used this technique is compiled in the catalog of Cayrel de Strobel (1992) and its subsequent editions: Cayrel de Strobel et al. (1997), and Cayrel de Strobel, Soubiran, and Ralite (2001). By reviewing these catalogs, Mishenina and Kovtyukh (2001) called attention to the high spread in the determinations of $T_{\rm eff}$ and [Fe/H] for the same stars by different authors: these are as large as 600 K and 0.5 dex, respectively. However, it is worth noting that the works cited in the catalogs are as old as from the beginning of the 50's, and atmosphere models and the quality of observational data changed significantly during 30 years of research. The temperatures and other parameters compiled in these catalogs are, in great part, derived by a variation of the excitation & ionization equilibrium of metal lines. This is the differential method, which evaluates the element abundances of one star with respect to those of another star taken as standard; the Sun is typically used for this task when FGK stars are studied. Since the same lines are analyzed when this technique is applied, the knowledge of the oscillator strengths is not needed. Another advantage is that the systematic errors that the equivalent widths measurements contain should be canceled, as long as the data acquisition and reduction are systematically performed. It also includes errors due to model generalizations, such as non-LTE effects or line enhancements by three-dimensional atmospheres dynamics, which are effectively canceled for stars with very similar properties, for example when applied to solar twins[4] (Meléndez et al., 2009; Ramírez, Meléndez, and Asplund, 2009).

[3]Available at `https://www.as.utexas.edu/~chris/moog.html`

[4]Stars with the same physical parameters as the Sun, thus with spectra indistinguishable to that of the Sun (Cayrel de Strobel and Bentolila, 1989b; Porto de Mello and da Silva, 1997; Meléndez, Dodds-Eden, and Robles, 2006).

By the end of the 90's Alonso, Arribas, and Martinez-Roger (1994), Alonso, Arribas, and Martinez-Roger (1996), Alonso, Arribas, and Martínez-Roger (1999a), and Alonso, Arribas, and Martínez-Roger (1999b) provided IRFM-based $T_{\rm eff}$–color calibrations for a wide range of atmospheric parameters. It then became good practice to validate temperature determinations from spectroscopic techniques, such as Hα fitting and excitation & ionization of Fe lines, by comparing them with those from IRFM; see for example Mishenina and Kovtyukh (2001), Meléndez, Barbuy, and Spite (2001), Meléndez and Barbuy (2002), Barklem et al. (2002), and Allende Prieto et al. (2004). After Barklem, Piskunov, and O'Mara (2000) and Barklem et al. (2002) introduced the "self broadening" theory of hydrogen atoms interaction for modeling Hα, the general consistency between the three main techniques, for parameters close to solar, implied the hottest temperature scale was that of the differential spectroscopic method, followed by Hα and IRFM with cooler temperatures by 50 to 100 K – Hα seemed slightly warmer for parameters close to solar. It was again an uncomfortable situation: both the differential spectroscopic method and IRFM were expected to be practically independent of models and hence to provide very similar results, while for Hα the physics of the hydrogen atoms interaction and the LTE approximation were addressed as possible causes (Allard et al., 2008; Barklem, 2007).

After the year 2000 several catalogs with homogeneously determined temperatures for a large number of stars were published. First large spectroscopic catalogs were provided by Allende Prieto et al. (2004), Santos, Israelian, and Mayor (2004), Santos et al. (2005), and Valenti and Fischer (2005); the last two dedicated to investigate the star-planet connection. Although their temperatures were derived by either variations of the excitation & ionization of metal lines or, simply, different implementations – for example, Valenti and Fischer (2005) used the global spectral fitting instead of equivalent widths – the three scales agreed; see Valenti and Fischer (2005, Fig. 18 and Table 11). Furthermore, Santos, Israelian, and Mayor (2004, Fig. A.2) showed a sharp offset of around +100 K with respect to the IRFM scale of Alonso, Arribas, and Martinez-Roger (1996). Around the same time, IRFM-based $T_{\rm eff}$–color calibrations were updated, for example: Ramírez and Meléndez (2005), Casagrande, Portinari, and Flynn (2006), González Hernández and Bonifacio (2009a), and Casagrande et al. (2010). The IRFM scale of Casagrande et al. (2010), which is an optimized version of Casagrande, Portinari, and Flynn (2006), was an important contribution because it took advantage of all recent works on modeling the flux distribution of Vega (the photometric standard) in the infrared to check the absolute flux calibration of previous IRFM implementations. It was found that the IRFM scale of Alonso et al. was biased by around 100 K, and that the origin of it was its absolute flux calibration, as suggested by divergent zero points estimated by the three interferometric methods employed for this task (Lunar Occultations, Michelson Interferometry, and Intensity interferometry); see literature provided in Casagrande et al. (2010, Appendix A) for more details. With these results, IRFM and the differential spectroscopic technique were reconciled for solar-like parameters as the comparisons with the three spectroscopic catalogs showed negligible offsets. On the other hand, the problem seemed to persist for metal-poor stars; see for example Casagrande et al. (2010, Fig. 5). This feature is however not easy to identify in more recent works because comparisons of the scales often lie within narrow metallicity ranges.

The problems above sum up the discrepancy of temperature scales along time, which have been a consequence of the absence of standard stars, aside from the Sun, with accurate atmospheric parameters, and by the difficulty of accurately measuring the solar photometric characteristics as a distant star. Interferometric $T_{\rm eff}$ measurements, if precise enough, could be the way to solve the problem given that they carry practically null modeling errors, but a useful precision was reached only in the present decade. First measurements were provided for giant stars, for example: Pease (1931) and Gezari, Labeyrie, and Stachnik (1972) by Michelson interferometry, Currie, Knapp, and Liewer (1974), Bonneau and Labeyrie (1973), and Worden (1976) by Speckle interferometry, Ridgway et al. (1980) and White and Feierman (1987) by Lunar ocultations, and Hanbury Brown, Davis, and Allen (1974) and Hanbury Brown et al. (1974) by intensity interferometry. They reached radius[5] precisions of 10 to 35% (0.015 to 0.055 arcsec) which in terms of $T_{\rm eff}$ reduce to the half, which is far from needed. Namely, a typical main sequence star has $T_{\rm eff}$ = 5000 K, the uncertainty of which would be of at least 250 K, which is greater than the scale discrepancies observed. The exception are the measurements by intensity interferometry that reached $\sigma T_{\rm eff} \sim 1\%$. Richichi, Percheron, and Khristoforova (2005, The CHARM2 catalogue) provided the first interferometric radius for 24 main sequence stars, with $T_{\rm eff}$ precision of around 5%. This record was improved by van Belle and von Braun (2009), who added 40 stars with measurements of same precision to the list, by using the Palomar testbed interferometer (Colavita et al., 1999). Later, Boyajian et al. (2012a) and Boyajian et al. (2012b) provided interferometric measurements for 69 main sequence stars, including M-type, with precisions between 1.5 to 5%, by using the CHARA array (ten Brummelaar et al., 2005).

Two technological advances in the last decade have promoted the accurate measurement of $T_{\rm eff}$ for main sequence stars, with which the accuracy of model-dependent techniques can be now reviewed: the improved quality of interferometric radius measurements translates to a precision/accuracy better than 90 K for $T_{\rm eff}$ thanks to new instruments (e.g., PAVO and VEGA beam combiners: Ireland et al., 2008; Mourard et al., 2011, respectively) in the powerful CHARA array, and the extremely precise distances measured by Gaia (Gaia Collaboration et al., 2016b) via parallax for stars in and out of the solar neighborhood. The radius measurement is much more limited than that of distance, for example, the distance of the solar twin 18 Sco is estimated with precision of 0.16% (0.032% in mas), while its best radius measurement has a precision of 0.89% (0.91% in mas, Bazot et al., 2011). Most of the available quasi-direct $T_{\rm eff}$, and $\log g$ measurements are for F, G, and K stars, of the solar neighborhood, but some of them also belong to the thick disc and halo, the distances of which are measured with practically null uncertainty (Heiter et al., 2015, The Gaia benchmark stars). The atmospheric parameters of these stars must be used to diagnose the accuracy of temperature scales and to calibrate their techniques; see for example Blanco-Cuaresma et al. (2014).

The precise parallaxes provided by Gaia need to be complemented with accurate $T_{\rm eff}$, [Fe/H], and L for obtaining reliable masses and ages, and thus reconstructing the stellar population distribution in our Galaxy. Gaia's astrometry and photometry will eventually cover a large sample of stars with enough statistics to be representative of the majority of the Galaxy population, and spectroscopic surveys started to reach stars at reasonable deep distances. On the other hand, the stellar type diversity of the Gaia benchmarks is restricted to nearby stars only, for which interferometric measurements can be resolved. This indirectly limits the sample of FGK benchmarks to high [Fe/H], hence the determination of $T_{\rm eff}$ for metal-poor and very metal-poor stars will be unavoidably based on indirect techniques until the next generation of

[5]Stellar radius measured via interferometric limb-darkened angular diameter $\theta_{\rm LD}$ can be converted into $T_{\rm eff}$ by applying a variation of the Stefan-Boltzmann relation given in Eq. 4.1

interferometers becomes available. Spectroscopic techniques are anyhow prime for T_{eff} determination, and for stellar characterization, due to the huge amount of information the spectra contain. Hence, it is essential to make available spectroscopic techniques with validated accurate T_{eff} diagnostics; otherwise full advantage cannot be taken of Gaia data.

Aware of the Gaia advent I proposed this PhD research at the beginning of the year 2015, shortly after the parameters of the Gaia benchmark stars were published (Jofré et al., 2015; Heiter et al., 2015), and the first release of the survey (Gaia Collaboration et al., 2016a) was published by the end of the year. This project is the first step of a long research scheme for accurate and precise stellar characterization. It attacks the problem of the determination of T_{eff} making a diagnostic of accuracy of the most used techniques, based on interferometric T_{eff} of the Gaia Benchmarks. By quantifying the biases, it attempts to identify their origin, and to assist theoreticians to improve models. Precisely quantified biases rationally lead to improvements of the application of the techniques by using empirical corrections.

The course of this thesis led me to work extensively on the Hα profile fitting. Namely, on the processing of the observational data to trace the errors related only to the physics of the theoretical models of the line profile. The results obtained enable the Hα profile fitting as a validated technique, aside IRFM, from which accurate T_{eff} can be derived for stars more distant than those resolved by interferometry. With accurate and very precise T_{eff} of a sample of 43 F-,G-, and K-type stars, equivalent to interferometric measurements, the accuracy IRFM was confirmed, and the accuracy of the excitation & ionization equilibrium of Fe lines was determined. The analysis of several large catalogs with precise temperatures derived by the excitation & ionization equilibrium of Fe lines is consistent with a significant bias as a function of metallicity, no matter the line-list selection, or even non-LTE corrections. These results, and upcoming extensions to stars with lower metallicity, will possibly impact on the abundance element distribution of the Galaxy and the ages, in particular significant changes in the abundance of Fe and Li are expected.

This thesis is organized as follows. In chapter 2, I present the data used in this work. The heart of this work consist on optimizing the removal of artificial spectral features, that may affect the application of the Hα profile fitting with large significance. In the chapter, the stars selected to test the method for removing such features are presented; these are 43 FGK stars called the Hα-test sample. Most of their data were acquired with instruments that have proven easy and precise instrumental pattern removal; Tables 2.1, and 2.2. The rest of the data and its characteristics are listed in Tables 2.3, and 2.4, to which the improved methods implemented in this thesis are applied. In chapter 3, the method proposed to assist on the diagnostic of the accuracy of the techniques for deriving T_{eff} is presented. The 'method' consist on applying the "Hα profile fitting" on the Hα-test sample, by which accurate T_{eff} was derived once its biases are determined and corrected. The chapter presents a normalization-fitting procedure I developed. It minimizes typical errors induced in wide line-profiles by custom normalization procedures. Chapter 4 presents the determination of the accuracy of the Hα model (from 1D model atmospheres) used in this work as a function of the atmospheric parameters, by comparison with the solar direct T_{eff} and the interferometric T_{eff} of the Gaia Benchmark Stars. The empirically corrected Hα T_{eff} scale is used in the work onwards as standard to determine the accuracy of other techniques. The accuracy of other Hα models (e.g. from 3D atmosphere models) are determined in this chapter as well. Chapter 5 presents the determination of the accuracy of other techniques, these are the IRFM, and the excitation & ionization equilibrium of Fe lines. In chapter 6, T_{eff} is determined for 52 stars members of the M67 open cluster. Two techniques were used for that: IRFM and Hα. The agreement between both techniques (applied the correction to Hα) is used to test the reddening for the cluster. In this chapter, the suitability of HARPS spectra for the application of Hα profile fitting is extensively tested with the Hα-test sample (it was done before applying the technique to the M67 spectra). Finally, in chapter 7, I expose the conclusions of this thesis, and I summarize ongoing and future projects that make use of the results presented here.

Chapter 2

Data and observations

The data used in this work are divided in four tables, and are presented at the end of this section.

- Table 2.1 presents the sample stars selected to test Hα theoretical profiles, this sample is called Hα-test-sample henceforth. This selection is justified in Sect. 2.1.
- Table 2.2 is an extension of Table 2.1, it displays the solar spectra used in this work to determine the accuracy of Hα profile models at solar parameters, and to determine the stability of HARPS' (High Accuracy Radial velocity Planet Searcher) blaze along time. The table lists the temperatures derived from Hα profiles from 1D LTE models ($T_{\rm eff}^{\rm H\alpha}$(1D LTE)) for each spectrum, as described in Sect. 4.1.1. Details of the spectra such as their date of acquisition, solar proxy, and signal-to-noise ratio (S/N) are provided as well.
- Table 2.3 presents the M67 cluster stars for which $T_{\rm eff}$ was derived from Hα profiles after the accuracy of the theoretical model has been determined and corrected using Eq. 4.2. The table also lists the astrometric data from Gaia DR2, photometric data, and $T_{\rm eff}$ derived using $(B-V)$–$T_{\rm eff}$ relations based on the InfraRed Flux Method (IRFM) (Casagrande et al., 2010) derredened by 0.041 mag (Taylor, 2007).
- Table 2.4 presents details of the spectra of the stars listed in Table 2.3 such as S/N and $T_{\rm eff}^{\rm H\alpha}$(1D LTE). These data are described in Sect. 2.2.

2.1 Hα-test sample

This sample contains 43 F-, G-, and K-type single stars and is presented in Table 2.1. They were selected from the HARPS/ESO archive of reduced and calibrated data[1], and have S/N of 200 at least, except for the Sun. The stars were restricted to be brighter than $V = 7$ in order to acquire good quality spectra of them (S/N > 350), with the MUSICOS and coudé instruments installed at the Perkin Elmer telescope of 1.6m in the Pico dos Dias Observatory (OPD/LNA) in acquisitions of 1-7 hours.

There was no a register of spectra with high quality in terms of resolution and S/N in the archives of the Pico dos Dias Observatory (OPD, Brazópolis, Brazil)[2] for stars with parameters similar to those in Table 2.1 to satisfy the objectives of this project. Henceforth, I submitted two time proposals of 16 days each; they were conceded. I also made use of partial time granted for a mission belonging to another project of the research group in order to acquire the MUSICOS spectra. In the first two missions I used the coudé[3] spectrograph, and in the last mission I used the

[1] http://archive.eso.org/wdb/wdb/adp/phase3_main/form

[2] Operated by Laboratório Nacional de Astrofisica (LNA/CNPq).

[3] Details of the instrument: http://www.lna.br/opd/instrum/manual/Manual_160mOPD_Cap3.pdf

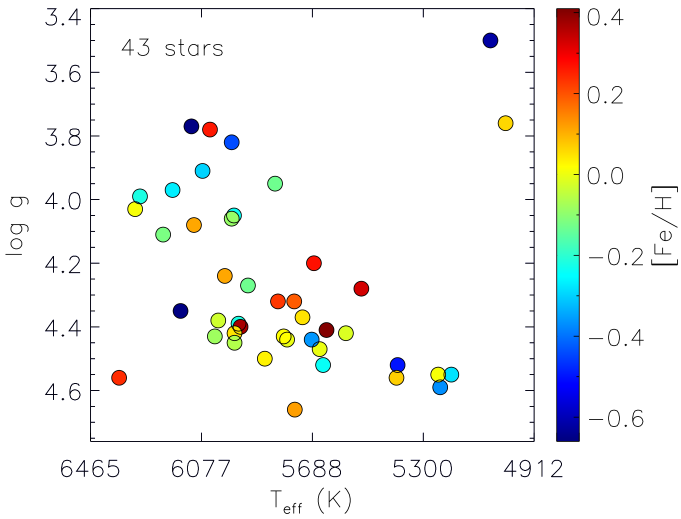

FIGURE 2.1: Parameter space covered by the Hα-test-sample. The values are listed in Table 2.1.

MUSICOS (e.g. Baudrand and Bohm, 1992) spectrograph. The missions were split between the second period of 2016 and both periods of 2017; different epochs of the year were necessary in order to observe several Gaia Benchmarks (Heiter et al., 2015).

MUSICOS and coudé spectrographs are fed by the 1.60 m Perkin-Elmer telescope. In the coudé spectrograph the slit width was adjusted to give a two-pixel resolving power R $= \lambda/\Delta\lambda =$ 45 000. A 1800 l/mm diffraction grating was employed in the first "direct-order", projecting onto a 13.5 μm, 2048 pixels CCD. The spectral region was centered on the Hα line $\lambda = 6562.797$ Å, with a spectral coverage of 155 Å. MUSICOS is a fiber-fed echelle spectrograph (on loan from Pic du Midi Observatory since 2012) available for the OPD/LNA. I employed the red channel, covering λ5400-8900 Å approximately, comprising about 50 spectral orders, at R $\sim$ 40 000 and 0.05 Å/pix dispersion in the Hα wavelength range. The exposure times for spectra acquisition with both instruments were chosen to obtain S/N ratios of at least 250 for the faintest stars ($V \sim 7$) and 300 in average for the other stars. Raw data from coudé were totally processed by myself, and raw data from MUSICOS were processed by Diego Lorenzo-Oliveira from IAG/USP. Data reduction was carried out by the standard procedure using IRAF[4]. Namely, bias and flat-field corrections were performed, background and scattered light were subtracted, and the one-dimensional spectra were extracted. The pixel-to-wavelength calibration was performed with Thorium-Argonium emission spectra taken the same nights of observation; the line data-base of IRAF was used as standard.

The coudé sample was acquired to develop the normalization method proposed in Chap. 3. Considering that the coudé is a single order spectrograph (non-echelle), its spectra are blaze-free, and their normalization errors should be quasi-exclusively related to the normalization method. MUSICOS spectra were acquired to validate the normalization method performed with coudé by applying an independent method. Namely, since the normalization of MUSICOS is performed by an independent method,

[4] *Image Reduction and Analysis Facility* (IRAF) is distributed by the National Optical Astronomical Observatories (NOAO), which is operated by the Association of Universities for Research in Astronomy (AURA), Inc., under contract to the National Science Foundation (NSF).

it should show systematic errors related to the method applied to coudé. The HARPS sample is collected to test the efficiency of the blaze removal by its flat-fielding procedure. Namely, the presence of residual blaze features in them should be indicated by divergent $T_{\rm eff}$ results when the same normalization method is applied to coudé and HARPS.

More stars were observed with the coudé spectrograph in order to cover as much as possible the $T_{\rm eff}$–[Fe/H]–$\log g$ parameter space. Therefore, every object in the HARPS and MUSICOS subsamples has associated coudé spectra. The parameter space covered by the sample stars is presented in Fig. 2.1. Stellar parameters were extracted from the compilation of catalogs from the literature listed in Table 2.1. In order to compare $T_{\rm eff}$ scales from the literature and determine their accuracy, I selected works that derived $T_{\rm eff}$ by three different techniques: *i)* excitation & ionization of Fe lines (Sousa et al., 2008; Ghezzi et al., 2010b; Tsantaki et al., 2013; Bensby, Feltzing, and Oey, 2014; Ramírez et al., 2014), *ii)* photometric calibrations based in IRFM (Ramírez, Allende Prieto, and Lambert, 2013), and *iii)* interferometry (Heiter et al., 2015). Most of the parameters in Table 2.1 belong to the catalog of Ramírez, Allende Prieto, and Lambert (2013) because this selection started using this catalog, which has a large number of stars with accurate parallaxes from the HIPPARCOS catalog (Perryman et al., 1997), observable in the southern hemisphere. These parameters are just referential because they were used for selection, thus their associated errors are not relevant. Even, in the case in case the parameters are subject to biases relative to the technique with which they are determined, which is the hypothesis of this work, such biases are not expected to be large.

Table 2.2 includes characteristics associated to the solar spectra, observed via reflection on the proxies Ganymede, Ceres, Callisto and the Moon. I acquired solar spectra for this work with coudé and MUSICOS in order to determine the accuracy of theoretical models at solar parameters. The Sun is the only star for which some spectra with S/N $<$ 200, and they were chosen with the purpose of verifying the influence of decreasing the S/N on the temperature determinations. HARPS solar spectra were retrieved to check if they have residual blaze features. In this sample, I added Ceres although I did not observe it with coudé, and MUSICOS. The purpose was to expand the data in the time dimension in order to check the temporal stability of the instrument; there were not available other proxies to evenly fill the time-line. Ten random spectra of the same object per day/year were extracted. The only 6 spectra available of 2010/10 were complemented with spectra of the close date 2010/12, and for 2007 and 2009 only the available spectra were used.

2.2 M67 sample stars

This sample contains 59 main sequence and turnoff stars of the open cluster (OC) M67. They are part of a sample of 91 stars, that also includes giants, with high probability of membership, discriminated by measurements of radial velocity (RV) from HARPS and Gaia (Gaia Collaboration et al., 2016b; Gaia Collaboration et al., 2018), and parallax and proper motion (PM) from Gaia. Figure 2.2 shows RV, parallax, and PM distributions of the 91 selected stars, and the Gaia color-magnitude diagram. The process for deriving $T_{\rm eff}$ for these stars is described in Chap. 6.

The stars were observed with HARPS for a long-term search program of massive planets, performed by Pasquini, Biazzo, Bonifacio, et al. (2008), Pasquini et al. (2012), Brucalassi et al. (2014), and Brucalassi et al. (2017), in which no sign of binarity or multiplicity was identified. Therefore, these stars are supposed to be single, that is, without any stellar companion-induced convection that can influence the photometry or contaminate the spectra. The 59 main sequence and turnoff stars are listed in Table 2.3 along with their parallax values, Johnson-Cousins BVI magnitudes (Yadav et al., 2008b; Yadav et al., 2008a), 2MASS JHK_S magnitudes (Cutri et al., 2003; Sarajedini, Dotter, and Kirkpatrick, 2009), Gaia $G_{BP}G_{RP}$ magnitudes, $T_{\rm eff}$ derived from $(B-V)$–$T_{\rm eff}$ relations based in InfraRed Flux Method (Casagrande et al., 2010) (the accuracy of this $T_{\rm eff}$ scale was conformed by Casagrande et al. (2014)), and $T_{\rm eff}$ derived from Hα lines from 1D LTE models (Barklem et al., 2002) bias-corrected (see Chap. 4 for details). All stars in the table have 2MASS photometry from the official catalog (Cutri et al., 2003), but some of them have more precise photometry from the catalog of Sarajedini, Dotter, and Kirkpatrick (2009), the extension of which is also 3 mag deeper. The latter catalog used all observations of M67 taken as part of the 2MASS calibration process. This data can be retrieved from the “Combined 2MASS Calibration Scan” source list (Title 90067) available from the 2MASS Web site[5].

Since the spectra used in this work were acquired for planet search, typically low S/N ratio, 12 in average, are available for each star. Table 2.4 lists the S/N of each spectrum along with their associated $T_{\rm eff}^{\rm H\alpha}$(1D LTE), and the weighted mean value for each star to which the bias correction of +28 K was applied (Eq. 4.2) In the table, seven stars appear with no information because it was not possible to normalize their spectra due to ripple-like profile distortions like that shown in Fig. 3.2. Hα profiles from giants were not analysed because unbiased $T_{\rm eff}$ are hardly possible to obtain due to their spectra highly crowded by metal lines.

[5] https://old.ipac.caltech.edu/2mass/releases/allsky/doc/seca7_4.html

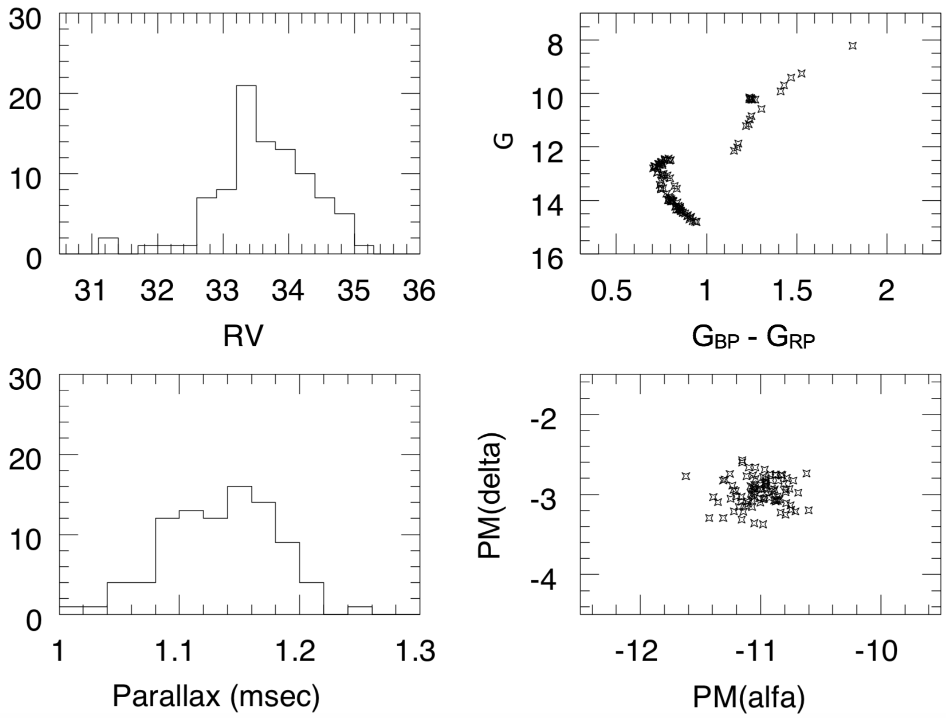

FIGURE 2.2: Final sample of 91 M67 stars selected. *Top left panel:* Distribution of radial velocity with mean 33.64 and dispersion 0.73 ms^{-1}. *Top right panel:* Gaia color-magnitude diagram. *Bottom left panel:* Distribution of parallax with mean = 1.133 and dispersion 0.053 mas, median = 1.139 and dispersion 0.0345 mas. *Bottom right panel:* Proper motion(α) mean $= -11.005$ and dispersion 0.186, Proper motion(δ) mean -2.968 and dispersion 0.175.

TABLE 2.1: **Hα-test-sample.**
The column 4 specifies the spectrograph of acquisition: coudé (Co), HARPS (HA) and MUSICOS (MU). The columns 5, 6 and 7 list the atmospheric parameters used to select the sample taken from the literature. The last column indicates the catalogs that provide parameters for the star, with which I determine the accuracy of various $T_{\rm eff}$ scales in Chaps. 4 and 5. The identification code is: (1) Sousa et al. (2008), (2) Ghezzi et al. (2010b), (3) Tsantaki et al. (2013), (4) Ramírez, Allende Prieto, and Lambert (2013), (5) Bensby, Feltzing, and Oey (2014), (6) Ramírez, Meléndez, and Asplund (2014), (7) Ramírez et al. (2014), (8) Maldonado et al. (2015), (9) Heiter et al. (2015). The catalog from which the parameters in columns 5, 6 and 7 were taken is highlighted in bold.

Name	HD	HIP	spectrum	$T_{\rm eff}$ [K]	log g	[Fe/H]	ctlg
Moon			Co/HA/MU	5772	4.44	0.00	
Ganymede			Co/HA/MU	5772	4.44	0.00	
Calisto			Co	5772	4.44	0.00	
Ceres			HA	5771	4.44	0.00	
ζ Tuc	1581	1599	Co/HA	5947	4.39	−0.22	1,2,3,**4**,5,8
β Hyi	2151	2021	Co	5819	3.95	−0.13	3,**4**,9
	3823	3170	Co/HA	5963	4.05	−0.24	1,2,3,**5**,8
τ Cet	10700	8102	Co/HA	5390	4.52	−0.50	1,2,3,**4**,8,9
ϵ For	18907	14086	Co/HA	5065	3.50	−0.62	**4**,9
α For	20010	14879	Co	6073	3.91	−0.30	**4**,5
κ Cet	20630	15457	Co	5663	4.47	0.00	2,**4**,8
10 Tau	22484	16852	Co	5971	4.06	−0.09	2,**4**,5,8
δ Eri	23249	17378	Co/HA	5012	3.76	0.06	1,3,**4**,8,9
40 Eri	26965	19849	Co/HA	5202	4.55	−0.28	1,3,**4**,8
	100623	56452	Co/HA	5241	4.59	−0.37	**4**,5,8
β Vir	102870	57757	Co/MU	6103	4.08	0.11	2,**4**,9
	114174	64150	Co	5723	4.37	0.05	**4**,7
59 Vir	115383	64792	Co	5995	4.24	0.11	2,**4**,5,8
61 Vir	115617	64924	Co/HA/MU	5571	4.42	−0.02	1,2,3,**4**,5,8
η Boo	121370	67927	Co/HA	6047	3.78	0.26	**4**,9
	126053	70319	Co	5691	4.44	−0.36	2,**4**,8
α Cen A	128620	71683	Co/HA	5809	4.32	0.23	**4**,8,9
ψ Ser	140538	77052	Co/HA	5750	4.66	0.12	7,**8**
	144585	78955	Co/HA	5940	4.40	0.37	1,3,**5**,6
18 Sco	146233	79672	Co/HA/MU	5789	4.43	0.02	1,3,**4**,7,8,9
	147513	80337	Co	5855	4.50	0.03	1,2,3,**4**,5,8
ζ TrA	147584	80686	Co/HA	6030	4.43	−0.08	**4**,5
12 Oph	149661	81300	Co/HA	5248	4.55	0.01	**4**,5,8
	150177	81580	Co/HA	6112	3.77	−0.66	**5**
	154417	83601	Co/HA	6018	4.38	−0.03	**4**,5
μ Ara	160691	86796	Co/HA/MU	5683	4.20	0.27	2,**4**,6,9
70 Oph	165341	88601	Co	5394	4.56	0.07	**4**,8
ι Pav	165499	89042	Co	5914	4.27	−0.13	**8**
	172051	91438	Co	5651	4.52	−0.24	**4**,5,8
	179949	94645	Co/HA	6365	4.56	0.24	1,2,3,**5**,6
31 Aql	182572	95447	Co/MU	5639	4.41	0.41	**5**
	184985	96536	Co/HA	6309	4.03	0.01	**2**,5
δ Pav	190248	99240	Co/HA	5517	4.28	0.33	1,2,3,**4**,8
15 Sge	190406	98819	Co	5961	4.42	0.05	2,**4**,8
ϕ^2 Pav	196378	101983	Co	5971	3.82	−0.44	**8**
γ Pav	203608	105858	Co/HA/MU	6150	4.35	−0.66	**4**,5,8
	206860	107350	Co/HA	5961	4.45	−0.06	**4**,8
ξ Peg	215648	112447	Co/MU	6178	3.97	−0.27	**2**
49 Peg	216385	112935	Co/HA	6292	3.99	−0.22	**4**
51 Peg	217014	113357	Co/HA/MU	5752	4.32	0.19	**4**,5,8
ι Psc	222368	116771	Co/HA	6211	4.11	−0.12	2,**4**,8

TABLE 2.2: **Solar proxies.**
The list is ordered by date of observation along with the S/N of the spectra and the effective temperature derived from Hα profiles from 1D LTE models (Barklem et al., 2002) with their associated errors.

Date	object	S/N	$T_{\rm eff}^{\rm H\alpha}$(1D LTE) [K]
coudé			
2014/10	Moon	300	5741 ± 32
2017/07	Moon	400	5748 ± 25
2017/07	Moon	400	5746 ± 28
2017/07	Moon	400	5751 ± 25
2017/07	Calisto	350	5740 ± 28
2017/07	Ganymede	350	5732 ± 35
MUSICOS			
2017/11	Ganymede	300	5726 ± 28
2017/11	Moon	250	5756 ± 45
2017/11	Moon	250	5759 ± 41
2017/11	Moon	250	5753 ± 30
HARPS			
2007/04	Ganymede	174	5746 ± 52
2007/04	Ganymede	172	5750 ± 76
2007/04	Ganymede	171	5745 ± 88
2007/04	Ganymede	173	5745 ± 68
2007/04	Ganymede	174	5735 ± 99
2007/04	Ganymede	391	5747 ± 54
2009/03	Moon	532	5747 ± 31
2010/10	Moon	263	5741 ± 65
2010/10	Moon	307	5759 ± 43
2010/10	Moon	288	5755 ± 53
2010/10	Moon	299	5743 ± 74
2010/10	Moon	308	5753 ± 60
2010/10	Moon	304	5759 ± 66
2010/12	Moon	578	5746 ± 29
2010/12	Moon	408	5735 ± 38
2010/12	Moon	412	5744 ± 38
2010/12	Moon	494	5732 ± 36
2012/06	Moon	479	5742 ± 45
2012/06	Moon	478	5737 ± 48
2012/06	Moon	488	5746 ± 38
2012/06	Moon	487	5742 ± 43
2012/06	Moon	485	5735 ± 44
2012/06	Moon	486	5735 ± 42
2012/06	Moon	488	5739 ± 39
2012/06	Moon	490	5742 ± 33
2012/06	Moon	478	5734 ± 33
2012/06	Moon	476	5753 ± 35
2014/02	Ganymede	119	5765 ± 98
2014/02	Ganymede	107	5750 ± 103
2014/02	Ganymede	117	5760 ± 105
2014/02	Ganymede	118	5750 ± 107
2014/02	Ganymede	109	5767 ± 97
2014/02	Ganymede	117	5757 ± 108
2014/02	Ganymede	116	5744 ± 139
2014/02	Ganymede	109	5757 ± 138
2014/02	Ganymede	109	5759 ± 118
2014/02	Ganymede	122	5760 ± 98
2015/07	Ceres	89	5754 ± 134
2015/07	Ceres	87	5748 ± 140
2015/07	Ceres	88	5751 ± 111

2015/07	Ceres	89	5745 ± 145
2015/07	Ceres	91	5755 ± 137
2015/07	Ceres	103	5753 ± 143
2015/07	Ceres	87	5751 ± 126
2015/07	Ceres	100	5753 ± 110
2015/07	Ceres	115	5754 ± 116
2015/07	Ceres	128	5746 ± 92

TABLE 2.3: **M67 main sequence and turnoff stars from Brucalassi et al. (2017).**
They are designated by their list number in the catalog of Yadav et al. (2008a). Parallaxes and their errors correspond to Gaia DR2 (Gaia Collaboration et al., 2018). B and V Johnson magnitudes, and I Cousins magnitudes were extracted from Yadav et al. (2008a). 2MASS J, H, and K_S magnitudes were extracted from Sarajedini, Dotter, and Kirkpatrick (2009) for the stars pointed in bold, and from Cutri et al. (2003) for the others. G, and $G_{BP} - G_{RP}$ were extracted from Gaia DR2. IRFM $T_{\rm eff}$ was derived using the $(B-V)$–$T_{\rm eff}$ relation of (Casagrande et al., 2010) using colors derredened by 0.041 mag (Taylor, 2007). $T_{\rm eff}$ and its internal uncertainty in the last two columns were derived by fitting Hα profiles from 1D LTE models (Barklem et al., 2002) corrected by Eq. 4.2

YBP	π (mas)	$\sigma(\pi)$	B	$\sigma(B)$	V	$\sigma(V)$	I	$\sigma(I)$	J	$\sigma(J)$	H	$\sigma(H)$	K_S	$\sigma(K_S)$	G	$G_{BP}-G_{RP}$	IRFM $T_{\rm eff}$	σ	$T_{\rm eff}$	σ
219	1.17672	0.02524	13.715	0.009	13.100	0.008	12.425	0.005	12.102	0.021	11.864	0.022	11.778	0.021	13.0543	0.7526	5993	100	6031	184
266	1.09917	0.02688	14.212	0.006	13.601	0.006	12.939	0.007	12.602	0.001	12.341	0.001	12.288	0.001	13.5487	0.7470	6007	89	6040	86
285	1.14768	0.03381	15.165	0.006	14.461	0.000	13.713	0.002	13.314	0.001	13.005	0.001	12.943	0.001	14.3824	0.8575	5707	78	5862	232
288	1.10494	0.02801	14.494	0.013	13.857	0.004	13.160	0.005	12.785	0.022	12.522	0.024	12.452	0.023	13.7872	0.7822	5920	99	–	–
291	1.14189	0.02550	14.090	0.010	13.478	0.009	12.807	0.018	12.492	0.023	12.245	0.023	12.245	0.023	13.4234	0.7425	6003	105	6082	65
349	1.12267	0.02941	14.978	0.006	14.301	0.002	13.614	0.007	13.176	0.023	12.889	0.026	12.830	0.023	14.2199	0.8293	5791	81	5858	89
350	1.08173	0.03226	14.226	0.005	13.624	0.010	12.955	0.006	12.578	0.001	12.310	0.001	12.249	0.001	13.5536	0.7603	6037	96	6025	72
401	1.17460	0.03145	14.268	0.006	13.661	0.007	13.009	0.003	12.639	0.001	12.381	0.001	12.324	0.001	13.5888	0.7475	6020	91	6074	56
473	1.11235	0.04271	15.142	0.011	14.443	0.008	13.731	0.004	13.292	0.001	12.991	0.001	12.918	0.001	14.3425	0.8318	5722	99	5739	134
587	1.10817	0.03069	14.753	0.006	14.107	0.006	13.405	0.020	12.971	0.023	12.730	0.024	12.648	0.025	13.9914	0.7875	5890	88	5986	89
613	1.05371	0.02619	13.907	0.015	13.254	0.006	12.594	0.022	12.172	0.001	11.910	0.001	11.848	0.001	13.1456	0.7670	5867	107	6031	65
637	1.13951	0.03660	15.191	0.017	14.489	0.010	13.751	0.011	13.284	0.001	12.977	0.001	12.910	0.001	14.3461	0.8432	5713	117	5660	118
673	1.15978	0.03155	15.062	0.002	14.356	0.009	13.569	0.001	13.058	0.022	12.746	0.023	12.628	0.025	14.2290	0.9073	5701	84	5718	83
689	1.09690	0.05524	13.783	0.012	13.120	0.011	12.436	0.010	12.030	0.001	11.762	0.001	11.709	0.001	13.0041	0.7623	5835	111	6029	76
750	1.12845	0.02605	14.215	0.007	13.576	0.014	12.865	0.005	12.403	0.023	12.102	0.022	12.065	0.020	13.4600	0.8233	5913	108	5873	75
769	1.12060	0.02593	14.119	0.004	13.478	0.003	12.771	0.005	–	–	12.054	0.049	11.943	0.021	13.3493	0.8012	5906	80	–	–
778	1.09554	0.03789	13.716	0.010	13.093	0.011	12.411	0.011	11.956	0.001	11.677	0.001	11.616	0.001	12.9605	0.7886	5966	109	5956	64
809	1.08098	0.04049	15.696	0.007	14.959	0.015	14.162	0.004	13.620	0.001	13.278	0.001	13.192	0.001	14.8004	0.9374	5607	104	5486	180
851	0.74973	0.06807	14.730	0.007	14.113	0.004	13.449	0.007	13.025	0.001	12.757	0.001	12.701	0.001	13.9847	0.7707	5986	87	6009	222
911	1.13059	0.03501	15.220	0.006	14.547	0.010	13.785	0.010	13.268	0.001	12.936	0.001	12.858	0.001	14.3927	0.8764	5803	94	–	–
988	1.11347	0.02886	14.819	0.005	14.180	0.001	13.475	0.002	13.004	0.022	12.750	0.022	12.682	0.023	14.0417	0.8065	5913	79	5961	126
1032	1.17007	0.03725	14.997	0.005	14.358	0.003	13.649	0.001	13.174	0.023	12.899	0.026	12.813	0.025	14.2360	0.8258	5913	81	5841	112
1036	1.10191	0.05013	15.678	0.018	14.947	0.003	14.164	0.005	13.608	0.001	13.260	0.001	13.186	0.001	14.7666	0.9247	5625	102	5578	103
1051	1.13203	0.02787	14.726	0.007	14.090	0.004	13.382	0.004	12.912	0.023	12.601	0.028	12.531	0.023	13.9571	0.8148	5923	86	5917	74
1062	1.15086	0.02999	15.144	0.001	14.477	0.008	13.745	0.004	13.216	0.022	12.921	0.024	12.844	0.025	14.3173	0.8488	5822	82	5717	70
1067	1.31676	0.05770	15.201	0.005	14.559	0.009	13.824	0.002	13.367	0.024	13.084	0.027	13.024	0.028	14.4338	0.8434	5903	92	5904	129
1075	1.12999	0.02752	14.386	0.000	13.712	0.006	12.992	0.004	12.501	0.021	12.199	0.022	12.146	0.023	13.5685	0.8361	5800	78	5835	82
1088	1.15607	0.03064	15.151	0.004	14.492	0.001	13.760	0.007	13.288	0.023	12.973	0.026	12.854	0.024	14.3440	0.8518	5848	77	5861	115
1090	1.13108	0.03041	14.450	0.004	13.800	0.005	13.040	0.010	12.516	0.001	12.161	0.001	12.079	0.001	13.6419	0.8567	5877	83	5843	209
1101	1.14705	0.03901	15.377	0.001	14.675	0.004	13.903	0.001	13.405	0.036	13.164	0.041	13.048	0.031	14.5538	0.8968	5713	77	–	–

YBP	π (mas)	$\sigma(\pi)$	B	$\sigma(B)$	V	$\sigma(V)$	I	$\sigma(I)$	J	$\sigma(J)$	H	$\sigma(H)$	K_S	$\sigma(K_S)$	G	$G_{BP}-G_{RP}$	IRFM T_{eff}	σ	T_{eff}	σ
1129	1.11548	0.02996	14.795	0.005	14.171	0.006	13.482	0.002	13.008	0.023	12.697	0.024	12.638	0.024	14.0280	0.8032	5963	87	5928	135
1137	1.11537	0.03724	15.571	0.002	14.873	0.008	14.107	0.009	13.564	0.001	13.227	0.001	13.161	0.001	14.7045	0.9073	5725	83	5813	59
1194	1.11641	0.03694	15.281	0.002	14.614	0.010	13.876	0.002	13.383	0.001	13.069	0.001	13.007	0.001	14.4666	0.8683	5822	87	5800	102
1197	1.11917	0.02858	13.921	0.006	13.315	0.003	12.618	0.024	–	–	–	–	–	–	13.1670	0.7976	6024	84	6037	85
1247	1.11657	0.03360	14.753	0.008	14.144	0.008	13.470	0.005	13.005	0.001	12.720	0.001	12.659	0.001	14.0004	0.7896	6013	98	6032	61
1303	1.09796	0.03471	15.318	0.008	14.641	0.008	13.899	0.009	13.396	0.023	13.042	0.022	12.958	0.028	14.4932	0.8814	5791	94	–	–
1304	1.14296	0.03633	15.454	0.015	14.731	0.009	13.916	0.006	13.362	0.001	12.990	0.001	12.908	0.001	14.5484	0.9290	5649	109	–	–
1315	1.15599	0.03267	14.990	0.013	14.297	0.011	13.544	0.008	13.027	0.022	12.667	0.025	12.597	0.025	14.1572	0.8778	5741	111	5787	118
1334	1.15628	0.03157	15.083	0.007	14.403	0.007	13.669	0.000	13.170	0.001	12.866	0.001	12.803	0.001	14.2481	0.8532	5781	90	5851	114
1387	1.13999	0.03015	14.724	0.004	14.098	0.002	13.398	0.000	12.935	0.001	12.650	0.001	12.592	0.001	13.9575	0.8059	5956	79	5907	94
1392	1.13010	0.03611	15.527	0.002	14.811	0.004	14.047	0.000	13.530	0.001	13.195	0.001	13.124	0.001	14.6593	0.9079	5670	78	5718	110
1458	1.08155	0.03711	15.716	0.010	14.977	0.005	14.186	0.004	13.632	0.001	13.282	0.001	13.206	0.001	14.8084	0.9459	5602	90	5693	94
1496	1.07358	0.03053	14.486	0.013	13.879	0.004	13.214	0.002	12.682	0.001	12.403	0.001	12.343	0.001	13.7448	0.7793	6020	100	6063	97
1504	1.13953	0.02881	14.796	0.001	14.171	0.011	13.474	0.000	13.009	0.001	12.719	0.001	12.661	0.001	14.0328	0.8160	5959	89	5877	105
1514	1.06454	0.03602	15.498	0.003	14.777	0.004	14.008	0.000	13.491	0.001	13.159	0.001	13.089	0.001	14.6201	0.9145	5655	79	5691	75
1587	1.15183	0.02748	14.804	0.015	14.163	0.004	13.469	0.006	13.009	0.001	12.721	0.001	12.662	0.001	14.0265	0.8077	5906	103	5956	69
1622	1.14626	0.02946	14.788	0.004	14.156	0.002	13.459	0.004	12.993	0.001	12.709	0.001	12.649	0.001	14.0168	0.8149	5936	79	5955	89
1716	1.09028	0.02380	13.918	0.010	13.299	0.009	12.625	0.005	12.161	0.001	11.874	0.001	11.812	0.001	13.1737	0.7970	5979	104	5900	94
1722	1.16529	0.02779	14.731	0.002	14.130	0.006	13.449	0.009	12.989	0.001	12.707	0.001	12.643	0.001	13.9924	0.7972	6041	82	5952	72
1735	1.09752	0.03521	14.993	0.012	14.332	0.010	13.617	0.007	13.144	0.022	12.820	0.024	12.789	0.025	14.2092	0.8455	5841	108	5919	123
1758	1.23333	0.03760	13.860	0.056	13.207	0.015	12.545	0.007	12.107	0.001	11.835	0.001	11.770	0.001	13.0987	0.7684	5867	251	5954	175
1768	1.07538	0.03284	15.060	0.003	14.404	0.004	13.684	0.004	13.195	0.023	12.882	0.023	12.799	0.022	14.2718	0.8517	5858	80	–	–
1787	1.07230	0.03020	15.214	0.006	14.547	0.004	13.813	0.003	13.327	0.001	13.015	0.001	12.955	0.001	14.4041	0.8598	5822	84	5807	94
1788	1.18134	0.02902	15.104	0.008	14.441	0.004	13.709	0.000	13.214	0.001	12.909	0.001	12.850	0.001	14.2976	0.8549	5835	87	5819	77
1852	1.15669	0.02993	14.575	0.011	13.962	0.008	13.286	0.005	12.855	0.024	12.556	0.022	12.514	0.026	13.8639	0.7919	6000	104	6080	121
1903	1.10327	0.03240	15.422	0.004	14.733	0.003	13.971	0.001	13.477	0.001	13.148	0.001	13.081	0.001	14.5853	0.8941	5753	79	5754	189
1948	1.09817	0.03123	14.627	0.009	14.015	0.004	13.327	0.002	12.887	0.021	12.569	0.025	12.504	0.023	13.9063	0.7978	6003	91	6066	247
1955	1.16992	0.02769	14.842	0.001	14.212	0.004	13.483	0.002	13.008	0.001	12.699	0.001	12.627	0.001	14.0855	0.8369	5943	77	5988	97
2018	1.08659	0.03044	15.237	0.000	14.565	0.005	13.832	0.007	13.370	0.021	13.022	0.027	12.952	0.026	14.4474	0.8684	5806	77	5828	76

TABLE 2.4: $T_{\rm eff}$ **for M67 stars.**
Temperatures from Hα 1D LTE profiles. Third and forth columns give individual determinations and corresponding errors, and fifth and sixth columns give mean bias-corrected (+28 K; Eq. 4.2), and the internal dispersion, respectively.

YBP	S/N	$T_{\rm eff}^{\rm H\alpha}$(1D LTE) [K]	σ [K]	$\langle T_{\rm eff}^{\rm H\alpha}$(1D LTE)$\rangle$ [K]	σ [K]
219	15	6003	266	6031	266
266	10	5855	256	6040	86
	13	5937	305		
	16	6109	161		
	13	6046	262		
	11	6006	176		
	20	5980	203		
285	11	5834	232	5862	232
288	–	–	–	–	–
291	14	6073	182	6082	65
	14	6167	245		
	14	6013	137		
	13	6195	265		
	15	5997	163		
	13	6013	300		
	18	6022	190		
	13	6079	190		
	10	6088	233		
349	12	5907	201	5858	89
	11	5795	170		
	11	5780	170		
	12	5912	263		
	7	5820	232		
350	17	5952	202	6025	72
	14	5972	105		
	14	6254	381		
	15	5974	236		
	11	6109	269		
	14	5874	198		
	9	6241	259		
401	16	6029	94	6074	56
	9	6056	223		
	11	6121	262		
	11	5955	217		
	11	6097	331		
	10	6084	255		
	6	6061	369		
	9	6095	339		
	13	6022	380		
	9	6066	298		
	8	6146	332		
	27	6047	114		
473	12	5606	256	5739	134
	11	5735	168		
	7	5851	437		
587	14	5926	131	5986	89
	13	6006	196		
	21	5973	156		
613	14	6117	134	6031	65
	21	6034	178		
	13	6000	224		
	24	5946	88		

YBP	S/N	$T_{\mathrm{eff}}^{\mathrm{H}\alpha}$(1D LTE) [K]	σ [K]	$\langle T_{\mathrm{eff}}^{\mathrm{H}\alpha}$(1D LTE)$\rangle$ [K]	σ [K]
637	10	5570	180	5660	118
	12	5678	156		
673	10	5674	443	5718	83
	8	5714	497		
	11	5712	353		
	11	5740	167		
	11	5779	211		
	11	5659	132		
	7	5482	303		
689	13	6090	200	6029	76
	15	5881	185		
	13	6020	254		
	13	5928	197		
	23	6039	115		
750	14	5898	130	5873	75
	16	5801	110		
	19	5860	164		
769	–	–	–	–	–
778	16	5979	157	5956	64
	24	5887	183		
	14	5972	196		
	15	5917	160		
	13	5908	278		
	14	6120	248		
	9	5726	271		
	12	5789	160		
	10	6059	185		
809	13	5498	281	5486	180
	9	5431	234		
851	17	5981	222	6009	222
911	–	–	–	–	–
988	13	5858	169	5961	126
	11	6026	189		
1032	12	5848	250	5831	112
	10	5857	213		
	17	5756	156		
1036	13	5539	139	5733	103
	8	5669	312		
	11	5450	176		
	12	5553	226		
	9	5663	211		
1051	16	5969	112	5929	58
	12	5776	157		
	12	6045	241		
	13	5964	148		
	13	5741	145		
	17	5865	177		
	11	5991	172		
1062	12	5801	253	5717	70
	8	5850	321		
	12	5584	244		
	11	5759	163		
	15	5635	122		
	11	5709	168		
	7	5680	318		
	9	5571	310		
1067	11	5897	236	5872	109
	6	5972	371		
	13	5983	273		
	12	5761	149		

YBP	S/N	$T_{\rm eff}^{\rm H\alpha}$(1D LTE) [K]	σ [K]	$\langle T_{\rm eff}^{\rm H\alpha}$(1D LTE)$\rangle$ [K]	σ [K]
1075	13	5920	206	5835	82
	13	5874	215		
	11	5880	296		
	13	5677	160		
	13	5880	211		
	16	5760	179		
1088	12	5798	161	5858	95
	10	5998	258		
	11	5859	171		
	13	5729	213		
1090	13	5815	143	5843	143
1101	–	–	–	–	–
1129	16	5900	135	5928	135
1137	11	5653	208	5813	59
	11	5661	172		
	11	5702	196		
	8	5882	243		
	33	5826	73		
1194	12	5815	237	5800	102
	13	5765	201		
	11	5898	378		
	14	5705	296		
	10	5601	270		
	9	5734	384		
	11	5851	415		
	6	5794	500		
	9	5928	477		
	8	5922	466		
1197	13	6084	234	6008	77
	14	5851	135		
	16	6039	218		
	13	6005	209		
	11	6071	254		
	14	6036	168		
1247	15	5969	197	6040	59
	11	6248	262		
	12	6123	157		
	20	5979	70		
1303	–	–	–	–	–
1304	–	–	–	–	–
1315	12	5916	205	5787	118
	15	5681	144		
1334	11	6034	176	5841	90
	14	5686	134		
	14	5778	239		
	13	5847	244		
1387	15	5655	121	5849	81
	13	6105	210		
	15	5875	173		
	18	5925	186		
1392	8	5441	367	5701	104
	10	5521	229		
	9	5751	194		
	9	5789	199		
	14	5830	269		
1458	11	5650	215	5693	94
	11	5616	223		
	11	5683	119		
1496	12	5945	203	6083	86
	12	6035	251		

YBP	S/N	$T_{\rm eff}^{\rm H\alpha}$(1D LTE) [K]	σ [K]	$\langle T_{\rm eff}^{\rm H\alpha}$(1D LTE)$\rangle$ [K]	σ [K]
	12	6067	200		
	14	6124	135		
	12	5983	251		
1504	17	5691	103	5815	82
	13	5941	159		
	14	5968	251		
1514	9	5745	195	5691	75
	10	5650	194		
	8	5637	215		
	10	5740	270		
	12	5763	312		
	12	5584	157		
	10	5649	255		
	9	5664	199		
1587	15	5898	235	5956	69
	14	5904	388		
	15	6033	405		
	14	5951	130		
	13	5823	325		
	16	5949	140		
	22	5905	129		
1622	16	5805	290	5947	84
	11	5848	172		
	14	5966	125		
	11	5848	278		
	12	6003	228		
1716	15	5780	191	5900	94
	22	5901	108		
1722	17	5961	107	5966	59
	13	5908	145		
	11	6087	172		
	10	5957	248		
	17	5883	177		
	11	6000	188		
	21	5806	151		
1735	13	5902	195	5890	108
	12	5764	158		
	8	6007	226		
1758	15	5926	175	5954	175
1768	–	–	–	–	–
1787	10	5797	273	5807	94
	12	5834	257		
	9	5727	252		
	13	5787	145		
	14	5748	212		
1788	13	5817	144	5819	77
	10	5726	177		
	10	5719	269		
	12	5837	237		
	11	5806	172		
	11	5858	258		
	11	5725	381		
1852	10	6266	251	6080	121
	13	6052	238		
	18	5954	170		
1903	9	5667	271	5766	167
	8	5781	211		
1948	12	6038	247	6076	247
1955	9	6021	274	5988	97
	13	5934	365		

YBP	S/N	$T_{\mathrm{eff}}^{\mathrm{H}\alpha}$(1D LTE) [K]	σ [K]	$\langle T_{\mathrm{eff}}^{\mathrm{H}\alpha}$(1D LTE)$\rangle$ [K]	σ [K]
	10	5954	164		
	14	5951	143		
2018	14	5797	129	5817	61
	10	5922	273		
	11	5715	165		
	13	5873	266		
	11	5699	167		
	12	5660	283		
	10	5727	177		
	10	5905	182		
	9	5986	218		
	10	5661	283		

Chapter 3

Method: Hα profile fitting

In this chapter I describe and solve the problems related to the normalization of Hα profiles. The method is also applicable to other profiles of the Balmer series and to other broad lines such as the calcium triplet, for instance. The discussion concerning the accuracy of theoretical Hα profiles is presented in Chap. 4.

The normalization of lines with broad profiles is not straightforward for precision spectroscopy: the wavelength ranges not influenced by the line profile in a spectral order are very short, and this makes the reconstruction of the spectrograph response by polynomial interpolation highly difficult. For example, the solar Hα profile fill the range 6510-6610 Å, which embraces $\sim$70% of the wavelength coverage of the single order coudé spectrograph. It thus allows only $\sim$15% on each side of the spectrum for selecting continuum wavelength bins (pixels) and interpolating them.

It is always desirable to apply the Balmer profile fitting to spectra with high resolution and sampling in order to perform robust fittings using many wavelength bins free from metal-line contamination. However, the higher the spectral resolution is, the shorter are the wavelength ranges free from the profile's influence. Therefore, the spectral characteristics have to be chosen according to a balance between the number of wavelength bins that the resolution allows for fitting the profile, and the extension of the free wavelength range. For Hα in solar-type stars, at least R = 30 000 is needed because few and narrow windows with no metallic lines are available. For example, in this work, in spectra with R = 40 000, eight windows were chosen containing a total of 26 to 27 wavelength bins. The widest windows are of 0.3 Å, which for typical CCD cameras of 2048 pixels allow between five and six wavelength bins.

The challenge in normalizing Hα profiles arises from the uncertainty of the continuum location, which is estimated defining "continuum windows" in the wavelength ranges free from the influence of the profile. Frequently, the continuum windows are determined using automatic or semiautomatic procedures, such as the IRAF task *"continuum"*, selecting the wavelength bins with the highest fluxes by applying clipping. Subsequently, the wavelength bins in the continuum windows are interpolated, determining so the normalization curve; this procedure is referred to as "custom normalization" henceforth. Nonetheless, for the analysis of Hα, the custom normalization can seriously distort the profile due to the lack of information about the extension of its wings: if the extension is overestimated/underestimated, the normalized profile result deeper/shallower. Another important problem is the presence of minute telluric features which can mimic the noise, and thus shift the continuum towards lower flux counts.

The normalization of Hα is even more challenging in cross-dispersed (echelle) spectra because of the instrumental blaze and the fragmentation of the profile into multiple orders. Figure 3.1 shows an example of the blaze shape of the fibre-fed

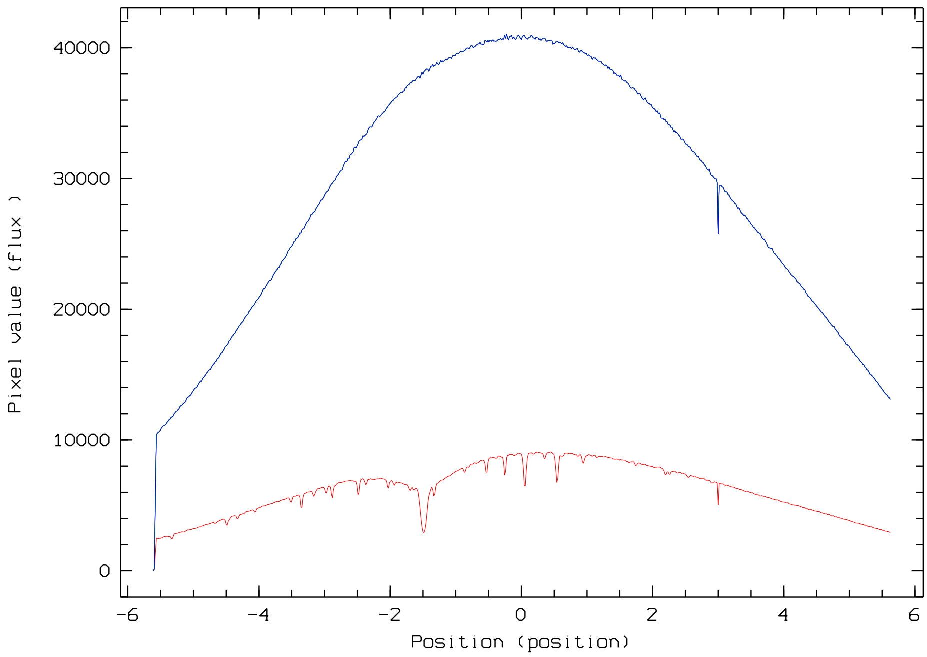

FIGURE 3.1: Adapted from Škoda, Šurlan, and Tomić (2008, Fig. 2). Extracted order containing a Balmer line and its corresponding flat by the HEROS spectrograph.

spectrograph HEROS (Slechta and Skoda, 2002) in one order containing an observed Balmer line. The deblazing by direct division of the acquired intensity counts from the star by the flat field exposures may not completely remove the shape of the blaze, and some residual structure hard to approximate by polynomials may remain underlying in the stellar spectrum (Škoda, Šurlan, and Tomić, 2008). Figure 3.2 shows an example of defective order merging in a spectrum containing a Balmer profile. Such defects are often produced by the data reduction software in slit echelle spectrographs but they are also possible in fiber-fed instruments. When this occurs, the spectra are useless and a new reduction from raw data should be applied following the recipe recommended by Škoda, Šurlan, and Tomić (2008). On the other hand, spectra with no obvious distortions need also to be tested because subtle residual blaze features may remain making the profiles shallower (especially close to the centre of the spectral order) thus mimicking profiles of cooler temperatures.

In the following section I describe a normalization-fitting method that minimizes the profile distortions related to the custom normalization. The method was performed indistinctly for coudé and HARPS pipeline-reduced spectra of the stars in Table 2.1, as is described in next section. The spectra normalized with this method allowed very precise temperature diagnostics with which I determine *i)* the accuracy of the Hα model used in this work (Chap. 4), and *ii)* the accuracy of other techniques (Chap. 5). Further, by comparing the temperature diagnostics from coudé and HARPS spectra I determine the quality of HARPS deblazing (Sect. 6.1). This is a mandatory step prior to the T_{eff} determination of the M67 stars by Hα profile fitting using HARPS (Chap. 6). Fits of all normalized coudé and HARPS spectra are displayed in Appendices A and B.

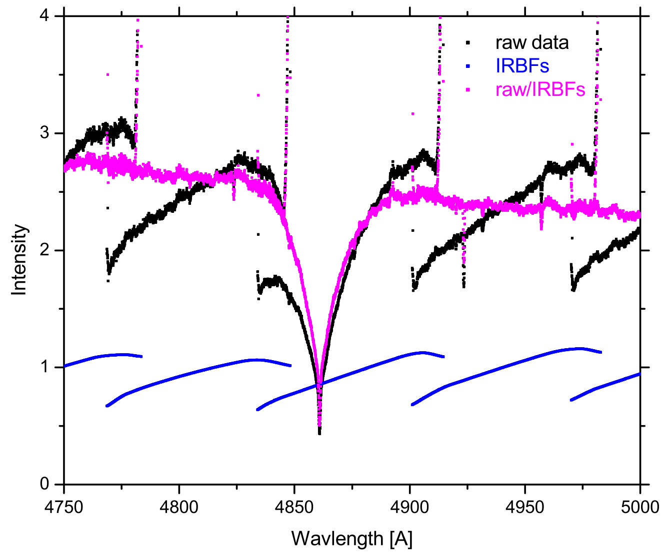

FIGURE 3.2: Adapted from Škoda, Šurlan, and Tomić (2008, Fig. 11). In black, spectrum discontinuities and ripple-like patterns in the orders containing the Hβ line of Vega. The corrected spectrum is plotted in magenta, which is product of the division between the black and the blue lines.

3.1 Normalization-fitting method

For this method to work properly, it is important to firstly assert that the instrumental profile of the acquired spectra is easy to model by low order polynomials. If this is not the case, a complex instrumental profile shape would make the interpolation hard to predict for the central part of the spectral order (where usually the line core is located), which would produce systematic errors in $T_{\rm eff}$. These errors can be large for small departures of the profile from the ideal normalized flux, for example changes of only 0.2% in normalized flux correspond to 20-25 K changes in temperature for the most sensitive regions. Some instruments that offer smooth instrumental features are, for example, FOCES (Pfeiffer et al., 1998), MUSICOS (Baudrand and Bohm, 1992), and coudé[1]. FOCES was used by Fuhrmann et al. (1997), Korn, Shi, and Gehren (2003), and Amarsi et al. (2018) for the same purposes as those of this work. MUSICOS and coudé are currently installed in the OPD/LNA. Coudé was used by Lyra and Porto de Mello (2005) and Porto de Mello, Lyra, and Keller (2008) to determine $T_{\rm eff}$ from Hα and other atmospheric parameters. The latter succeeded in distinguishing small differences in chemical abundances between A and B components of α Cen by applying this technique. Unlike the other two spectrographs, coudé is a single order instrument, so it offers also the advantage of no spectral fragmentation and it has enough wavelength coverage to fully include Hα lines of stars with $T_{\rm eff}$ up to $\sim$6400 K. Accordingly, the OPD coudé spectrograph was chosen to acquire the main set of spectra in which this study is based.

Even with the advantages of the use of coudé spectra, the custom normalization usually leads to distorted profiles because the extension of the profile is unknown. The underestimation/overestimation of the profile extension leads to profile wings

[1] http://www.lna.br/opd/instrum/manual/Manual_160mOPD_Cap3.pdf

with higher/lower fluxes than actual. These errors can be better detected as small flux incompatibilities between the observed and synthetic profiles in the regions where the continuum turns into profile wings (they are referred to as "transition regions" henceforth). Although these incompatibilities seem small in flux, they may imply large errors in T_{eff} because, during the normalization, small flux errors in the transition regions trigger large flux errors close to the line core, where the Hα profile is more sensitive to the temperature. Sect. 4.1.1 provides examples of this problem, where solar normalized profiles, and their associated temperatures are compared. I optimize the custom normalization by iterating on the normalization and fitting processes as described below, in this way the compatibility between the observed and synthetic profiles in the transition regions are checked after every fit and corrected. With this method, I minimize the main source of uncertainty in the Hα profile T_{eff} diagnostic.

3.1.1 Normalization algorithm

The normalization is applied by interpolating Legendre polynomials of 4$^{\mathrm{th}}$ order with the IRAF task *"continuum"*, integrated with the fitting code described in Sect. 3.1.2 in an iterative procedure:

1. A first gross normalization is performed using the blue and red regions outside the range $6514 - 6610$ Å. Although the extension of the Hα wings is variable, this region is kept the same for all the sample stars with the purpose of keeping enough room to apply weights in nearby regions to modulate the normalizing curve.

2. The obtained profile is used to fit a precipitable water vapor (PWV) spectrum that will be used to verify the continuum level after every iteration (Sect. 3.1.3).

3. The same normalized profile is compared with the grid of synthetic profiles using the fitting code described in Sect. 3.1.2 to find the most compatible one.

4. The compatibility between the normalized and synthetic profiles must be visually checked at the transition regions, defined in this procedure as $\lambda < 6536$ Å and $\lambda > 6590$ Å. This procedure makes the normalizations dependent on the model, but only very weakly, because metallicity and surface gravity (the parameters set beforehand) do not greatly influence the shape of the line, especially in the transition regions. I verified that changes as large as ± 0.3 dex in both parameters do not significantly modify the shape of the normalized profiles, while larger changes may truncate the procedure. For consistency, the HARPS spectra were degraded to the resolution of the coudé spectra in this step (only for this step, not for the fitting procedure).

5. Usually the first normalization is deficient; in this case a second one is performed **from scratch** applying weights to the wings around 6514 and 6610 Å to make the profile deeper or shallower as required to match the flux of the synthetic profile. Subsequently, another fit is applied and the matching check described in step 4 is repeated. The procedure finishes when the observed and synthetic profiles are compatible in the transition regions, as shown in Fig. 3.3 for coudé, and in Fig. 3.4 for HARPS. An example of the difference between the first gross normalization and the final normalization is shown in Fig. 3.5.

TABLE 3.1: **Windows of fits**
These windows were used to fit theoretical with observed Hα profiles.

Window	wavelength range (Å)
1	6556.45 – 6556.55
2	6559.00 – 6559.20
3	6559.86 – 6560.08
4	6561.30 – 6561.60
5	6566.00 – 6566.30
6	6567.90 – 6568.10
7	6577.10 – 6577.40
8	6589.55 – 6589.80

Notes: No more windows in the blue wing of the profile were included because the spectra appear systematically contaminated by telluric features in this region.

Notice that in the first iteration the synthetic and observed profiles are incompatible in the outermost regions; the flux of the observed profile cannot be higher than that of the synthetic profile.

3.1.2 Fitting

This study is based on the grid of synthetic profiles of (Barklem et al., 2002) computed using the self-broadening theory developed in Barklem, Piskunov, and O'Mara (2000) and the 1D LTE plane-parallel model atmospheres from the MARCS code (Asplund et al., 1997). The atmospheric parameters of the grid are $T_{\rm eff}$: 4400 to 7500 K with steps of 100 K, [Fe/H]: -3.0 to $+0.5$ dex with steps of 0.5 dex, log g: 3.4 to 5.0 dex with steps of 0.5 dex and microturbulence velocity of 1.5 $\rm Kms^{-1}$. In order to derive very precise $T_{\rm eff}$ values around solar parameters, a more detailed grid from the same theoretical recipe used by Ramírez et al. (2011) (provided by the first author by private communication) is also used here, its parameters are $T_{\rm eff}$: 5500 to 6100 K with steps of 10 K, [Fe/H]: -3.0 to $+0.3$ dex with steps of 0.05 dex, log g: 4.2 to 4.65 dex with steps of 0.05 dex and microturbulence velocity of 1.5 $\rm Kms^{-1}$. The fitting between the observed and synthetic profiles is performed only considering the wavelength bins within "windows of fits" which are free from metallic lines; they are listed in Table 3.1. These windows are shown in all fit plots of this work by vertical shades.

I wrote a program in IDL[2] to perform the fits eliminating the influence of contaminated wavelength bins. It first interpolates the resolution of the grids to 1 K, 0.01 dex, 0.01 dex in $T_{\rm eff}$, [Fe/H], log g. Subsequently, for each wavelength bin, the temperature related to the interpolated synthetic profile with the closest flux value is chosen, [Fe/H] and log g previously fixed by the user. The most probable temperature and its uncertainty are determined by the median and the robust standard deviation (1.4826 times the median absolute deviation) of the histogram, see e.g. Fig. 3.3 and 3.4.

[2] Interactive Data Language, version 7.0

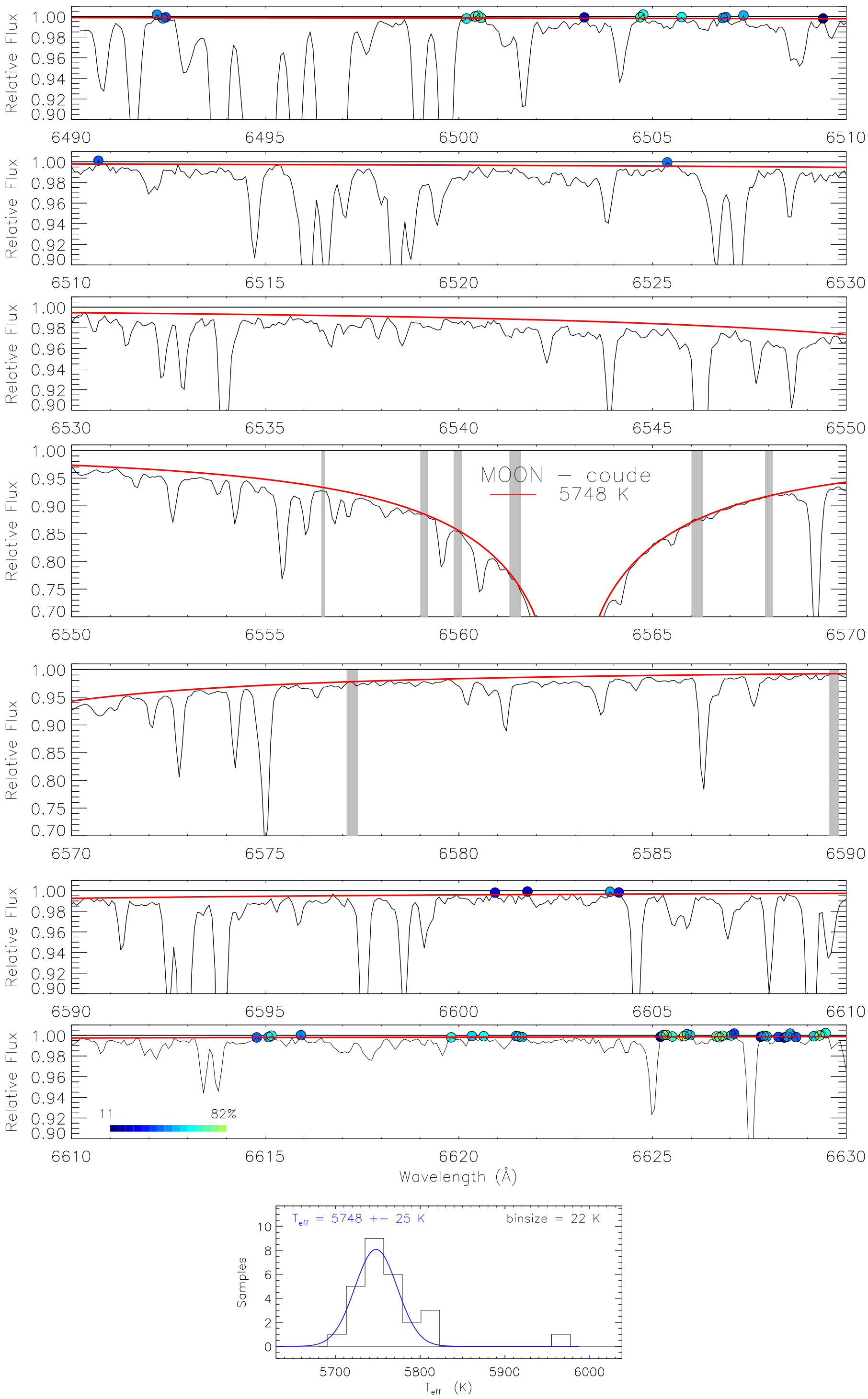

FIGURE 3.3: Coudé Hα spectrum of one of the solar proxies in Table 2.2. The black line represents the observed normalized profile, and the red line represents the synthetic profile from the grids of Barklem et al. (2002, synthesised with 1D LTE atmosphere models) that best fits the observed profile. The shaded regions are the windows of fits listed in Table 3.1, and the circles represent the continuum bins color-coded according to their frequency of appearance in all coudé spectra. The most frequent continuum windows are listed in Table 3.2. *Bottom panel:* Histogram of temperatures related to the wavelength bins within the windows of fits. A Gaussian is fitted to its median and robust standard deviation.

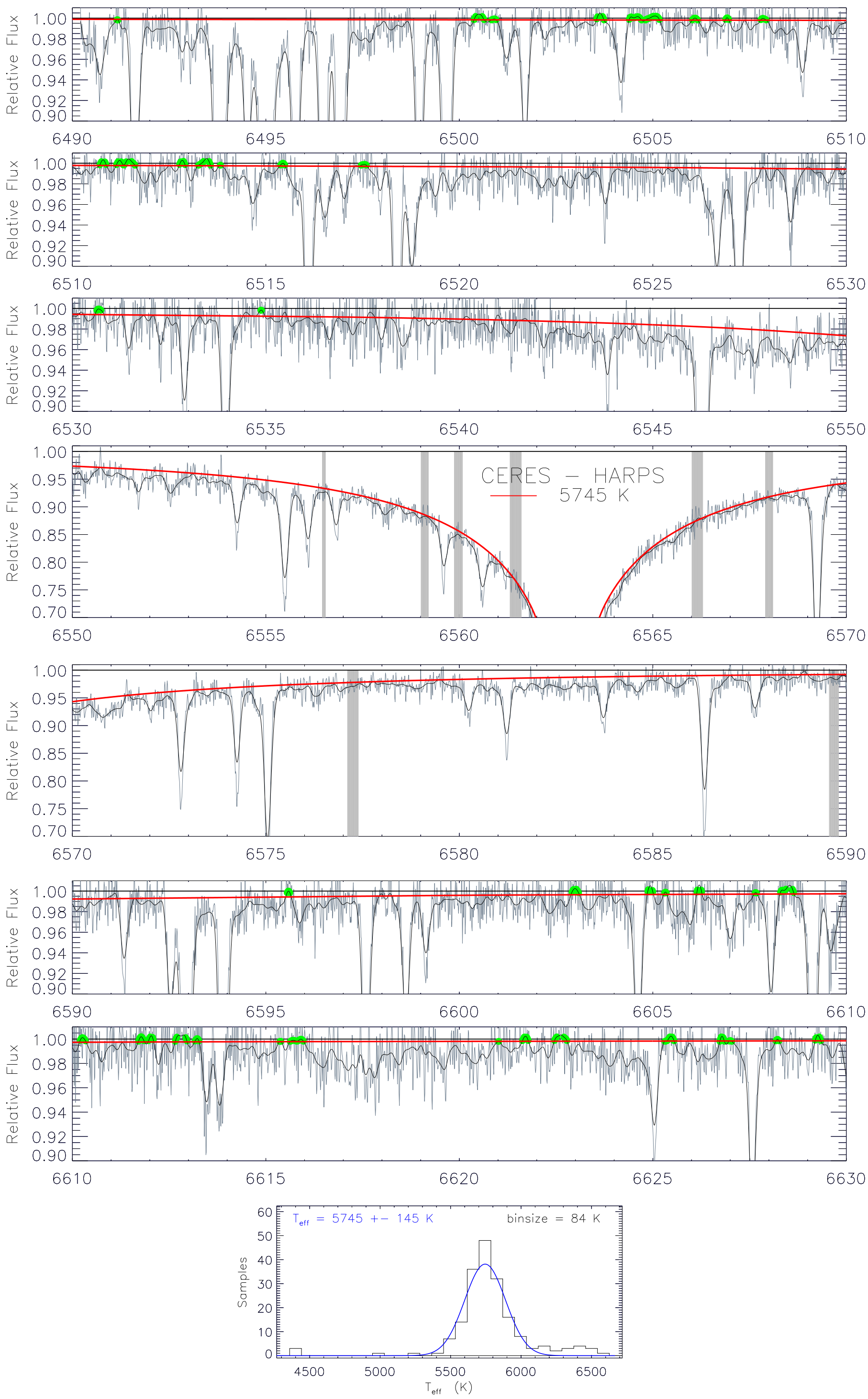

FIGURE 3.4: Similar to Fig. 3.3 but with a HARPS spectrum of one of the solar proxies from Table 2.2. The gray line represents the spectrum in its original resolution and the black line represents the spectrum degraded to the resolution of coudé. Continuum bins in the degraded spectrum are highlighted in green; notice that they mostly match those of Fig. 3.3.

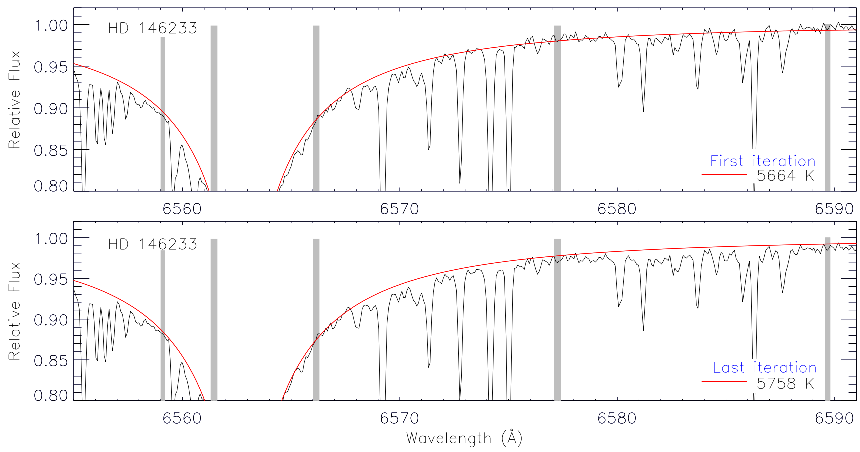

FIGURE 3.5: Results from the iterative Hα normalization-fitting of one of the two coudé spectra of 18Sco (HD 146233). The synthetic profile is represented by the red line, and the windows of fits (Table 3.1) are represented by the shades.

TABLE 3.2: **Continuum windows**
The table lists the most frequent continuum windows in the coudé sample.

Window	Wavelength range (Å)	Rate (%)
1	6500.25 – 6500.50	77
2	6504.50 – 6505.00	73
3	6619.70 – 6620.50	63
4	6625.60 – 6625.80	82
5	6626.50 – 6626.80	82

Notes: Third column lists the maximum rate of appearance of the wavelength bins inside the window according to the color-code in Fig. 3.3

3.1.3 Continuum fine-tune

The solar KPNO2005 atlas and the line catalogue of Moore, Minnaert, and Houtgast (1966) were used to select windows free from metallic lines to check the continuum during the normalization procedure. The availability of these windows diminishes progressively in cool metal-rich stars and because of the presence of telluric lines. Since the humidity at OPD/LNA often exceeded 90% during the observations, the contribution of many minute telluric lines is relevant in the coudé spectra. To fine-tune the continuum level, as part of the procedure described in Sect. 3.1.1, I separated telluric features from noise, fitting the observed spectra with synthetic telluric spectra from the PWV library of Moehler et al. (2014)[3], as shown in Fig. 3.6. This library is available at resolutions R = 300 000 and R = 60 000, for the air-masses 1.0, 1.5, 2.0, 2.5, and 3.0 and water content of 0.5, 1.0, 1.5, 2.5, 3.5, 5.0, 7.5, 10.0, and 20.0 mm. The fitting is performed degrading the resolution of the original PWV spectra to match those of the spectrograph used, and selecting the set of PWV spectra with the air-mass closest to that of the observation. Essentially the same results were found as with the *Molecfit* software package (described in detail in Sect. 3.2), but the latter produce more precise fittings which are more suitable for spectral correction.

[3] ftp://ftp.eso.org/pub/dfs/pipelines/skytools/telluric_libs

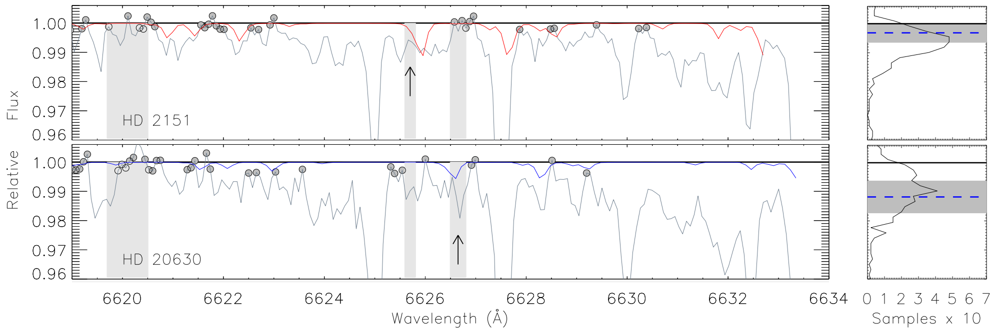

FIGURE 3.6: *Left panels:* fitting of two coudé spectra (gray line) with synthetic spectra of PWV with concentrations of 7.5 and 5 mm (red and blue lines, respectively) for the same air-mass. The circles are the continuum wavelength bins on $1 \pm \sigma$(noise). The shades represent 3 of the 5 continuum windows selected in Fig. 3.3 and listed in Table 3.2. The arrows point the windows contaminated by telluric features. *Right panels:* flux histograms of the spectra on the left panels with the same flux scale; only ranges not affected by Hα were taken. The black horizontal line points the continuum, the dashed line is the average flux of the 5 continuum windows in Table 3.2, and the shades are the spread.

I quantified the displacement of the continuum due to the presence of telluric features as follows. After normalizing all coudé spectra, continuum wavelength bins were identified in the solar spectrum of Fig. 3.3 applying σ-clipping. The fluxes of these wavelength bins were then checked in all other normalized coudé spectra, and none of them were found to remain as continuum in the whole sample. The colour code of the plot in the figure represents the percentage rate, the windows listed in Table 3.2 are the most frequent, and they are called henceforth "continuum windows". Figure 3.6 shows two cases where two of these windows are affected by the presence of minute telluric lines, and how much the average flux of the five mentioned windows decreases (see counts in the right panels of the figure). Analysing all of the sample spectra, I find that when the content of PWV is high, that is, over 5.0 mm, minute telluric features are almost omnipresent and displace the continuum flux by about 0.5%. In my experience, this issue may cause the stellar temperature to be underestimated by between 10 and 30 K. It is however difficult to provide a precise estimate because the flux displacement produced is often not homogeneous, but a distortion of the continuum shape. I stress that no correction is applied during this procedure, only a visual check. The correction is done later, and is explained in Sect. 3.2.

3.2 Telluric-corrected spectral library

The resolution and sampling of the coudé spectra allow a total of 26 to 27 wavelength bins inside the windows of fit, enough to perform the fitting procedure described in Sect 3.1.2. Several coudé spectra presented one or more windows of fits contaminated by telluric lines, therefore the wavelength bins inside were not useful for the fittings, which limits the robustness of the error estimates. A further reason that justifies the effort of applying telluric correction is to provide a library of observed Hα profiles for purposes of empirical spectra index–$T_{\rm eff}$ calibrations (e.g. Hanke et al., 2018), for studies of cromospheric activity (e.g. Pasquini and Pallavicini, 1991; Lyra

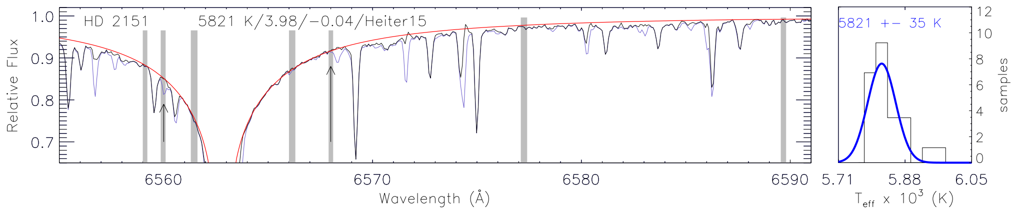

FIGURE 3.7: Telluric correction and profile fitting of the coudé spectrum of HD 2151. *Left panel:* Corrected and non corrected spectra are represented by the black and blue lines, respectively. The windows of fits are represented by the shades, and the arrows point those where the relative flux was perfectly recovered. The red line represent the synthetic profile fitted. *Right panel:* Histogram of temperatures related to the wavelength bins inside the windows of fits. The most probable temperature from the grids of Barklem et al. (2002) is shown in the top part of the plots, also log g and [Fe/H] values used for the fittings along with their source in the literature (Table 2.1).

and Porto de Mello, 2005), and for templates to perform measurements of stellar activity cycles (e.g. Flores et al., 2016).

Solène Ulmer-Moll from Instituto de Astrofísica e Ciências do Espaço, Universidade do Porto (CAUP), corrected the normalized coudé spectra with the *Molecfit* software package (Smette et al., 2015; Kausch et al., 2015). This software computes the transmission of the Earth's atmosphere at the time of the observations with the radiative transfer code LBLRTM (Clough et al., 2005), taking into account spectroscopic parameters from the HITRAN database (Rothman et al., 2013) and an atmospheric profile. The atmospheric transmission is fitted to the observed spectrum, and the telluric correction is done dividing the observed spectrum by the atmospheric transmission. The average equatorial atmospheric profile was used, which is *Molecfit*'s default profile. H_2O (the main absorber around Hα), O_2, and O_3 molecules were chosen to model. The line shape was fitted by a boxcar profile; as starting value for the boxcar FWHM, 0.36 times the slit width was used. The wavelength solution of the atmospheric transmission is adjusted with a first degree polynomial. First, *Molecfit* was ran automatically on all spectra, avoiding the center of the Hα line from 6560 to 6566 Å. If the residuals of this first telluric correction were larger than 2% of the continuum, the starting value of the water abundance was adapted and a second fit was subsequently performed. This telluric correction allowed to recover with precision the stellar flux inside the contaminated windows of fits in most cases. An example is shown in Fig 3.7 where the corrected and non-corrected spectra of HD 2151 are over-plotted. The telluric corrected and non-corrected normalized coudé spectra of the sample stars in Table 2.1 can be accessed at an online repository[4], and by CDS[5], or by contacting the author of this thesis.

3.3 Validation of the normalization method

An efficient method for removing the spectral blaze of echelle spectra is described in detail by Barklem et al. (2002). It is referred as 2D-normalization because it uses the two spacial dimensions of the CCD detector to determine the blaze of the orders that

[4] `https://github.com/RGiribaldi/Halpha-FGKstars`
[5] `http://cdsarc.u-strasbg.fr/viz-bin/qcat?J/A+A/624/A10`

contain the line-profile. Since this method was applied to validate the normalization method presented in Sect. 3.1, I reproduce the description in the following lines.

It is a prerequisite the profile to be well centered in one of the spectral orders, where the S/N is higher. It ensures that the normalization of the regions more sensitive to the temperature will be more precise, and also the fittings will be performed with the wavelength bins of best quality. Hence, an optimal use of the spectra is guaranteed, which translates into a more precise T_{eff} determination. To determine the shape of the normalization curves of the spectral orders that contain the profile, the contiguous orders are normalized first. The normalization curves of these orders contain information of the blaze shapes imprinted by the spectrograph. Hence, with normalization curves from several contiguous orders, those of the orders that contain the wide profile can be computed by interpolation. This procedure is represented in Fig. 3.8, where the Hβ line acquired by the MUSICOS instrument is normalized. In the figure, several normalization curves related to each spectral order (with no influence of the Balmer profile) are represented by the continuous lines. Notice that since the blaze shape is dependent on the two dimensions of the CCD detector, the normalization is performed on 1D-spectra in the extracted pixel domain, namely before to apply the wavelength calibration. The normalization curves relative to the three orders that contain the Hβ profile (discontinuous lines) are then obtained by polynomial interpolation of the continuous lines pixel-to-pixel. So that, the thick dashed line is the normalization curve of the spectral order of most interest, which contains the wavelength ranges of greatest temperature sensitivity. This procedure corrects smooth wide flux variations related to residual blaze features. Although it can be also applied without subtracting flat-field images, I recommend not to skip this step because it corrects pixel-to-pixel variations that are more important to reduce the noise in the windows of fits.

MUSICOS spectra were acquired for eight stars that have coudde spectra, including the Sun; these stars are indicated in Table 2.1. MUSICOS spectra were only normalized with the 2D-normalization as described above; their fits are presented in in the Appendix C. Accepted that the 2D-normalization applied to MUSICOS spectra do remove its blaze, for the stars listed in Table 2.1, the temperature values retrieved from coudé, HARPS, and MUSICOS spectra should be equivalent in ideal conditions: *i)* the normalization method of Sect. 3.1 does not lead to unreal/distorted profiles, and *ii)* HARPS spectra present no remaining blaze features – the truth of this preposition is proven in Sect. 6.1. Fig. 3.9 shows the temperatures derived with coudé and MUSICOS spectra compared vs. their atmospheric parameters from the literature listed in Table 2.1. No trend with respect to any atmospheric parameter is observed in the three plots, while the offset between the two sets of temperature is -1 K, and the scatter is 25 K. Solar spectra reflected in the Moon and Ganymede were also normalized with this method, from which I derive the average value 5745 ± 16 K (see comparative values in Table 2.2, the profile fits are shown in Fig. 4.6), perfectly consistent with the temperatures listed in Table 4.1 derived from coudé and HARPS spectra.

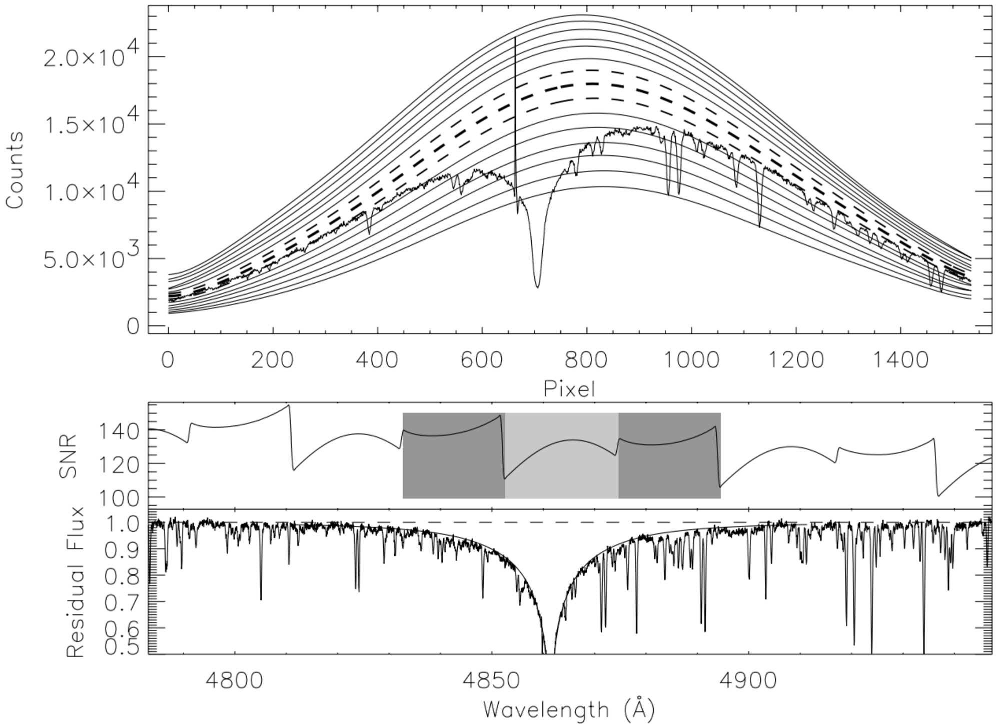

FIGURE 3.8: Adapted from Barklem et al. (2002). *Top panel:* 2D-normalization of the Hβ line in MUSICOS spectra. The continuous lines represent the normalization curves of the spectral orders contiguous to that containing the profile. The dashed lines are the normalization curves of the orders that contain the profile, obtained by interpolation of the continuous lines pixel-to-pixel. The thick dashed line is the normalization curve of the order containing the center of the profile. *Bottom panels:* show the final wavelength-calibrated profile fitted to a synthetic profile, aligned to the estimate of the S/N along the spectrum in the continuum. The composition of the two plots allow to visualize the position of each order. The upwardly convex regions are the regions where the orders overlap.

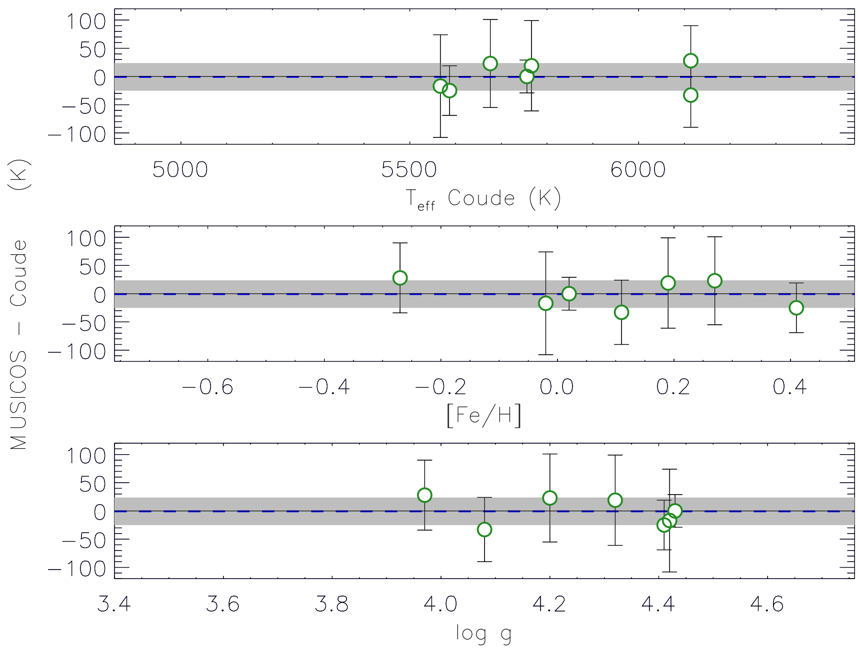

FIGURE 3.9: Temperature diagnostics from MUSICOS with respect to those of coudé vs. atmospheric parameters; related fits for both kind of spectra are presented in Appendices A and C. [Fe/H] and $\log g$ values from Table 2.1 were used here. The -1 K offset and 25 K scatter are represented by the dashed lines and the shades.

Chapter 4

Results: Accuracy of theoretical Hα profiles

In late-type stars, hydrogen lines of the Balmer series ($n = 2$) are extremely precise indicators of temperature; they are believed to form very close to LTE in the deepest photospheric layers. The well populated lowest levels of the atom produce considerable opacity at the center of the lines, and interactions with charged ions, electrons, and other hydrogen atoms results in extended wings in high-density atmospheres. hydrogen influences the main continuum opacity source, thus changes in its abundance are hardly reflected in the lines' strengths. Therefore, the strengths are much more weakly affected by gravity and metal abundances than perturbations to the temperature (Barklem et al., 2002; Barklem, 2007).

The line broadening due to the interaction between hydrogen atoms and charged particles is accounted by the Stark effect, the model of which was enhanced several times, for example: Griem (1962), Griem (1967), Edmonds, Schluter, and Wells (1967), Vidal, Cooper, and Smith (1970), Vidal, Cooper, and Smith (1973), Stehle (1994), and Stehlé and Hutcheon (1999). The line broadening due to the interaction between hydrogen atoms was also several times modeled (e.g. Cayrel and Traving, 1960; Ali and Griem, 1966; Barklem, Piskunov, and O'Mara, 2000; Allard et al., 2008), and the related temperature changes produced have been more notable. For example, according to the tests performed by Barklem et al. (2002), the difference in temperature provided by the theory developed by Barklem, Piskunov, and O'Mara (2000) with respect to that developed by Ali and Griem (1966) accounts $\sim$+100 K for $T_{\rm eff}$ and [Fe/H] around solar values. On the other hand, for instance, the temperature difference between the Stark effect models of Griem (1967) and Stehlé and Hutcheon (1999) accounts only 11 K for solar parameters. I show this change in terms of flux in Fig. 4.1: the difference between both profiles at 3-5 Å around the line core, where the sensitivity to temperature is maximum, reaches 0.1%, which is equivalent to 11 K. The profiles in this comparison were synthesised with the CO^{5}BOLD package as described in Sect. 4.2.

The analysis of Balmer lines attempts to establish a tool for determining $T_{\rm eff}$. It therefore demands a prior knowledge of the accuracy of the theoretical model atmospheres, that is, the ability of the models to reproduce the wings of the observed Balmer lines from actual physical parameters. The core of the line is out of this context because it is related to cromosphere flux. The primary reference object for testing the accuracy of models is naturally the Sun: it is still the only star for which we access its fundamental parameters accurately by direct measurements. The fundamental test with the Sun was performed for every model at least once, for example: Gehren (1981), Fuhrmann, Axer, and Gehren (1993), Fuhrmann, Axer, and Gehren (1994), Gardiner, Kupka, and Smalley (1999), Barklem et al. (2002), Ramírez et al. (2011), Ramírez et al. (2014), Pereira et al. (2013), Cornejo, Ramirez,

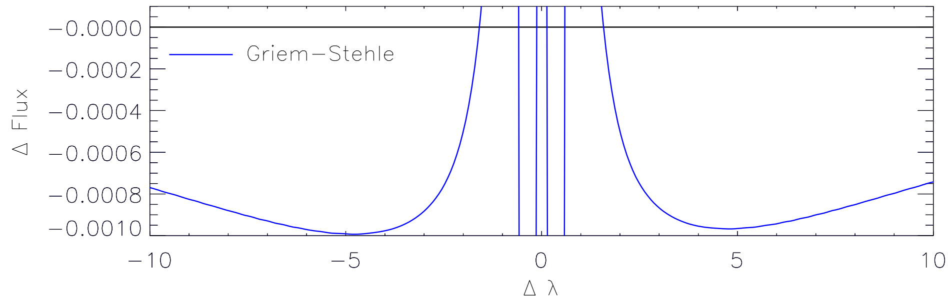

FIGURE 4.1: Difference between Hα profiles with Stark broadening models of Griem (1967) and Stehlé and Hutcheon (1999) for solar parameters. The impact broadening of hydrogen atoms of Allard et al. (2008) was used in the synthesis of both profiles.

and Barklem (2012), and Önehag, Gustafsson, and Korn (2014). In particular, the model of Barklem, Piskunov, and O'Mara (2000) and Barklem et al. (2002) which presents the "self broadening theory" of hydrogen atoms under 1D LTE atmosphere assumptions, showed through several tests a significant advance to the completeness of the physics of the Balmer lines formation. Most tests agreed with a 'hot' $T_{\rm eff}$ value of ∼5730 K, not far from the solar value 5772 K directly measured (Heiter et al., 2015; Prša et al., 2016), while some others retrieve a 'cool' value ∼5670 K. Furthermore, cool $T_{\rm eff}$ values are all associated to tests with KPNO atlases (Kurucz et al., 1984; Kurucz, 2005; Wallace et al., 2011), while hot values are associated to spectra taken by other spectrohraphs. Such discrepance exemplify the extent of the temperature variation when $T_{\rm eff}$ is retrieved from heterogeneous observed/normalized profiles. Given that extremely good quality with which KPNO solar spectra are acquired in terms of resolution, S/N, and sampling, such difference must come from artificial information introduced during the data processing, which is reflected in the final normalized profile and its associated temperature. An extensive discussion regarding to the causes of this problem have been presented in Chap. 3.

Later studies explored the improvement on the Balmer lines modeling by 3D atmosphere models. For example, Ludwig et al. (2009a) performed a differential analysis for Hα, Hβ, and Hγ lines, for various atmospheric parameters. They found that 3D models, in general, produce hotter temperatures, and that the difference between the temperatures of 3D models and 1D models increases as the metallicity decreases. Pereira et al. (2013) found similar results for the solar case when profiles from 3D models were compared with those from MARCS and PHOENIX 1D models (Gustafsson et al., 2008; Hauschildt, Allard, and Baron, 1999).

Changes in Balmer lines by non-LTE were explored separately. For example, Przybilla and Butler (2004), Barklem (2007), and Pereira et al. (2013) performed tests for the solar case. The first prototype model of Hα from non-LTE models (Przybilla and Butler, 2004) resulted slightly shallower than that from LTE. Pereira et al. (2013) found moderate effects: Hα wings up to ∼1.008 times shallower (∼+0.0064 in normalized flux, which translates in ∼70 K in terms of temperature). Notice that shallower synthetic profiles imply hotter temperature diagnostics because a higher temperature input is required to match the same relative flux.

Only two works presented results of simultaneous 3D and non-LTE implementation on Balmer line modeling. In the first, done by Pereira et al. (2013), only the solar case was evaluated and it was found that the Hα profile from 3D non-LTE models is ∼1.004 times shallower than that from 3D LTE, thus it produces diagnostics hotter by ∼35 K; see blue line in Fig. 4.2. According to the results presented in their Table 2,

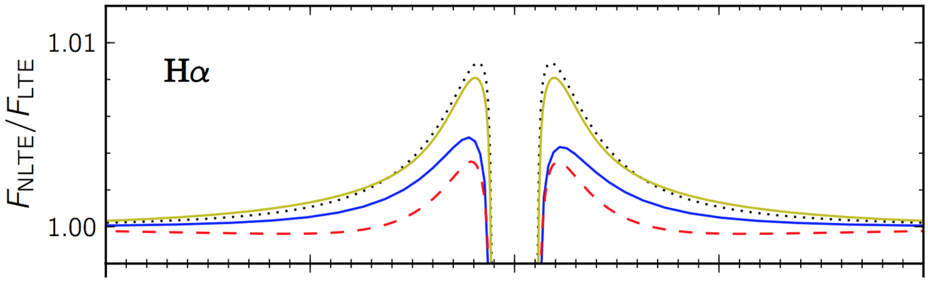

FIGURE 4.2: Adapted from Pereira et al. (2013, Fig. 7). Flux rates between synthetic Hα lines from non-LTE and LTE. The blue line was synthesised with 3D models. The other lines with 1D models: Holweger and Mueller (1974) (red discontinuous line), MARCS (yellow continuous line), and PHOENIX (black dotted line). Marks in the horizontal axis display 1 Å spacing.

they obtained from 3D LTE models a $T_{\rm eff}$ value 50 K cooler than the direct solar $T_{\rm eff}$, so 3D non-LTE results in a diagnostic of −15 K with respect to the direct solar $T_{\rm eff}$. In Sect. 4.1.1, I present a correction of this estimate, the error of which was caused by fitting an imperfectly normalized template. The work performed by Amarsi et al. (2018) is the most extensive in terms of theoretical development and observational test so far. The non-LTE excitation and ionization balance were solved together for hydrogen species H I and H II, and only H^- was treated in LTE conditions, considering that its abundance is small enough to not affect those of H I and H II. Collisional excitation and ionization between neutral hydrogen (in the $n = 1$ ground state), electrons, and hydrogen ions H^+ and H^- was modeled following Barklem (2007). From the theoretical recipe, a grid of Balmer profiles was synthesized with parameters: $4000 \leq T_{\rm eff} \leq 6750$ K with steps of 50 K, $-4.0 \leq$ [Fe/H] ≤ 0.5 with steps of 0.1 dex, and $1.5 \leq \log g \leq 5.0$ dex with steps of 0.1 dex. Hα, Hβ, and Hγ lines of the template stars Sun, Procyon (HD 61241), HD 103095, HD 84937, HD 140283, and HD 122563, with interferometric $T_{\rm eff}$ (the technique is described in Sect. 4.1.2), were fitted with the grid of synthetic profiles. They found that, from Hα lines, $T_{\rm eff}$ of all stars can be reproduced with high precision, but for the Sun; see Fig. 4.3 where the only temperature values not matching are those of the Sun. Similar to the solar case of Pereira et al. (2013), this discrepancy is caused by fitting an imperfect normalized template; I present in Sect. 4.1.1 an estimate of the correction. It deserves to be highlighted that even the most metal-poor stars, for which discrepancies between diagnostics from different techniques are usually large, present perfect agreements.

The discussion above shows that most works used the Sun-only as the unique reference star with accurate atmospheric parameters. However, radius interferometric measurements of nearby dwarfs now allow semi-direct $T_{\rm eff}$ measurements with accuracy to better than 100 K, thus reasonably good comparisons with standards with non-solar atmospheric parameters can be performed, as done by Cayrel et al. (2011) and Amarsi et al. (2018). The catalog presented by Heiter et al. (2015) is one of the most accurate sources of atmospheric parameters of reference stars or "benchmark stars": it provides $T_{\rm eff}$ and $\log g$ from the least model-dependent technique, and [Fe/H] from the most sophisticated physics. Its stars also evenly cover the parameter space, and many of them are observable in the southern hemisphere, which favored the development of this project using the instruments in the OPD/LNA.

Given the extreme good quality of normalized spectra achieved with the method described in Chap. 3, I determined with them the accuracy of theoretical models of

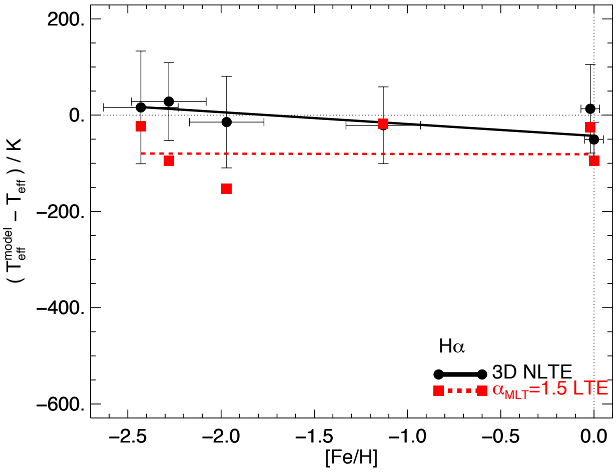

FIGURE 4.3: Adapted from Amarsi et al. (2018, Fig. 14). In black, difference between T_{eff} from Hα profiles and interferometric T_{eff} vs. [Fe/H] values, for 3D non-LTE in black symbols, and for 1D LTE in red symbols. The two stars with solar metallicity are Procyon and the Sun; the latter is the only star with discrepant temperatures. The discontinuous line is the linear regression of the red points, the temperatures of which were determined using 1D models; these results are out of the discussion of this work.

the Hα line. The accuracy of Hα from 1D LTE atmosphere models (Barklem et al., 2002) is determined in Sect. 4.1. The accuracy of Hα from other 1D LTE models for solar parameters are also determined in the same section by performing differential analysis with the same spectra. The accuracy of Hα lines enhanced by 3D modeling is determined in Sect. 4.2. Such models are those of Ludwig et al. (2009b, in LTE conditions), especially synthesized for this work with a wide parameter space coverage, and those of Pereira et al. (2013), and Amarsi et al. (2018), both in LTE/non-LTE conditions for the solar case only. The accuracy of temperature scales from different Hα models is reviewed in Sect. 4.3. These scales are those that not modeled the solar profile only: Barklem et al. (2002), Allard et al. (2008), and Amarsi et al. (2018). Related tests are performed by indirect comparisons with several stars.

4.1 Accuracy of 1D + LTE atmosphere models

For testing the accuracy of Hα lines synthesized from 1D LTE atmosphere models I used the grids of Barklem et al. (2002), which, as mentioned above, used the self broadening theory of hydrogen atoms developed by Barklem, Piskunov, and O'Mara (2000). For practical purposes these grids will be called Hα from 1D LTE models and the temperatures derived using them will be represented by $T_{\mathrm{eff}}^{\mathrm{H}\alpha}$(1D LTE) henceforth. I highlight however that the diagnostic of accuracy presented in this section is not only related to the influence of 1D LTE models, but it depends on several factors such as the version of atmosphere models, completeness and/or physical approach of stark broadening and self broadening, and the choice of mixing-length value α_{MLT}. I refer the reader to Table 4.1 and Fig. 4.4 to follow the differences discussed below. For example, Barklem et al. (2002) and Önehag, Gustafsson, and Korn (2014) derived different temperatures from the same theoretical recipes of stark broadening and self broadening and from the same solar spectrum (KPNO1994).

The former synthesized profiles from the MARCS models of Asplund et al. (1997), while the later used the version of Gustafsson et al. (2008) which, although irrelevant for the solar case, uses a different value of α_{MLT} within its updates; corresponding tests are commented below. Another example is given by the difference between the results of Cayrel et al. (2011) and Pereira et al. (2013). Both derived temperatures from the same solar template (KPNO2005) fitted to synthetic profiles in 1D LTE conditions (the latter also derived temperatures from 3D and non-LTE models), but the atmosphere models and the self broadening approximations were different. Namely, the profiles of Cayrel et al. (2011) were synthesised by ATLAS9, BALMER9 codes (Castelli and Kurucz, 2004) and an enhanced recipe of the self broadening (Allard et al., 2008), that includes more transitions than that of Barklem, Piskunov, and O'Mara (2000). On the other hand, the profiles of Pereira et al. (2013) were synthesised with MARCS atmosphere models (Gustafsson et al., 2008) and the self broadening recipe of Barklem et al. (2002).

In 1D atmosphere models, the convective energy transport is described by the mixing-length approximation (Böhm-Vitense, 1958), which is characterised by the dimensionless parameter α_{MLT}. It, together with the convective structure parameter (y_{MLT}), account for the contribution of convection to the line broadening when the atmosphere is assumed static. Balmer lines in late-type stars are formed in very deep layers of the photosphere (but not equally deep), where the structure is significantly affected by convection, and therefore α_{MLT} and y_{MLT} are of strong impact (Fuhrmann, Axer, and Gehren, 1993). These two parameters are highly degenerated and, for Hα, combinations of them (favoring a high value for one parameter and a low value for the other parameter) have shown to produce profiles equally similar to observed , but always associated to T_{eff} lower than actual (Barklem et al., 2002). The sensitivity of T_{eff} to α_{MLT} varies according to which Balmer line is analysed and to the atmospheric parameters of the star. For example, for $y_{\mathrm{MLT}} \approx 0$ and solar metallicity, α_{MLT} changes do not affect T_{eff}, and for low metallicity values only minor T_{eff} changes of the order of tens of Kelvins are produced (Barklem et al., 2002; Ludwig et al., 2009a; Amarsi et al., 2018). On the other hand, for other lines of the series, T_{eff} changes easily surpass 100 K for any metallicity (Amarsi et al., 2018, Table 4).

4.1.1 The zero point

I used the six blaze-free coudé solar spectra listed in Table 2.2 to determine the accuracy of Hα profiles from 1D LTE model atmospheres of Barklem et al. (2002) for solar parameters. Their fits are shown in Fig. 4.5, and the fits of the solar profiles acquired in MUSICOS spectra are shown in Fig. 4.6. The average value from coudé-only spectra is 5744 ± 7 K, and from MUSICOS-only spectra is 5745 ± 16 K; see Sect. 3.3 for information about the purpose of the use of MUSICOS spectra in this work. These results are compatible with those from solar profiles in HARPS spectra in Sect. 6.1, thus totally consistent temperatures are retrievable from the three kind of spectra. It allows to determine the zero-point of the model by averaging the inferred temperature values from the three sets of solar spectra analysed in this work, these are 57 spectra of very good quality. It results in an offset of -28 ± 1 K with respect to the 5772 K (Prša et al., 2016; Heiter et al., 2015) measured by the fundamental relation.

This zero point supports the temperature values initially determined by Barklem et al. (2002) with their MUSICOS spectrum and the KPNO1984 atlas, and those found later by Ramírez et al. (2011), Cornejo, Ramirez, and Barklem (2012), and Ramírez et al. (2014) with MIKE spectra. On the other hand, it disagrees with any value

TABLE 4.1: **Effective temperature values from solar Hα lines fitted with different models.** Third column lists T_{eff} values from 1D model atmospheres (top table) and from 3D model atmospheres (bottom table). Forth column lists the correction factor related to the normalization errors of the corresponding KPNO atlas in second column. The last column lists the corrected values. Fits of the spectra are shown in Fig. 4.7.

Author	**spectrum**	T_{eff} **(K)**	ΔT_{eff} **(K)**	T_{eff} correct
	1D models			
Barklem et al. (2002)	KPNO1984	5733	—	5733
Barklem et al. (2002)	MUSICOS	5743	—	5743
Ramírez et al. (2011)	MIKE	5732 ± 32	—	5732
Cayrel et al. (2011)	KPNO2005	5678 ± 5	+37	5715
Cornejo, Ramirez, and Barklem (2012)	MIKE	5752 ± 16	—	5752
Ramírez et al. (2014)	MIKE	5731 ± 21	—	5731
Pereira et al. (2013)	KPNO2005	5674	+37	5711
Önehag, Gustafsson, and Korn (2014)	KPNO1984	5670	—	5670
Amarsi et al. (2018)	KPNO2011	5681 ± 40	+49	5730
This work	coudé	5744 ± 7	—	5744
This work	HARPS	5744 ± 10	—	5744
This work	MUSICOS	5745 ± 16	—	5745
This work	KPNO2005	5707 ± 6	—	—
This work	KPNO2011	5695 ± 18	—	—
	3D models			
Pereira et al. (2013)	KPNO2005	5722	+37	5759
Pereira et al. (2013)[a]	KPNO2005	5757	+37	5794
Amarsi et al. (2018)[a]	KPNO2011	5721 ± 40	+49	5770

[a] Also non-LTE conditions were assumed in this model.

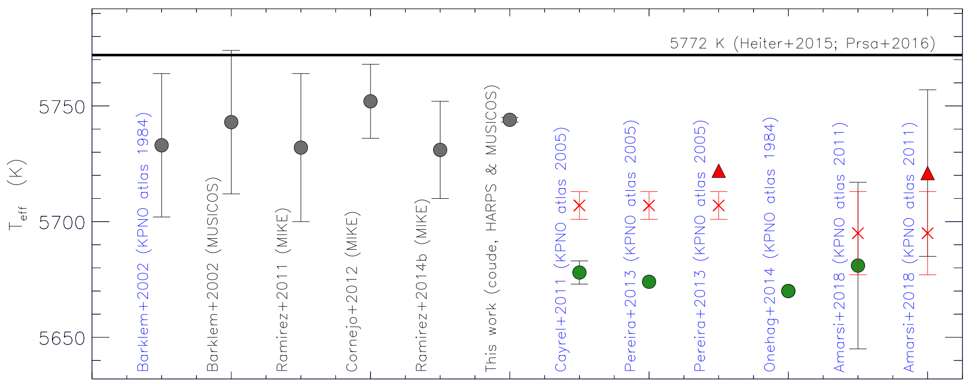

FIGURE 4.4: Graphic representation of solar T_{eff} values in Table 4.1. The horizontal line represents the solar T_{eff} measured by the Stefan-Boltzmann equation. Works that used theoretical models based on 1D atmosphere models are represented by circles, and those that used 3D models by triangles. Gray circles represent works that used the theoretical model of Barklem et al. (2002), and green circles represent a different/enhanced recipe. Works that used KPNO solar atlases are labeled in blue. For them, for comparison purposes, my measurements from corresponding KPNO spectra are included as red crosses in the same line.

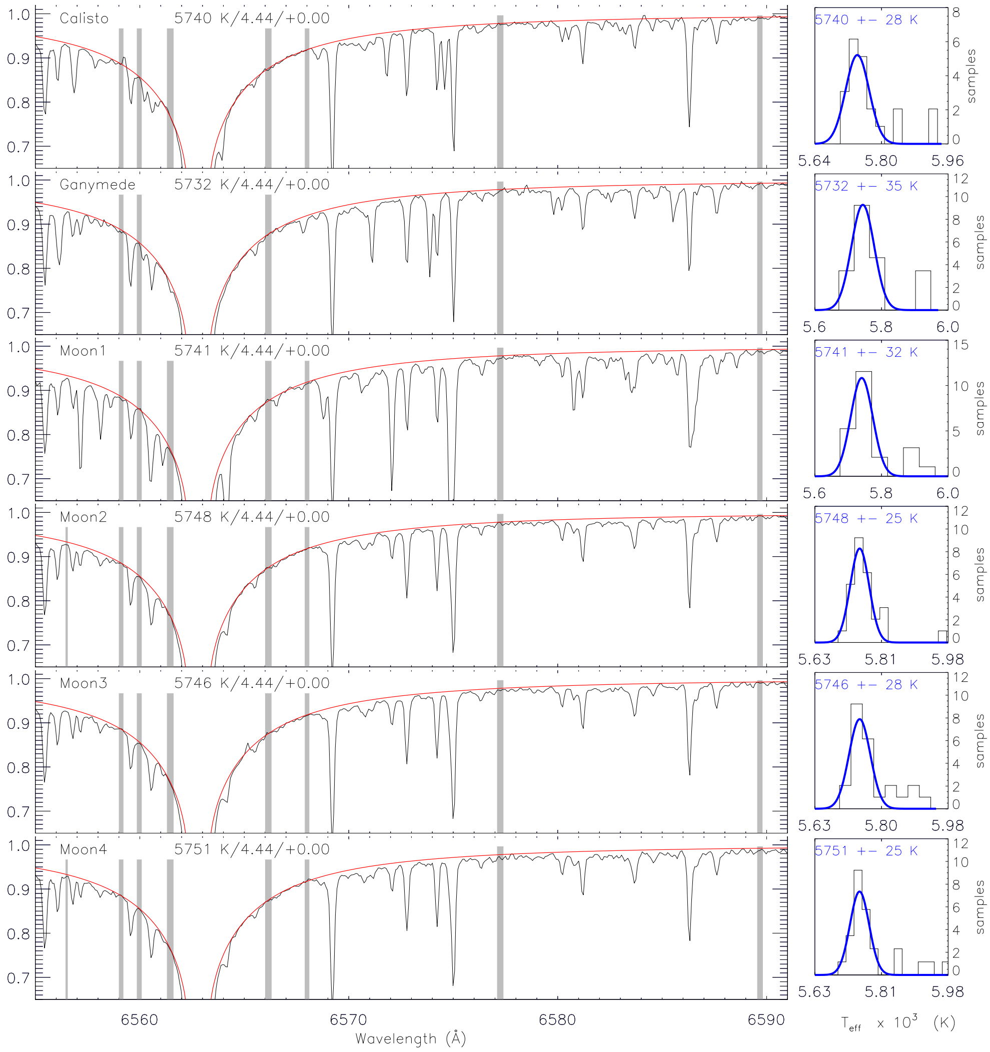

FIGURE 4.5: Profile fits of coudé solar spectra.

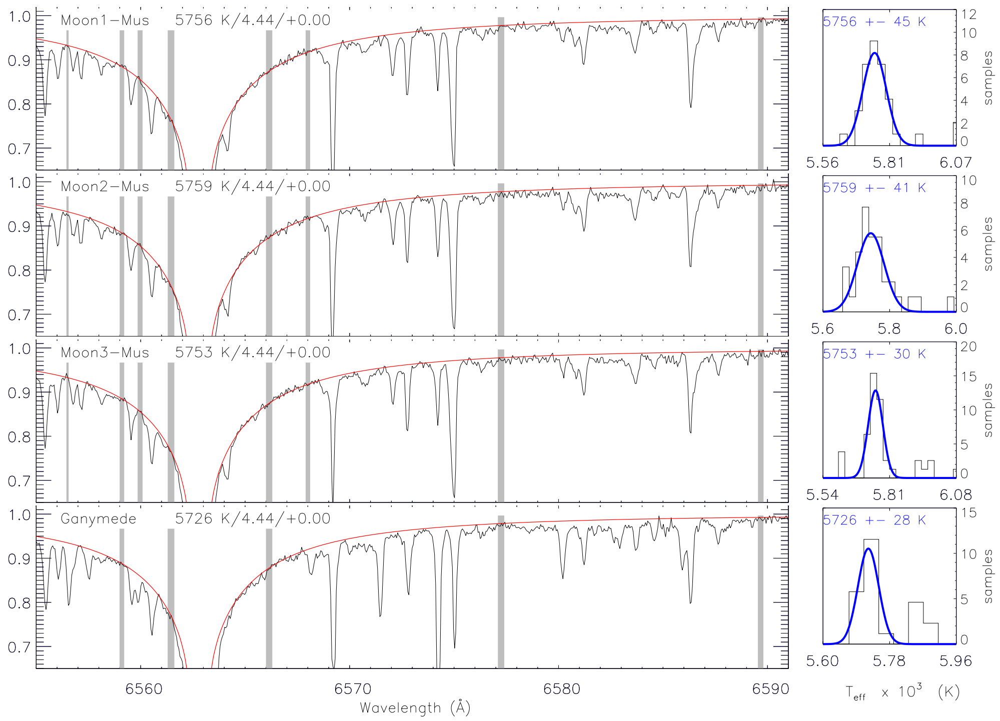

FIGURE 4.6: Profile fits of MUSICOS solar spectra.

derived from KPNO2005 and KPNO2011 solar atlases, including my own determinations (from fitting-only without further normalization). Table 4.1 and Fig. 4.4 present a compilation of $T_{\rm eff}$ values derived from solar spectra, including KPNO atlases, by various authors in the literature and myself in this work. $T_{\rm eff}$ values derived by 3D models in LTE, and non-LTE conditions are discussed later in Sect. 4.3.

Hα profiles in KPNO2005 (Kurucz, 2005), and KPNO2011 (Wallace et al., 2011) atlases are the best cases to quantify the impact of normalization errors on $T_{\rm eff}$. I derived $T_{\rm eff}^{\rm H\alpha}$(1D LTE) from both atlases by fitting by fitting the synthetic with observed profiles without further normalization. Their fits are presented in Figs. 4.7, 4.8, and 4.9 for different spectral regions, to which I refer the reader for illustrating the discussion below. The interior regions of the two observed profiles fit very well with the synthetic ones, while the external regions do not, which is an evidence of normalization errors. Namely, it is natural that line profiles are well fitted in the interior regions because there the sensitivity to the temperature is maximum; the fits will always look good if there is no a gross normalization error. Thus, when the profile is a little distorted, incompatibilities with synthetic profiles will more likely appear in the outermost regions. An observed profile showing relative defect/excess of flux in the transition regions implies that its extension was overestimated/underestimated by the normalization process, and it could be due to several factors: insufficient continuum wavelength bins for interpolation, the presence of minute telluric lines diverting the normalization curve to lower flux counts, excess of white noise in the continuum windows that allows too many degrees of freedom for interpolating, or a combination of all the above. Since I used the same theoretical model to infer the $T_{\rm eff}^{\rm H\alpha}$(1D LTE) associated with coudé/HARPS/MUSICOS spectra, the estimate of the temperature biases induced by the normalization errors in KPNO atlases are differential. From KPNO2005 and KPNO2011 atlases I obtain 37 K and 49 K cooler values than obtained with coudé/HARPS/MUSICOS (average value of 5744 ± 1 K), respectively, and they are used to correct the zero point values for the models listed

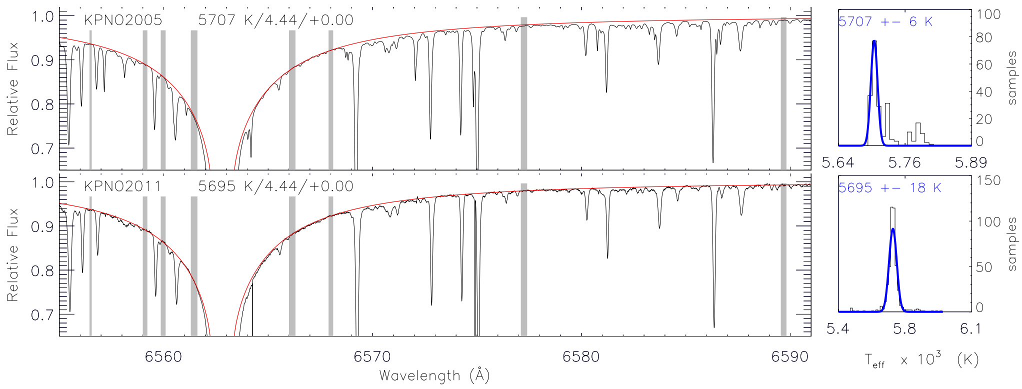

FIGURE 4.7: Profile fits of KPNO2005 (top), and KPNO2011 (bottom) spectra.

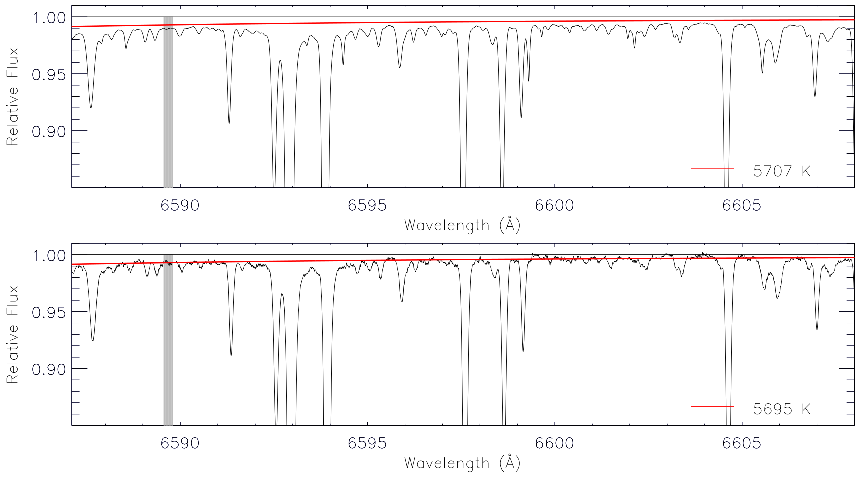

FIGURE 4.8: From the top to the bottom, transition regions at the red wings in fitted KPNO2005 (top), and KPNO2011 (bottom) spectra.

in Table 4.1. These values are similar although the normalization of the former spectra seem to have been more careful than that of the latter; see for example in Fig. 4.9 clear normalization errors in KPNO2011. Therefore, these values are the corrections for the temperature determinations from both atlases.

The top part of Table 4.1 list three works that determined temperatures from Hα 1D LTE models for the Sun using KPNO atlases. These models are different between them and to that used in this work: they use either an enhanced model of hydrogen atom collisions (Cayrel et al., 2011) or an updated model atmosphere (Pereira et al., 2013; Amarsi et al., 2018). Nevertheless, even with the temperature corrections, applied none of them recover the solar temperature.

4.1.2 Accuracy for non-solar parameters

Atmospheric parameters $T_{\rm eff}$, $\log g$, and [Fe/H] of 34 stars were published by Heiter et al. (2015) and Jofré et al. (2015), to be used as benchmark stars for calibrating and validating Gaia data sets. They are known as the "Gaia benchmark stars" and their $T_{\rm eff}$ are based on the fundamental relation $L = 4\pi R^2 \sigma T_{\rm eff}^4$, where L is the luminosity, R is the stellar radius, and σ is the Stefan-Boltzmann constant. In it, the bolometric flux $F_{\rm bol}$[1] and the limb-darkened angular diameter $\theta_{\rm LD}$ replace L and R, to obtain

[1]The term "bolometric flux" refers to the total radiative flux from the star received at the Earth.

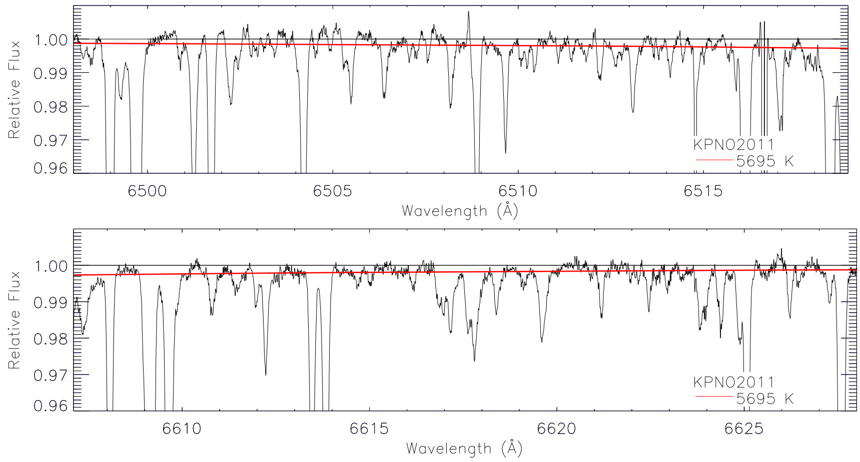

FIGURE 4.9: For the KPNO2011 atlas, spectral regions that contain the continuum windows 1 and 2 (top), and 3, 4 and 5 (bottom) listed in Table 3.2.

$T_{\rm eff}$ by the equation rearranged:

$$T_{\rm eff} = \left(\frac{F_{\rm bol}}{\sigma}\right)^{0.25} (0.5\theta_{\rm LD})^{-0.5} \tag{4.1}$$

I acquired coudé spectra of nine Gaia benchmarks to determine the accuracy of 1D non-LTE models at non-solar parameters assuming the $T_{\rm eff}$ scale of these stars as the standard. They are: β Hyi, τ Cet, ϵ For, δ Eri, β Vir, η Boo, α Cen A, 18 Sco, and μ Ara. Their $\theta_{\rm LD}$ measurements, compiled by Heiter et al. (2015) and listed in their Table 4, were measured by interferometry (hence, their associated temperatures are referred as interferometric $T_{\rm eff}$) and are the most recent with the lowest formal uncertainty. They include limb-darkening effects, estimated by coefficients from Claret (2000) or Claret, Diaz-Cordoves, and Gimenez (1995), both based in 1D LTE atmosphere models. Only two stars of the above list, ϵ For and μ Ara, have no direct $\theta_{\rm LD}$ measurements, but estimated from the surface-brightness relations of Kervella et al. (2004) based in $B-K$ and $V-K$ colors (Eq. 22 and 23 in the paper). Hence, the authors do not recommend the use of their interferometric $T_{\rm eff}$ for calibration purposes. I show in the analysis below that the interferometric $T_{\rm eff}$ of μ Ara totally disagrees with the typical behavior of $T_{\rm eff}$ of the other stars with respect to $T_{\rm eff}^{\rm H\alpha}$(1D LTE); see Fig. 4.11.

In this work, the test of the accuracy of Hα profiles as a tool to derive effective temperature scale, and its comparison with the other scales analyzed in the next chapter, is fundamental. Namely, it is based on $T_{\rm eff}$ measured by the fundamental relation, the closest approximation of which is the interferometric $T_{\rm eff}$. Two main options for this task were available: the Gaia Benchmarks of the catalog of Heiter et al. (2015), which is a compilation of interferometric $T_{\rm eff}$ from several sources in the literature, and the catalogs of Boyajian et al. (2012a) and Boyajian et al. (2012b), the interferometric measurements of which are homogeneous. Although the former catalogs seem, in principle, a better option, Casagrande et al. (2014) showed that they are biased in their zero point (i.e $T_{\rm eff}$ values for solar $\theta_{\rm LD}$ and $F_{\rm bol}$) to lower $T_{\rm eff}$ values that can reach -400 K in the worse cases; see Fig. 4.10. Individual examples are the $T_{\rm eff}$ values inferred for the solar twin 18 Sco (Porto de Mello and da Silva, 1997):

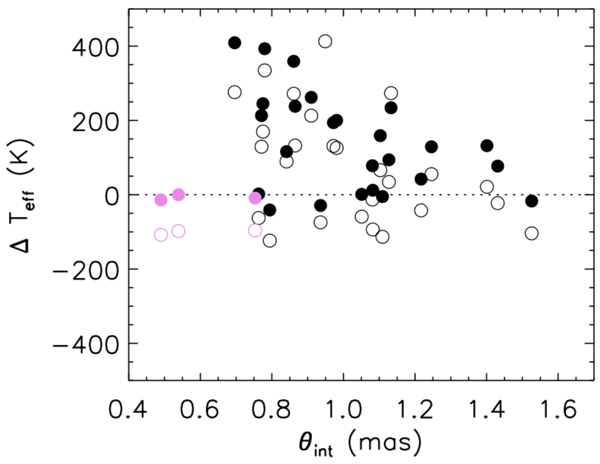

FIGURE 4.10: Adapted from Casagrande et al. (2014, Fig. 4). $T_{\rm eff}$ of Casagrande et al. (2011, filled circles) and Holmberg, Nordström, and Andersen (2009, open circles) with respect to interferometric measurements of Boyajian et al. (2012a, black circles) and White et al. (2013, purple circles).

Boyajian et al. (2012a) obtain $T_{\rm eff} = 5433 \pm 69$ K from $\theta_{\rm LD} = 0.780 \pm 0.017$ mas (implying $R = 1.166 \pm 0.026\ R_\odot$), while Bazot et al. (2011), confirming the solar radius and temperature of this star, obtain $T_{\rm eff} = 5810$ K from $\theta_{\rm LD} = 0.676 \pm 0.0062$ mas (implying $R = 1.010 \pm 0.009 R_\odot$). This difference was explained by White et al. (2013), who found underestimated errors and systematic offsets in the sample of Boyajian et al. (2012a). They performed measurements with CHARA, the same instrument as Boyajian et al. (2012a), but with a different beam combiner: PAVO (Ireland et al., 2008) instead of Classic, which allows to probe the visibility curve at higher spatial frequencies (White et al., 2013, Fig. 3), and thus to derive robust $\theta_{\rm LD}$.

Limb-darkening correction is the source that introduces the model dependence (although marginal) in interferometric $T_{\rm eff}$, and 1D models corrections impact angular diameters by reducing them by 0.5–1.0% (i.e. increase $T_{\rm eff}$ by 15–30 K) when compared with those from 3D models, depending on the stellar parameters and wavelength of observation (Allende Prieto et al., 2002; Aufdenberg, Ludwig, and Kervella, 2005; Bigot et al., 2006; Chiavassa et al., 2010; Chiavassa et al., 2012). These offsets were not accounted in the absolute frame $T_{\rm eff}$–[Fe/H]–log g of this work. However, these references are relevant to consider in order to assert the consistency with the IRFM $T_{\rm eff}$ scale in Sect. 5.1.

The plot in Fig. 4.11 shows the comparison of $T_{\rm eff}^{\rm H\alpha}$(1D LTE) with interferometric $T_{\rm eff}$ for the above mentioned stars. I find a constant offset of 30 K between the two scales (the Hα scale having cooler $T_{\rm eff}$), that is broadly equal to the -28 K zero point found with the solar spectra in Sect. 4.1.1. No temperature dependence is found with log g but a trend is present with metallicity according to the equation in the right plot in Fig. 4.11; the temperature values of μ Ara appear highly discrepant and were ignored to compute the trend. The trend shows that Hα from 1D LTE models underestimates $T_{\rm eff}$ progressively for metal-poorer stars; at the metal-poor extreme of the sample, -0.6 dex, the underestimation is larger than 100 K. The precision of the zero point given by the trend is high considering the average errors of the temperatures from the two scales (22 K for Hα and 43 K for interferometry), but the zero point obtained with solar spectra in the previous section is much more precise: $T_{\rm eff} = T_{\rm eff}^{\rm H\alpha}$(1D LTE) + 28($\pm$1) K. Therefore, the trend in the plot is improved in its zero

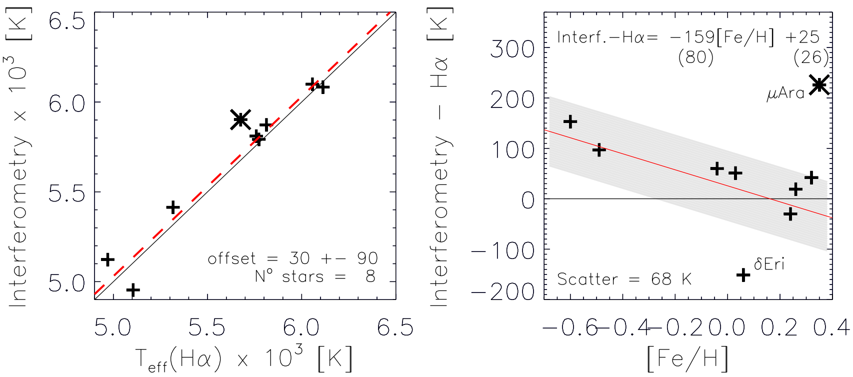

FIGURE 4.11: *Left panel:* Comparison of $T_{\rm eff}^{\rm H\alpha}$(1D LTE) with interferometric $T_{\rm eff}$ of the Gaia Benchmark stars (Heiter et al., 2015). The red dashed line represent the offset. *Right panel:* Relative temperatures in function of [Fe/H]. The red line and the shade represent the trend and its scatter. The corresponding function and the errors of its coefficients (in brackets) are shown in the plot. The cross symbol in both plots point μ Ara (HD 160691) considered as outlier.

point to the following equation:

$$T_{\rm eff} = T_{\rm eff}^{\rm H\alpha} - 159(\pm 80)[{\rm Fe/H}] + 28(\pm 1)\ {\rm K} \quad (68\ {\rm K\ scatter}) \tag{4.2}$$

I list in Table 4.2 the best $T_{\rm eff}$ estimates for the stars of the Hα-test sample (Table 2.1), and their respective uncertainties. These are the weighted averages of $T_{\rm eff}^{\rm H\alpha}$(1D LTE) values corrected by Eq. 4.2, derived from all coudé, HARPS, and MUSICOS spectra when available. The tests performed in Sects. 3.3 and 6.1 show that equivalent temperatures can be retrieved from the three kind of spectra, thus allow averaging the values. The $T_{\rm eff}$ values in the table are not exactly, but are practically the same as those compared in the right panels of Figs. 5.2 and 5.4, which correspond to coudé spectra only.

4.2 Hα profiles from 3D models

I showed in the previous section that the comparison of Hα with the accurate interferometric $T_{\rm eff}$ scale is quite robust, showing only a dependence with respect to metallicity. In order to investigate such a trend, I analysed Hα profiles from 3D models, specially produced for this work by Hans-G Ludwig from Zentrum für Astronomie der Universität Heidelberg. With this analysis I quantify the impact of the 1D approximation.

Eight line profiles were produced from the CIFIST grid of CO^{5}BOLD models (Ludwig et al., 2009b; Freytag et al., 2012), calculated using the spectral synthesis code Linfor3D (version 6.2.2) in LTE approximation. These profiles were synthesized following a recipe as close as possible to that of Barklem et al. (2002) in order to perform a differential analysis. Thus, the expected improvement of the temperature discrepancy implicit in Eq. 4.2, can be attributed to the 3D modeling itself. The self broadening model (Barklem, Piskunov, and O'Mara, 2000) and the stark broadening model of Griem (1967) were used for the synthesis. The former is not the same stark broadening model used by Barklem et al. (2002), however it does not significantly

TABLE 4.2: $T_{\rm eff}$ of the sample stars. Column 4 lists the [Fe/H] values used to derive $T_{\rm eff}^{\rm H\alpha}$(1D LTE), and their sources are shown in last column according to the codification: (1) Sousa et al. (2008), (2) Ghezzi et al. (2010b), (3) Tsantaki et al. (2013), (4) Ramírez, Allende Prieto, and Lambert (2013), (5) Bensby, Feltzing, and Oey (2014), (6) Ramírez, Meléndez, and Asplund (2014), (7) Ramírez et al. (2014), (8) Maldonado et al. (2015), (9) Heiter et al. (2015). Column 5 lists the weighted mean of the temperatures derived with coudé, HARPS, and MUSICOS spectra. Column 6 lists $T_{\rm eff}$ corrected from the Hα diagnostics by Eq. 4.2. The errors presented are internal and are associated to the dispersion of the fit. These are the best estimates for $T_{\rm eff}^{\rm H\alpha}$(1D LTE), and $T_{\rm eff}$. Fits of coudé, HARPS, and MUSICOS normalized spectra are displayed in Appendix A, B, and C, respectively.

Name	HD	HIP	[Fe/H]	$T_{\rm eff}^{\rm H\alpha}$(1D LTE) [K]	best $T_{\rm eff}$ [K]	ctlg
SUN			+0.03	5744	5772 ± 1	9
ζ Tuc	1581	1599	−0.22	5866	5930 ± 17	4
β Hyi	2151	2021	−0.04	5813	5848 ± 20	9
	3823	3170	−0.34	5947	6030 ± 18	8
τ Cet	10700	8102	−0.49	5311	5417 ± 22	9
ϵ For	18907	14086	−0.60	4984	5108 ± 48	9
α For	20010	14879	−0.30	6112	6188 ± 23	4
κ Cet	20630	15457	0.00	5675	5704 ± 22	4
10 Tau	22484	16852	−0.09	5947	5990 ± 25	4
δ Eri	23249	17378	+0.06	5090	5110 ± 12	9
40 Eri	26965	19849	−0.28	5109	5182 ± 33	4
	100623	56452	−0.37	5101	5188 ± 17	4
β Vir	102870	57757	+0.24	6096	6087 ± 18	9
	114174	64150	+0.05	5703	5724 ± 32	4
59 Vir	115383	64792	+0.11	5975	5987 ± 23	4
61 Vir	115617	64924	−0.02	5557	5589 ± 18	4
η Boo	121370	67927	+0.32	6042	6020 ± 25	9
	126053	70319	−0.36	5663	5749 ± 58	4
α Cen A	128620	71683	+0.26	5765	5753 ± 12	9
ψ Ser	140538	77052	+0.12	5653	5663 ± 21	8
	144585	78955	+0.29	5816	5799 ± 27	6
18 Sco	146233	79672	+0.06	5760	5780 ± 20	9
	147513	80337	+0.03	5805	5829 ± 24	4
ζ TrA	147584	80686	−0.08	6012	6054 ± 17	4
12 Oph	149661	81300	+0.01	5209	5236 ± 34	4
	150177	81580	−0.66	6056	6189 ± 60	5
	154417	83601	−0.03	5950	5984 ± 12	4
μ Ara	160691	86796	+0.35	5690	5664 ± 13	9
70 Oph	165341	88601	+0.07	5305	5323 ± 33	4
ι Pav	165499	89042	−0.13	5891	5941 ± 32	8
	172051	91438	−0.24	5565	5632 ± 71	4
	179949	94645	+0.2	6134	6131 ± 32	6
31 Aql	182572	95447	+0.41	5581	5545 ± 14	5
	184985	96536	+0.01	6255	6282 ± 21	2
δ Pav	190248	99240	+0.33	5633	5610 ± 14	4
15 Sge	190406	98819	+0.05	5904	5925 ± 16	4
ϕ^2 Pav	196378	101983	−0.44	5979	6078 ± 28	8
γ Pav	203608	105858	−0.66	5991	6124 ± 31	4
	206860	107350	−0.06	5878	5916 ± 27	4
ξ Peg	215648	112447	−0.27	6125	6197 ± 21	2
49 Peg	216385	112935	−0.22	6193	6257 ± 35	4
51 Peg	217014	113357	+0.19	5785	5784 ± 15	4
ι Psc	222368	116771	−0.12	6150	6198 ± 25	4

affect the temperature determinations. As I show in Fig. 4.1, the flux difference between profiles from both models translates to 11 K, favoring hotter temperature diagnostics for the model of Stehlé and Hutcheon (1999). The profiles compared in the figure were synthesized not with self broadening (Barklem, Piskunov, and O'Mara, 2000) but with impact broadening (Allard et al., 2008), which is an enhanced version of the self broadening.

The progress of the present work with respect to previous works that performed the comparative 3D-1D model analysis is the wide parameter space here considered. The atmospheric parameters of four profiles were chosen to bracket a solar metallicity with different $T_{\rm eff}$ and $\log g$ values. The four bracketing models were accompanied by four further models of sub-solar metallicity with [Fe/H]$= -0.5$ dex. The chemical composition follows Grevesse and Sauval (1998) with the exception of the CNO elements which were updated following Asplund (2005). For the metal-depleted models, an α-enhancement of $+0.2$ dex was assumed. The variation of the continuum across the Hα profile was modeled by assuming a parabolic[2] dependence of the continuum intensity on wavelength, as assumed for the profiles of Barklem et al. (2002).

Doppler shifts stemming from the underlying velocity field were fully taken into account – albeit they have a minor effect on the overall profile shape. The final flux profiles were horizontal and temporal averages over typically 20 instants in time. The center-to-limb variation effect on the line profiles (the effect of using 3D models, basically) was calculated using three limb-angles. Figure 4.12 illustrates the center-to-limb variation predicted by the 3D models used in this work compared with solar observations for four different limb-angles as a function of the wavelength. It is observed that the predictions from 3D models match the observations even for the shortest wavelengths where 1D models fail. Increasing the number of limb-angles in the profiles modeling imply more use of computational resources, hence the choice of three limb-angles in this work. This is not the optimum minimum number of angles, but it is still a good approximation. Namely, the line profile is given by the integrated light from every infinitesimally thick ring for every radius from the center to the limb. The optimum minimum number of rings (or limb-angles) n is that for which the change of flux between profiles from n and $n+1$ rings translates to less than the internal error of the temperature measurement. This is illustrated in Fig. 4.13, where the flux of Hα profiles synthesised using three, four, and five angles with respect to that from two angles is shown. Given the internal precision of 10 K expected in this work, the convergence is reached for four angles: the change of flux between profiles from five and four angles is $\sim$0.05% $\equiv$ 5.5 K at 2 Å around the line core. The error in temperature by assuming three angles instead of four angles is then given by the difference between the green and red lines in the plot: 0.12% $\equiv$ 13 K at most in the left wing, the asymmetry of which is caused by granulation. It favors cooler temperature diagnostics for the current models by $\sim$13 K, this effect along with the use of the Stark broadening approximation of Griem (1967) instead of that of Stehlé and Hutcheon (1999) discussed above, account for temperatures cooler than ideal by $\sim$25 K in total.

To estimate the effects of 3D models on $T_{\rm eff}$, I analyzed the synthetic Hα profiles as they were observed profiles. Therefore, in the ideal case in which the Hα profiles from 3D models are identical to observed, the trend that relates interferometric $T_{\rm eff}$ and $T_{\rm eff}^{\rm H\alpha}$(1D LTE) as a function of [Fe/H] in Fig 4.11 should be reproduced.

[2] Although I tested that these empirical normalizations produce almost no difference with theoretical ones: $\pm$1 K difference in terms of temperature.

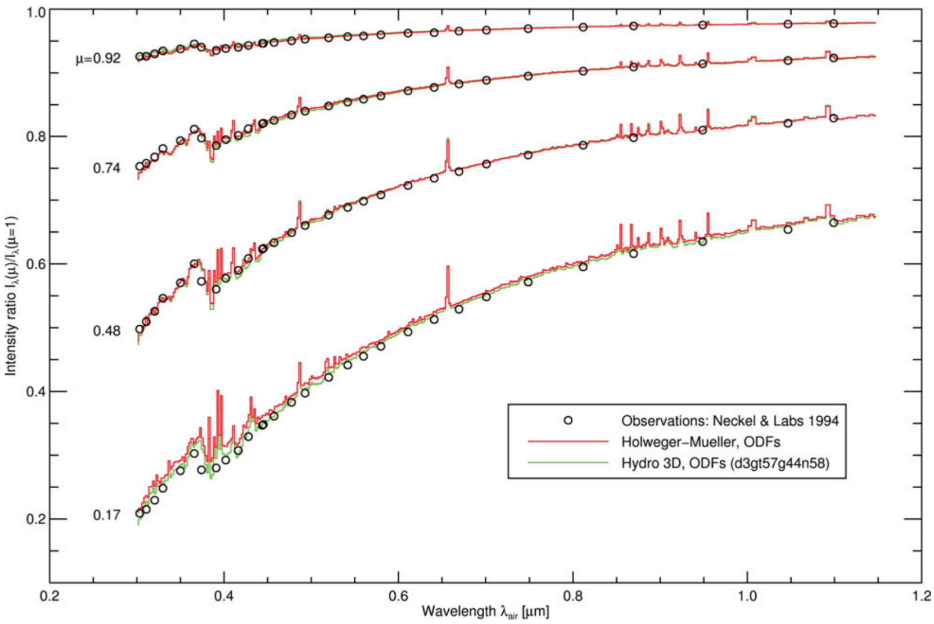

FIGURE 4.12: Adapted from Ludwig et al. (2010). Comparison of the predicted center-to-limb variation as a function of wavelength by 3D models (green line), and by the 1D semi-empirical model of Holweger and Mueller (1974) against observations (Neckel and Labs, 1994). The results are given for four different viewing angles from close to the center ($\mu = cos\theta = 0.92$) to close to the limb ($\mu = 0.17$).

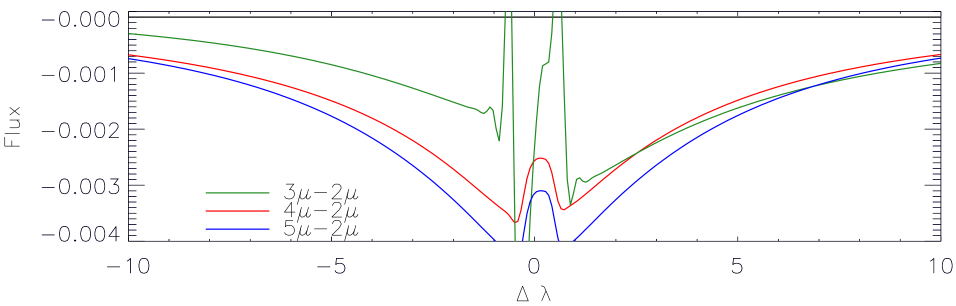

FIGURE 4.13: Flux difference for Hα profiles from different limb-angles ($\mu = cos\theta$).

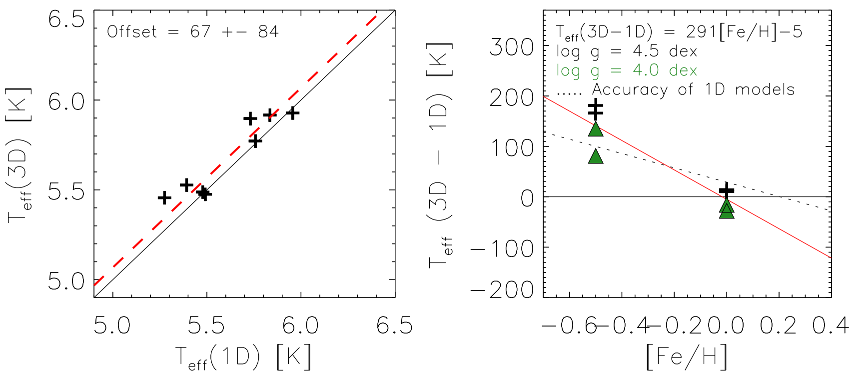

FIGURE 4.14: As in Fig. 4.11 but for 3D models. In the panel on the right, different symbols and colours are used for the two log g values according to the legends. The accuracy of 1D models Eq. 4.2 is represented by the dotted line.

The synthetic profiles from 3D models were resampled with the same pixel size of HARPS and 0.1% of white noise was added to allow the fitting. The fits are shown in Fig. 4.15 and the temperatures retrieved from 1D models are compared with the nominal temperatures of the 3D models in Fig. 4.14, as done in Fig. 4.11. In the plot on the right panel, a linear trend was fitted to the points, thus it can be compared with the trend related to Eq. 4.2 which is also overplotted. The comparison shows that the offset relative to 1D models is almost reproduced at [Fe/H] = 0 dex, and at [Fe/H] = −0.5 dex 3D models produce temperatures that tend to be hotter by 0-100 K depending on log g. Hence, temperatures from 3D models are significantly closer to those from interferometry at [Fe/H] = −0.5 dex, and they show particularly high levels of agreement for low log g values.

I conclude that the most likely cause for the trend with metallicity represented by Eq. 4.2 is the use of 1D models, and that the impact of LTE is subtle for the metallicity range analysed. On the other hand, I consider that the use of 1D models together with the correction for metallicity given by Eq. 4.2 is an excellent approximation.

The differential analysis between coudé/HARPS/MUSICOS spectra and KPNO solar atlases performed in Sect. 4.1.1 allowed me to determine temperature corrections that counter the normalization errors present in KPNO2005 and KPNO2011. These corrections applied to the solar-case determinations in the bottom part of Table 4.1 show the actual improvement of 3D models on the accuracy of Hα modeling; the temperatures derived are very close to solar. Remarkably, Hα from 3D non-LTE models of Amarsi et al. (2018) exactly reproduce the solar T_{eff}, at 5770 K (see Table 4.1), when it is considered 5721 + 29 K. This is a prefect agreement with the fundamental value 5772 K as given by Prša et al. (2016) and Heiter et al. (2015).

4.3 Comparison with other Hα scales

In the previous sections I determined the accuracy of various Hα models for the solar case. These results are summarized in Table 4.1, where the original temperature predictions, as provided by the authors, are listed along with their bias-corrections related to the normalization errors in their observational templates. In this section I compare not only the zero points but the temperature scales. I again discuss the possible sources of differences between them and how the enhanced models improve the results across the parameter space. The scales compared below have only

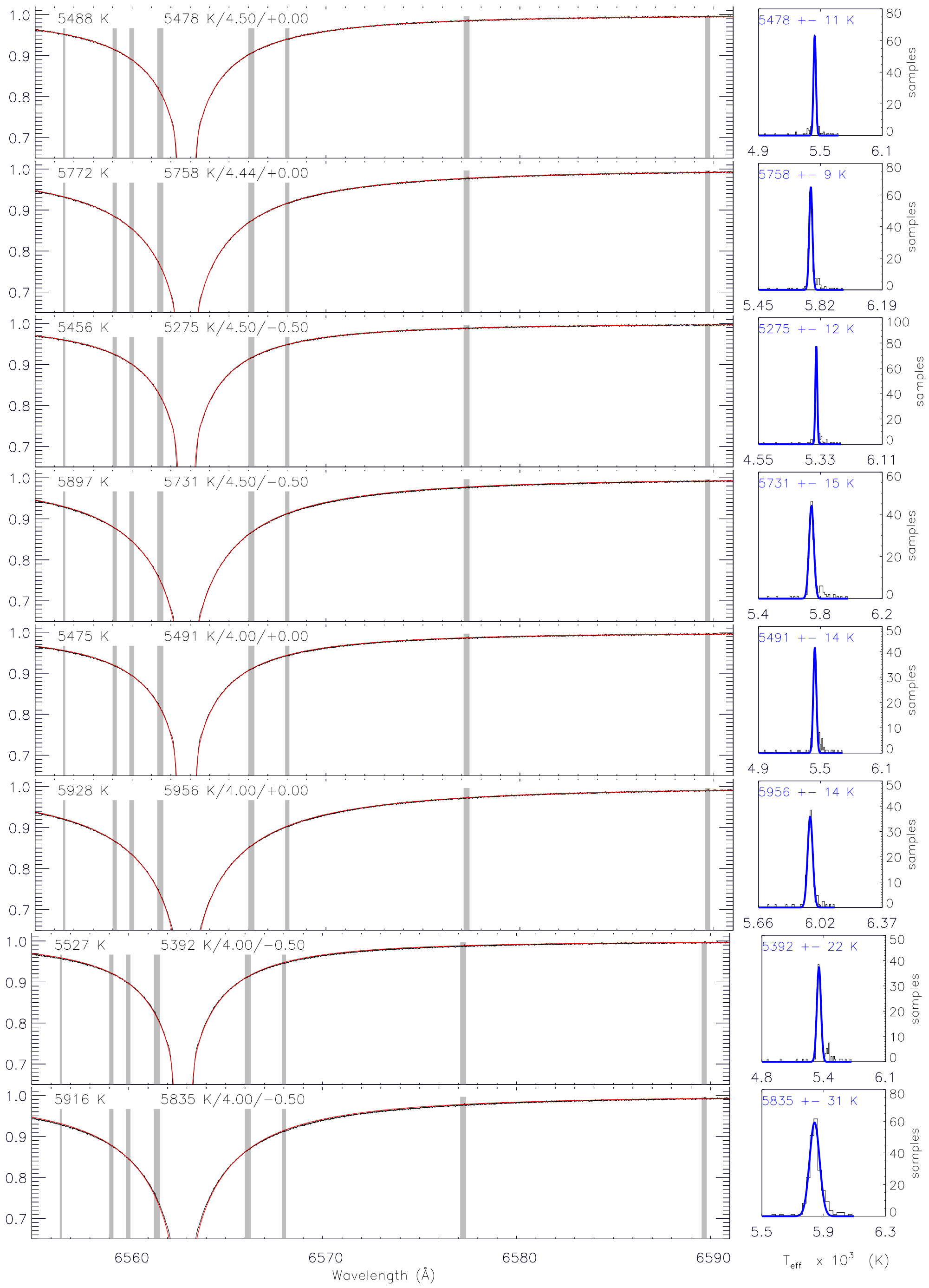

FIGURE 4.15: Fits of 3D profiles (black) with 1D profiles (red). The nominal temperature values of the 3D profiles are noted in the left, while the parameters of the 1D profiles are at the right side.

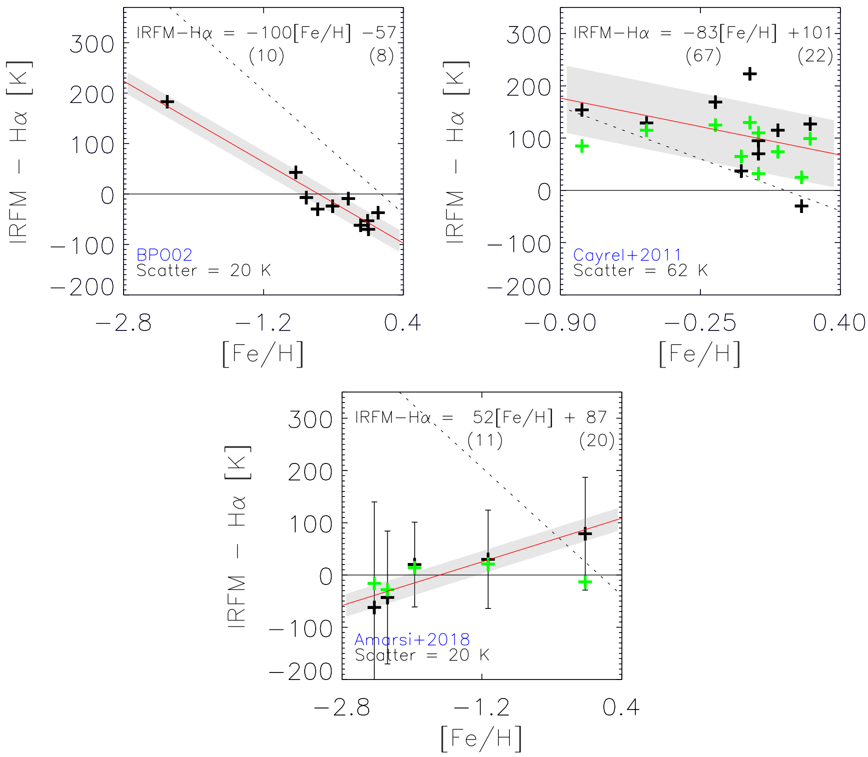

FIGURE 4.16: From left to right, analogous comparisons to the right panel in Fig. 4.11 for the Hα scales of Barklem et al. (2002), Cayrel et al. (2011), and Amarsi et al. (2018). In all plots, the red line and the shade represent the trend and the spread fitted to dark crosses. For a quick comparison, the trend of Eq. 4.2 is represented by the dotted line. Green symbols represent interferometric $T_{\rm eff}$ and black symbols represent $T_{\rm eff}$ from IRFM. Note the much larger [Fe/H] range of the first and third plots.

a few or no stars in common with this work. However, they have all or most of their stars in common with the catalogue of Ramírez, Allende Prieto, and Lambert (2013), the temperatures of which were derived by means of the IRFM calibrated by Casagrande et al. (2010). In Sect. 5.1 I confirm that the $T_{\rm eff}$ scale from IRFM is equivalent to $T_{\rm eff}$ from interferometry, as reported by Casagrande et al. (2014). Accordingly, the comparisons between the $T_{\rm eff}^{\rm H\alpha}$(1D LTE) scale with the scales below are performed indirectly using IRFM of Ramírez, Allende Prieto, and Lambert (2013) as the standard, which replaces interferometric $T_{\rm eff}$. I refer the reader to check the plots in Fig. 4.16, which are analogous to those in Figs. 4.11 to follow the discussions below. The plots in the figure show also the trend corresponding to the accuracy of $T_{\rm eff}^{\rm H\alpha}$(1D LTE) (Eq. 4.2) to help the reader to compare the scales.

- Scale of Barklem et al. (2002, 1D LTE): Ten stars are in common with the catalog of Ramírez, Allende Prieto, and Lambert (2013). The discrepancy of this scale with respect IRFM/interferomety as a function of [Fe/H] is similar to Eq. 4.2, but it is shifted by $\sim +70$ K for the metallicity range I analyse in this work (-0.65 to $+0.40$ dex). A probable cause for the shift is that the synthetic spectra seem to be predominantly fitted with lower observed fluxes; see two examples in Fig. 4.17. This may be caused by the χ^2_{min} fitting method without sigma clipping applied in low-S/N spectra. For example, Ramírez et al. (2014) find systematically high Hα temperatures for larger χ^2_{min}. It should however be mentioned that the results of Barklem et al. (2002) agree with ours in that a trend with metallicity exists. It should be noted that the quality of their spectra and their fitting method were not conceived in order to achieve the high precision that the current study is aiming for.

- Scale of Cayrel et al. (2011, 1D LTE): The comparison against $T_{\rm eff}$ from IRFM as a function of [Fe/H] shows a slight trend. In the comparison against $T_{\rm eff}$ from interferometry the trend disappears leaving only a flat offset of $\sim$100 K (see green symbols in the plot), as shown by the authors. The plot suggest that the Hα model of Allard et al. (2008), in which the analysis of Cayrel et al. is based, enhances the difference between the model of Barklem et al. (2002) and interferometry close to the solar [Fe/H]. This result is consistent with the result for the solar case in Table 4.1: after the bias-correction corresponding to the use of KPNO2005 (+37 K), I estimate that this model produce a cooler temperature than from Barklem et al. (2002), that is $5678 + 37$ K. The discrepancy for low metallicity values remains almost the same as that of the scale of this work (Eq. 4.2).

- Scale of Ramírez et al. (2014, 1D LTE) (not shown in Fig. 4.16): Precise $T_{\rm eff}$ was derived for 88 solar analogues (i.e. stars that share the same atmospheric parameters with the Sun within an arbitrary narrow range of errors, according to the definition in Porto de Mello et al., 2014) from IRFM of Casagrande et al. (2010), Hα profiles using the model of Barklem et al. (2002) (as I do), and the spectroscopic technique described in Sect. 5.2. In their Fig. 13, Ramírez et al. (2014) compare their determinations from Hα with spectroscopy and find, after a zero point correction, a small trend, as I find in Sect. 5.2 comparing $T_{\rm eff}^{\rm H\alpha}$(1D LTE) with their spectroscopic scale and several others. No comparison were presented against [Fe/H], which is to be expected given that the range of their sample is very narrow, that is, ± 0.1 dex around solar metallicity.

- Scale of Amarsi et al. (2018, 3D non-LTE): Spectra of six templates were used to test the model. Two of these stars, the Sun and Procyon, lie within the [Fe/H]

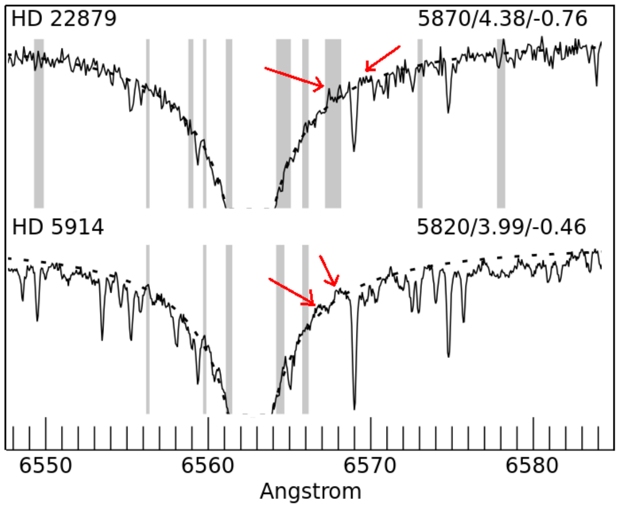

FIGURE 4.17: Adapted from Barklem et al. (2002, Fig. 6). Fits of Balmer lines of two stars. The arrows point possible excesses of flux of the observational spectra with respect to the synthetic profiles.

range of the sample in this work, while the other four with [Fe/H] between −2.8 and −1.2 dex exceed the range. The comparison with $T_{\rm eff}$ from IRFM as a function of [Fe/H] shows a trend, but this trend disappears when interferometric $T_{\rm eff}$ is compared instead. The change in slope is mainly given by the interferometric measurement of Procyon, which agrees closely with that from Hα. Accordingly, interferometry perfectly agrees with this Hα scale along the [Fe/H] range of analysis. Further, I also determined in Sect. 4.1.1 (Table 4.1) that these 3D non-LTE models do reproduce the solar $T_{\rm eff}$ from direct measurement (5772 K) when the error due to profile distortions in the used template is removed.

In this chapter I summarized the modeling of Hα lines and its improvement in a time-line from early researches. The accuracy of the Hα profile as a tool for the diagnostic of $T_{\rm eff}$ has been unquestionably improved significantly in the previous decade by enhancing the model of hydrogen interaction (Barklem, Piskunov, and O'Mara, 2000; Barklem et al., 2002). No test with the Sun found the model accurate, although some reported close agreement with the direct $T_{\rm eff}$. The most intriguing fact of such reports was the excessive spread of solar determinations for the same model (Fig. 4.4), which I took as the initial clue to develop the research I present. Until the date when the paper that presents the bulk of this thesis to the community was accepted (Giribaldi et al., 2019), it was believed that the most sophisticated physics applied on modeling the Hα line was still insufficient, as shown by the results of Amarsi et al. (2018). Namely, this was the first grid of Hα profiles synthesized from 3D and non-LTE model atmospheres, with which the solar $T_{\rm eff}$ could not be recovered. The results presented in this chapter have shown that the model of Amarsi et al., supported by 50 years of theory development, is indeed accurate to a high degree of precision, as required by current researches. This contribution was achieved by means of an extremely detailed analysis of observational profiles, which derived into a 'cookbook' of methods for a proper treatment of the observational data to take full advantage of the models, as described in Chap. 3.

Chapter 5

Results: Accuracy of other techniques

In this chapter I test the accuracy of IRFM and spectroscopic T_{eff} scales in Sects. 5.1 and 5.2, respectively. For testing IRFM T_{eff} I analyse only the implementation of Casagrande et al. (2010), while for testing spectroscopic T_{eff} I analyse individually several implementations of wide current use.

The strategy I use is different from that used by Heiter et al. (2015), although the diagnostic of accuracy of this work is based on their interferometric T_{eff} scale as the standard. Heiter et al. (2015) take the average T_{eff} values from many implementations of the same technique (i.e. IRFM or spectroscopic) and compare it with their interferometric T_{eff}. In such a way they estimate the underlying offset related to the accuracy of one technique, thus avoiding the offsets related to particular implementations of it. This strategy works well when comparing spectroscopic T_{eff} scales because, as I show in Sect. 5.2, spectroscopic T_{eff} scales produce very similar diagnostics. On the other hand, this is not true for IRFM scales: most of the IRFM implementations previous to that of Casagrande et al. (2010) produce systemetically different T_{eff} diagnostics. Those IRFM T_{eff} scales were analysed in detail by Casagrande et al. (2010), and the origin of their differences were identified. Accordingly, for the purposes of this thesis, there is no need to analyse them. Further, taking the average T_{eff} values of several IRFM implementations would increase the noise of the comparisons, making the results less precise.

For determining the accuracy of IRFM and spectroscopic T_{eff} scales I proceed as follows: $T_{\mathrm{eff}}^{\mathrm{H}\alpha}$(1D LTE) was derived for the sample stars Table 2.1 using as stellar input $\log g$ and [Fe/H] parameters provided by each author, so that each comparison is consistent as far as the stellar parameters are concerned. Subsequently, $T_{\mathrm{eff}}^{\mathrm{H}\alpha}$(1D LTE) values are corrected by applying Eq. 4.2, thus a reference frame of accurate T_{eff} is settled to determine the accuracy of each T_{eff} scale. Finally, the accuracy of the T_{eff} scales are the offsets computed from the comparisons.

5.1 InfraRed Flux Method

IRFM was introduced by Blackwell and Shallis (1977), Blackwell, Shallis, and Selby (1979), and Blackwell, Petford, and Shallis (1980), and it is considered the second less model-dependent technique after interferometry for determining angular diameters and T_{eff}. This technique consist on comparing the bolometic flux (F_{bol}) with the flux in infrared bands (F_{IR}) as shown by Eq. 5.1. In it, σ is the Stefan-Boltzmann constant, F_{bol} and F_{IR} are directly measured by spectrophotometry, and $F_{\mathrm{IR}}(\mathrm{model})$ must be computed by models to match F_{IR}. The marginal influence of modeling is introduced by the latter.

$$\frac{F_{\text{bol}}}{F_{\text{IR}}} = \frac{\sigma T_{\text{eff}}^4}{F_{\text{IR}}(\text{model})} \tag{5.1}$$

For stars hotter than about 4200 K, infrared photometry longward of $\sim$1.2 μm ensures that the fluxes are measured in the Rayleigh-Jeans part of a stellar spectral energy distribution, a region largely dominated by the continuum which linearly depends on T_{eff}, and thus only mildly on model atmospheres (Casagrande et al., 2010, see Fig. 2). This spectral region also has little dependence on other atmospheric parameters such as metallicity and surface gravity (Alonso, Arribas, and Martinez-Roger, 1996; Casagrande, Portinari, and Flynn, 2006; Casagrande et al., 2010), and it is nearly free from non-LTE and granulation effects (Asplund and García Pérez, 2001).

Several IRFM temperature scales have been implemented since the technique was proposed, for example Saxner and Hammarback (1985), Bell and Gustafsson (1989), Alonso, Arribas, and Martinez-Roger (1996), Ramírez and Meléndez (2005), Casagrande, Portinari, and Flynn (2006), and González Hernández and Bonifacio (2009b). Casagrande et al. (2010) optimized the IRFM scale presented previously in Casagrande, Portinari, and Flynn (2006); its accuracy was later tested and confirmed by Casagrande et al. (2014) by tests performed against interferometric measurements of good quality. Casagrande et al. (2010), by comparison with their scale, showed that previous IRFM scales of wide use present large systematic errors, and that the errors originate in the absolute flux calibration of the photometric system of use. For example, in Fig. 5.1, the top panel shows the offset of the scale of Alonso, Arribas, and Martinez-Roger (1996) with respect to that of Casagrande et al. (2010), and the bottom panels shows the difference between the absolute flux for JHK_S bands determined by both groups of authors for Vega which is the star used as the calibration standard. It clearly shows that the increase of the absolute flux of Vega is related to cooler T_{eff} diagnostics.

More in detail, photometric systems are calibrated by Eq. 5.2, where the magnitude m_ξ in a given photometric band ξ is converted in into a physical flux (i.e. erg cm^{2}s^{-1} Å^{-1}) for its use in Eq. 5.1

$$F_\xi = F_\xi^{std} 10^{-0.4\left(m_\xi - m_\xi^{std}\right)} \tag{5.2}$$

In the equation, F_ξ^{std} is called the *absolute flux calibration* and m_ξ^{std} is called the *zero point* of the photometric system. Thus, varying any of these two parameters, or both simultaneously, the photometric system may be re-calibrated, but variations of m_ξ^{std} are of greater impact because it is an exponent. For instance, a change of 0.01 mag corresponds to a change of about 1% in flux, and in turn, increasing the flux of the standard star in the JHK_S bands simultaneously by 2% translates into a decrease of around 40 K in T_{eff} determinations, according to the tests made by Casagrande et al. (2010).

Johnson-Cousins and 2MASS photometric systems, that are often used to implement IRFM, use Vega as zero point standard. However, Vega is not the ideal standard, even though it have been used as such since the UBV system was established (Johnson and Morgan, 1953). The problem is that the spectral distribution of Vega is not characterized by a single set of atmospheric parameters due to its rapid pole-on rotation (Aufdenberg et al., 2006; Peterson et al., 2006) and its debris disc (Aumann et al., 1984; Wilner et al., 2002; Su et al., 2005). The pole-on rotation view of Vega sets a strong change of surface temperature and gravity as functions of the latitude due to fast rotation. For instance, T_{eff} varies from the pole (in the center of

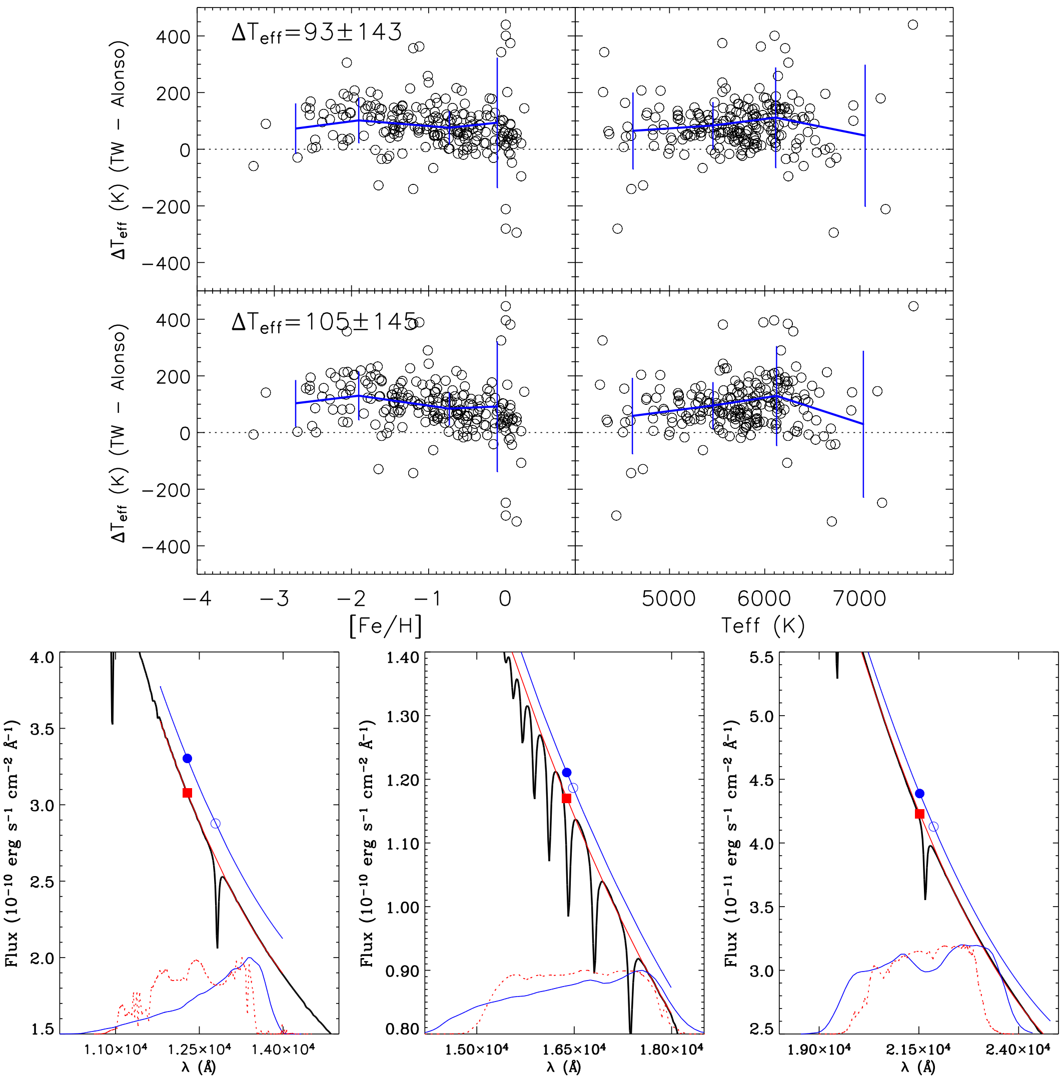

FIGURE 5.1: Adapted from Casagrande et al. (2010, Figs. 3 and A.1). *Top and mid panels:* Difference between the effective temperatures derived by Casagrande et al. (2010) and those derived by Alonso, Arribas, and Martinez-Roger (1996) for 220 stars in common. For both panels, different model atmospheres were used to derive IRFM temperatures. *Bottom panels:* Comparison between absolute fluxes of Vega, for each effective wavelength of JHK_S photometric bands (from the left to the right, respectively), determined by Casagrande et al. (2010, red squares) and Alonso, Arribas, and Martinez-Roger (1996, blue filled circles). Red and blue lines are fittings to the spectral energy distributions considered by each group of authors. The black line is the synthetic spectrum of Vega (Bohlin, 2007). Dotted and continuous curves in the bottom of the plots are the transmission curves of 2MASS filters and those used by Alonso, Arribas, and Martinez-Roger (1996), respectively.

the disc) to the equator (in the border of the disc) between 10 150 and 7900 K (Aufdenberg et al., 2006). On the other hand, the spectrum of Vega presents a flux excess in the infrared due to its debris disc, which is located not far from the star. This excess varies depending on the photometric band, for example 1.29% in K (Absil et al., 2006), and 2-3% in 2.2 μm (Ciardi et al., 2001). A more detailed discussion regarding the problems of Vega as standard can be found in Gray (2007).

It is therefore evident where large systematics between IRFM implementations arise from. Implementing an IRFM temperature scale requires accurate absolute calibrations for the terms in the left part of Eq. 5.1. For computing $F_{\rm bol}$, the absolute calibrations of optical bands are essential, while the calibrations of infrared bands are not of great influence; except for stars cooler than 5000 K, for which $(RI)_C$ bands are important because they are centered on the peak of the energy distribution of the star. On the other hand, the absolute calibrations of infrared bands are the key to obtain $F_{\rm IR}$.

5.1.1 Casagrande et al. (2010) IRFM scale

The IRFM $T_{\rm eff}$ scale of Casagrande et al. (2010) was implemented using a sample of 104 nearby stars (within a distance of 30 pc) with BVR_CI_C and JHK_S photometry acquired at La Palma observatory by Casagrande, Portinari, and Flynn (2006). The sample stars were confirmed to be free from reddening by means of polarimetric measurements of dust. They were selected from an initial sample of 186 stars in the northern hemisphere listed by Gray et al. (2003), which was reduced in order to separate double/multiple systems and variable stars. The final sample was complemented with metal-rich stars from Ramírez and Meléndez (2005), and with metal-poor[1] stars from several sources in the literature.

Casagrande et al. (2010) derived IRFM $T_{\rm eff}$ through $F_{\rm bol}$ and $F_{\rm IR}$ based on very carefully calibrated optical and infrared photometry, respectively. Subsequently, they determined empirical color–$T_{\rm eff}$ relations for Johnson-Cousins $BV(RI)_C$, 2MASS JHK_S, Tycho2 $(BV)_T$ and Strömgreen by photometric systems. I summarize below the calibration of infrared and optical bands used by the authors in their IRFM implementation. The details I mention are essential to understand why the accuracy of this IRFM scale is substantially improved in comparison with previous scales. An the end of the section I show the equivalence of this scale to the interferometric scale of the Gaia Benchmark stars.

- JHK_S 2MASS flux calibrations: Casagrande et al. (2010) used a slightly modified 'fine-tuned' version of the absolute flux calibrations of Cohen, Wheaton, and Megeath (2003). Namely, they modified the zero points for the three bands in order to obtain consistent temperatures for their sample stars with Tycho2 photometry, the bands of which were absolutely flux calibrated for computing $F_{\rm bol}$, instead of using Johnson-Cousins photometry.

  The calibrations of Cohen, Wheaton, and Megeath (2003) were performed using a synthetic spectrum of Vega (Cohen et al., 1992) with which magnitudes and their corresponding fluxes in each band (m_ξ and F_ξ in Eq. 5.2) were determined. The zero points were determined comparing the observed 2MASS magnitudes of 33 stars with the values predicted from absolutely calibrated templates. The use of a synthetic spectrum of Vega instead of ground-based

[1] I call metal-poor stars those below the limit of metallicity in considered in this work: [Fe/H] < -0.70 dex. The parameters related to these stars and their sources are not mentioned because they fall out of the range of analysis of this work.

measurements was justified by Blackwell et al. (1990) and Blackwell and Petford (1991), who found that higher precision can be obtained from synthetic models than from observationally determined absolute calibrations. The calibrations of Cohen, Wheaton, and Megeath (2003) were further validated by new zero points computed by Maíz Apellániz (2007) from an updated synthetic spectrum of Vega (a model from the grids of Kurucz (2005) with $T_{\rm eff}$ = 9400 K, log g = 3.9 dex, [Fe/H] = -0.5 dex, and null microturbulence; see Fig. 5.1) determined by Bohlin (2007). The latter fitted the model with re-calibrated spectrophotometric measurements from the STIS instrument in the Hubble Space Telescope (Goudfrooij and Bohlin, 2006), obtaining a precision of 1-2% for the wavelength region between 3200 and 10 000 Å which is of main interest for IRFM.

The modification made by Casagrande et al. (2010) with respect to that of Cohen, Wheaton, and Megeath (2003), turned into a decrease of the absolute calibration by 1.6% in the J band and an increase by 1.5 and 0.3% in the H and K_S bands, respectively. These changes in terms of magnitudes make H and K_S redder by 0.016 and 0.003 and J bluer by 0.017.

- BVR_CI_C Johnson-Cousins flux calibrations: They were presented by Casagrande, Portinari, and Flynn (2006) in a previous version of the scale, which was slightly corrected for the version of (Casagrande et al., 2010). The former used the magnitudes of Vega determined by Bessel (1990) to fit a synthetic spectrum of Kurucz (2003) with the parameters $T_{\rm eff}$ = 9550 K, [Fe/H] = -0.5 dex, log g = 3.95 dex, microturbulent velocity = 2 Km s^{-1}. The flux of the synthetic model was scaled to the flux detected at the top of the Earth atmosphere, according to the equation:

$$F_{Earth}(\lambda) = \left(\frac{R}{d}\right)^2 F_{model}(\lambda) \tag{5.3}$$

where $(R/d)^2$ is the dilution factor that represents the ratio between the radius of Vega and its distance to the Earth. The dilution factor was obtained not from interferometric measurements of the radius of Vega, but from the flux value at 5556 Å measured by Megessier (1995) divided by the flux predicted by the model at the same wavelength, which offers a more precise measurement. The computed value was $(R/d)^2 = 6.2891286 \times 10^{-17}$, which implied an angular diameter of 3.272 mas in agreement with the latest direct measurements: 3.28 ± 0.06 mas (Ciardi et al., 2001), and 3.225 ± 0.032 mas (Mozurkewich et al., 2003).

The choice of the synthetic spectrum with the parameters above followed the results of Bohlin and Gilliland (2004), who found that this model best fitted the spectrophotometric measurements of the STIS instrument in the Hubble Space Telescope. Although the re-calibration of STIS made by Goudfrooij and Bohlin (2006) – applied for the calibration of 2MASS bands described above – changed the infrared fluxes determined by Bohlin and Gilliland (2004) by about 2%, it does not represent a strong conflict for optical bands because for wavelength regions below 7000 Å, flux changes are lower than 0.5% (Bohlin, 2007). Nonetheless, those differences were taken into account by Casagrande et al. (2010) in their updated flux calibration. Namely, the flux differences along with the differences arising from $F_{\rm bol}$, computed by Tycho2 bands accounted for systematic offsets of 0.15% in $F_{\rm bol}$ and 8 K in $T_{\rm eff}$, which were removed in

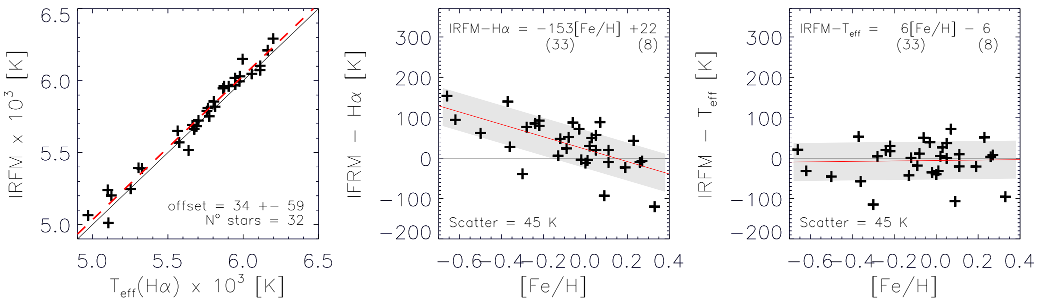

FIGURE 5.2: *Left and middle panels:* As in Fig. 4.11 but for the IRFM $T_{\mathrm{eff}}$of Ramirez13. *Right panel:* Relative temperatures as a function of [Fe/H] after applying the correction relation given by Eq. 4.2 to $T_{\mathrm{eff}}^{\mathrm{H}\alpha}$(1D LTE).

the final calibrations to obtain consistent T_{eff} from both optical photometric systems.

- $B_T V_T$ Tycho2 flux calibrations: As for the Johnson-Cousins system, Casagrande et al. (2010) based the absolute calibration of the Tycho2 system on the synthetic spectrum of Vega (Bohlin, 2007), adopting the $B_T V_T$ zero points of Maíz Apellániz (2007) and the corresponding filter transmission curves of Bessell (2000). This flux calibration was done to perform an accuracy test of the IRFM implementation using ten of the best known solar twins, the atmospheric parameters of which were derived by means of a differential spectroscopic method with respect to the Sun reported not to be model-dependent (Meléndez, Dodds-Eden, and Robles, 2006; Meléndez and Ramírez, 2007). Optical colors are required to compute F_{bol} in Eq. 5.1, but Johnson-Cousins photometry was available only for a few of these twins, while Tycho2 photometry was available for all them.

I determine the accuracy of the IRFM T_{eff} using the temperatures of Ramírez, Allende Prieto, and Lambert (2013), that were derived by the metallicity-dependent color–T_{eff} relations of Casagrande et al. (2010) using the Johnson-Cousins, 2MASS, Tycho2, and Strömgreen available photometry. To obtain these temperatures, the authors used an homogeneous set of metallicity derived from Fe lines, for which T_{eff} from IRFM was provided as input, thus performing an iterative procedure minimizing the T_{eff}–[Fe/H] degeneracy.

The left panel in Fig. 5.2 shows the comparison between IRFM T_{eff} and $T_{\mathrm{eff}}^{\mathrm{H}\alpha}$(1D LTE) derived using coudé-only spectra. The comparison shows a constant offset of 34 K between the two scales with a scatter of 59 K. The difference of the two scales show a trend with metallicity according to the equation displayed in the plot in the middle panel. This trend is equivalent to Eq. 4.2 found in the comparison with interferometric measurements. Thus, after applying the relation given in Eq. 4.2 to $T_{\mathrm{eff}}^{\mathrm{H}\alpha}$(1D LTE), the trend is indeed removed, as shown in the right panel of the figure. This result asserts the equivalence between interferometry and IRFM reported by Casagrande et al. (2010), and subsequently confirmed by (Casagrande et al., 2014). Both authors agree on a maximum systematic offset of 15 to 30 K favoring hotter values for IRFM depending on the exact system in use. However, the latter authors highlighted that the small offset lies on the interferometric T_{eff} values used in their test. That is, a slight temperature underestimation mostly caused by overestimated angular diameters (0.5–1.0%) due to the use of 1D models to compute limb-darkening corrections; see several cited tests that agree on this result in Sect.4.1.2.

The remaining scatter of 45 K is close to the average formal errors of IRFM T_{eff} of the stars compared (52 K), which implies that it is dominated by the uncertainties of the color measurements. Therefore the contribution of random errors of $T_{\text{eff}}^{\text{H}\alpha}$(1D LTE) related to the normalization is negligible, supporting the precision of the method described in Sect. 3.1.

5.2 Spectroscopic effective temperatures

The need of deriving accurate stellar T_{eff} got more attention with the discovery of exoplanets because their characterization depends directly on how accurately and precisely the physical parameters of the host stars are determined. Other studies also require a refined determination of T_{eff}. For example, finding the nature of the connection between stellar metallicity and planetary presence (e.g. Gonzalez, 1997; Santos et al., 2003; Fischer and Valenti, 2005; Sousa et al., 2008; Ghezzi et al., 2010b), the detection of diffusion effects in stellar atmospheres (e.g. Korn et al., 2006; Korn et al., 2007), and the search for chemical signatures of planetary formation (e.g. Meléndez et al., 2009; Ramírez, Meléndez, and Asplund, 2009).

Some of these studies deal with a large amount of stars, for which automatic spectroscopic procedures have been developed, that provide results with high internal precision. However, when results from different spectroscopic procedures are compared, significant discrepancies may appear implying that the quoted precisions are far from the accuracy. One example that perfectly displays this problem is presented in Fig. 5.3. It shows the comparison between atmospheric parameters derived by the ROTFIT tool (Frasca et al., 2003) and by the ARES+MOOG tool (e.g. Sousa et al., 2008). The latter is based on measurements of equivalent widths (its details are given below), while the former determines atmospheric parameters by fitting a library of observed spectra of 220 reference stars, whose parameters were compiled mostly from works in the literature that performed spectral synthesis or equivalent widths spectroscopic analysis (Molenda-Żakowicz et al., 2013, Table 2). The comparison in the figure shows that, although both sets of atmospheric parameters are based on the same (or similar) spectroscopic technique, T_{eff} values disagree from the solar to hotter values.

In this work I test catalogues with small internal errors. Among them Ramírez et al. (2014, Ramirez14a) and Ramírez, Meléndez, and Asplund (2014, Ramirez14b) are the most precise with $\sim$10 K, followed by Sousa et al. (2008, Sousa08), Tsantaki et al. (2013, Tsantaki13) and Maldonado et al. (2015, Maldonado15) with $\sim$20 K, then Ghezzi et al. (2010b, Ghezzi10) and Heiter et al. (2015, Heiter2015) with $\sim$30 K, and Bensby, Feltzing, and Oey (2014, Bensby14) with $\sim$70 K. The characteristics of the spectroscopic methods implemented by each author are mentioned below in order to interpret their influence in the accuracy of the scales. The plots in Fig. 5.4 show the comparison of the Hα temperatures determined from coudé-only spectra with those derived by the different sources. As in Fig. 5.2, the comparisons in the right panels of the figure show the accuracy of the T_{eff} scales, given that $T_{\text{eff}}^{\text{H}\alpha}$(1D LTE) corrected by Eq. 4.2 are converted into accurate T_{eff}.

- **Scales of Sousa08, Ghezzi10 and Tsantaki13:** Their T_{eff} are derived assuming LTE and 1D geometry by the Kurucz Atlas 9 (Kurucz, 1993) model atmospheres. They used the 2002 version of MOOG (Sneden, 1973) and the ARES code for automatic measurement of equivalent widths (Sousa et al., 2007). They differ in the line lists used and in the atomic data adopted. Tsantaki13's line list is an upgrade of that used by Sousa08 selected with HARPS, where 'bad' lines were suppressed to correct $T_{\rm eff}$ overestimation in cooler stars. Both works computed oscillator strength values (log gf) from an inverted solar analysis using equivalent widths measured in solar spectra. The list of Ghezzi10 is short in comparison with those of Sousa08 and Tsantaki13, and was selected for the FEROS spectrograph (Kaufer et al., 1999) at lower resolution; they used laboratory log gf values. The comparison with these three works shows a trend with $T_{\rm eff}^{\rm H\alpha}$(1D LTE): the larger $T_{\rm eff}$, the larger the discrepancy. For Ghezzi10, the comparison with $T_{\rm eff}^{\rm H\alpha}$(1D LTE) shows a positive trend with [Fe/H], while for Sousa08 and Tsantaki13 no trend with [Fe/H] is found, but offsets of 48 and 33 K, respectively.

- **Scale of Bensby14:** $T_{\rm eff}$ was derived considering non-LTE corrections on spectral lines measured manually. The 1D MARCS model atmospheres (Asplund et al., 1997) were used with their own code of convergence of atmospheric parameters. They used a large line list and spectra from different instruments of medium and high resolution, with laboratory log gf values. The comparison of their $T_{\rm eff}$ scale against $T_{\rm eff}^{\rm H\alpha}$(1D LTE) is similar to those of Sousa08 and Tsantaki13. Indeed, Sousa08 found their scale to be compatible to an offset of +18 K with respect to that of Bensby14 (see Fig. 3 in paper). I find a slightly significant positive trend with [Fe/H].

- **Scales of Ramirez14a and Ramirez14b:** $T_{\rm eff}$ were derived using a differential method (Meléndez, Dodds-Eden, and Robles, 2006) with which the atmospheric parameters of high internal precision are obtained. By means of the "q^2" package[2] both groups of authors used the 2013 version of MOOG and 1D + LTE model-atmosphere grids. They, measured spectral lines manually and used laboratory log gf values. There are two main differences between the procedures of Ramirez14a and Ramirez14b. Firstly, Ramirez14a used the "odfnew" version of Kurucz, while Ramirez14b used the MARCS atmosphere model (Gustafsson et al., 2008). However, according to Ramirez14b the use of different models does not significantly affect the parameter diagnostics because of the differential method applied. Secondly, the stars analysed in both works differ in [Fe/H]: Ramirez14b analysed solar twins while Ramirez14a more metal-rich stars, that is [Fe/H] $\gtrsim 0.2$. Thus, Ramirez14b naturally used the Sun as standard for the solar twins, while in Ramirez14a the differential method was applied with respect to every star of the sample. For the Ramirez14b scale of solar twins I find an offset of $+42 \pm 13$ K with respect to Hα, which agrees with the 28 ± 1 K needed to correct the Hα zero point. For the Ramirez14a scale I find an offset of $+72 \pm 17$ K. Considering Ramirez14a and Ramirez14b as a unique sample, I find a positive trend with [Fe/H].

- **Scale of Maldonado15:** $T_{\rm eff}$ was derived assuming LTE and 1D geometry by the Kurucz Atlas 9 model atmospheres as Sousa08, Ghezzi10, and Tsantaki13, but they used the line list from Grevesse and Sauval (1999) and spectra from several sources including HARPS. For the convergence of the atmospheric parameters they used TGVIT (Takeda et al., 2005). The comparison of their $T_{\rm eff}$ scale against Hα does not show a significant trend, but an offset of +34 K. I

[2]The Python package "q^2" `https://github.com/astroChasqui/q2`

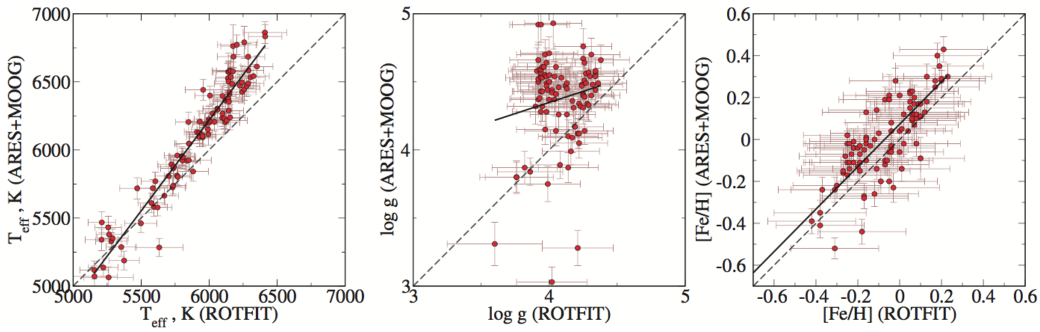

FIGURE 5.3: Adapted from Ryabchikova, Piskunov, and Shulyak (2015). Comparison between the atmospheric parameters derived by different spectroscopic procedures. Based on the results published in Molenda-Żakowicz et al. (2013). The discontinuous lines represent the prefect agreement, and the continuous lines are the linear regressions of the points.

find the same offset for IRFM against Hα (Sect. 5.1), which confirms the agreement[3] between this T_{eff} scale and IRFM reported by the authors –when [Fe/H] is not considered. On the other hand I find a positive trend with [Fe/H].

The spectroscopic scales analysed show a general agreement with Hα up to ~5700 K and hotter values for hotter T_{eff}. The trends with [Fe/H] are opposite to what is observed with interferometry and IRFM. After applying the correction relation for metallicity of Eq. 4.2 to $T_{\text{eff}}^{\text{H}\alpha}$(1D LTE), the H$\alpha$ scale becomes T_{eff}, in the same frame of the interferometry scale, allowing to study the accuracy of the spectroscopic scales. This is shown in the right panels of Fig. 5.4, the common pattern shows that spectroscopic temperatures are underestimated by 100-200 K at [Fe/H] = -0.6 dex and overestimated by ~100 K at [Fe/H] = $+0.4$ dex. The most accurate [Fe/H] range is around the solar value, that is, between -0.3 and $+0.1$ dex. The relations presented in the plots in Fig. 5.4 can be used to empirically correct such spectroscopic scales. These corrections become important as T_{eff} depart from solar to derive unbiased [Fe/H] values. An example of the impact of the T_{eff} scale on [Fe/H] is provided in Fig. 5.5. The plots compare the T_{eff} and metallicity scales of Sousa08 and Ramirez13 (the latter is an IRFM scale determined as accurate in Sect. 5.1). No offset between both temperature scales appears, but their difference plotted against [Fe/H] replicates the trend obtained in the top-right panel of Fig. 5.4. The difference between metallicity scales also shows a trend with T_{eff}, associating larger [Fe/H] discrepancies with T_{eff} farther from solar.

The main difference between all spectroscopic scales analysed is the line list, however all them show equal trends with [Fe/H]. It therefore implies that the selection of the line list does not significantly improve the accuracy of spectroscopic T_{eff}, at least not for [Fe/H] values far from solar. Another result important to highlight is that even though the T_{eff} scale of Bensby, Feltzing, and Oey (2014) considers non-LTE corrections, it shows the same trend with [Fe/H] as the others. This result could be however misleading because the scatter of the trend is large and the comparison is only comprised by 10 stars. A larger sample and tests with other non-LTE T_{eff} scales should provide stronger results. From this analysis I conclude that, besides the LTE

[3]Maldonado et al. (2015) find an offset of 41 K, which is not significant considering the ~ 100 K error bar relative to their IRFM calculations.

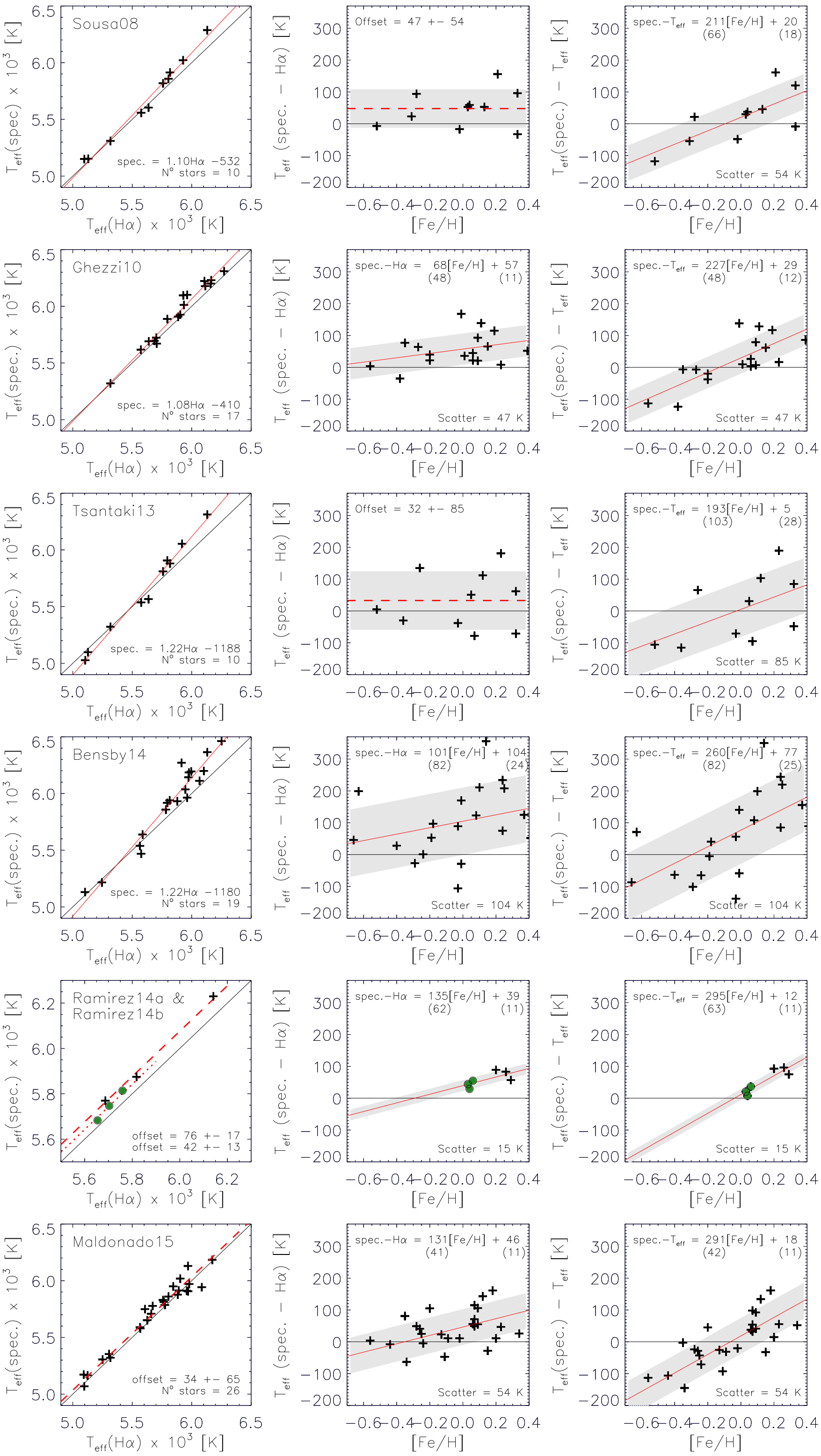

FIGURE 5.4: As in Fig. 5.2 but for spectroscopic T_{eff}. The authors are indicated in the plots in the left panels. In all plots, the black lines represent the perfect agreement, the red lines represent the trends, and the shades represent the scatter. When the trends are not significant, the offsets are drawn with dashed red lines. T_{eff} from Ramirez14a (plus symbols) and Ramirez14b (green circles), derived with the same method, are compared in the same plots. The right panels show comparisons of the spectroscopic scales with respect to accurate interferometric T_{eff}, obtained by applying Eq. 4.2 to $T_{\mathrm{eff}}^{\mathrm{H}\alpha}$(1D LTE)

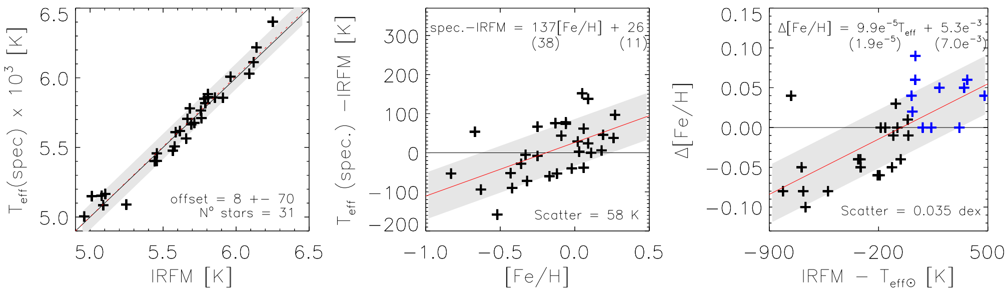

FIGURE 5.5: *Left and middle panels:* Similar to Fig. 4.11 but for the IRFM $T_{\rm eff}$ of Ramirez13 against the spectroscopic $T_{\rm eff}$ of Sousa08. *Right panel:* Δ[Fe/H] represent the metallicity values of Sousa08 with respect to those of Ramirez13. The blue symbols are the stars with over-solar $T_{\rm eff}$.

assumption, the most probable culprit for such trends is the $T_{\rm eff}$–[Fe/H] degeneracy that is maximized when several atmospheric parameters are derived simultaneously by the excitation/ionization equilibrium of Fe lines.

Chapter 6

Results: Effective temperature of M67 stars

The Open cluster (OC) M67 is a Rosetta Stone for understanding the lithium evolution in F- and G-type stars. The study of the lithium evolution can help validate theories of the origin of the Universe, and of the formation and evolution of solar-like planetary systems. The Li abundance measurement in stellar spectra is strongly dependent on T_{eff}, which must be determined with models for the vast majority of stars, the reason why the exhaustive effort for developing more realistic models is plenty justified.

There are three observations that that support the Big bang model: the cosmic expansion, the cosmic microwave background radiation, and the big bang nucleosynthesis (BBN). The BBN (Wagoner, Fowler, and Hoyle, 1967; Burles, Nollett, and Turner, 2001) predicts the primordial abundances of the elements: He, H (as deuterium), and Li, that were produced during the first minutes of the Universe when it was dense and cool enough for nuclear reactions to take place. Using the measurements of the density of the baryonic matter obtained with the Planck satellite mission (Coc, Uzan, and Vangioni, 2014), and previously with the Wilkinson Microwave Anisotropy Probe (WMAP) mission (Spergel et al., 2007), the abundances of the elements above were calculated. Subsequently, they were compared with spectroscopic observations of the atmospheres of the oldest stars, where the abundances were expected to be preserved. The comparisons were satisfactory for all elements except for Li: BBN predicts the precise value [Li/H] = 2.66-2.73 dex, while the observed value is around three times lower (Spite and Spite, 1982; Ryan, Norris, and Beers, 1999, the "Spite plateau"), which constitutes the so called "Lithium Problem".

The interpretation of the stellar observations is however not trivial because Li can be destroyed in the stellar interior at temperatures above 2.5×10^6 K and, at the same time it is produced in the Galaxy by several mechanisms. Furthermore, it is not clear which are the dynamical processes in the stellar interiors that could deplete Li from the stellar atmosphere without necessarily destroying it. Li is measured using its most prominent line Li I at 6707.81 Å – usually the only one measurable in low S/N spectra from cluster stars –, for which T_{eff} changes of 100 K translate to 0.1 dex changes in [Li/H].

A smart way to study the Li evolution is the analysis in stellar clusters: under the reasonable assumption that the cluster members have a common birth from a chemically homogeneous primordial cloud, the effects of the stellar evolutionary variables are isolated. However, it is not straightforward to perform such analysis because of the limited precision imposed by the observation of faint cluster stars. Other more complicated problems to solve are related to the techniques from which T_{eff} is derived. All stellar parameters involved (e.g. mass, radius, age, chemical composition, stellar rotation, asteroseismological properties, luminosity, and distance) are dependent on T_{eff}, which has to be derived from models because direct measurements are not available for distant stars. Among all techniques, T_{eff}–color relations are used most frequently, and some times the fitting of evolutionary tracks or Balmer lines are used. The diagnostic by excitation & ionization equilibrium of Fe lines is usually avoided to prevent degenerate atmospheric parameters, considering that only small variations in abundances between stars are expected. The problems of deriving T_{eff} from T_{eff}–color relations are the accuracy and precision of the scale, and the possible uneven distribution of reddening in the cluster. An inaccurate T_{eff} scale produces systematic biases in other parameters only when the star-to-star [Fe/H] variation is negligible (consider that T_{eff}–color calibrations are always dependent on [Fe/H]), otherwise the effect of T_{eff} biases are difficult to predict. The precision of the T_{eff} scale depends on the color precision and the technique with which it was calibrated, and it directly impacts on the Li abundance spread. Reddening is probably the worst problem: estimates from dust maps often allow a single average value for all cluster members, but individual values could be significantly different. For example, non-homogeneous interstellar absorption was observed around Ca II lines for some M67 cluster stars (Curtis, 2017).

A series of discussions that illustrate the problems above are, for example, summarised in Korn (2008). It cites the studies of Korn et al. (2006) and Korn et al. (2007) on the evolution of Li and other elements in the metal-poor globular cluster NGC 6397 ([Fe/H] ≈ -2 dex). Their observational measurements suggest that the evolution of the abundances can be explained by 'non-standard' models that consider mixing processes further than convection. Fig. 6.1 shows that a model that includes "atomic diffusion" reasonably agrees with the observed Li depletion along the evolutionary path, and that from the observed abundances, the models predict an initial abundance value [Li/H] = 2.54 $\pm$0.1 dex very close to the BBN predictions. These results were however criticised by Bonifacio et al. (2007), who argued that the T_{eff} scales from Hα and photometric colors are not fully consistent, and that using only T_{eff} from photometric colors could remove the evolutionary signatures shown, and hence the meaning of the results.

Plenty of Li abundance measurements in similar field stars, as in stars belonging to associations, support the incompatibility with predictions from evolutionary models that only consider convection as a mixing agent. For example, a large Li spread is observed in solar-type stars in the main sequence, whose convective zone bases do not reach the layers in the stellar interiors where the temperature is high enough to burn Li, the reason why Li depletion should not occur (Deliyannis, Barrado y Navascues, and Stauffer, 2000; Pasquini, 2000, among others). Lithium depletion in solar-type stars can be caused, otherwise, by mixing of the material of photospheric layers with hot interior layers, trough processes such as diffusion, meridional circulation, and internal gravity waves (Talon, 2008). Many observational tests have been performed to constrain the relevance of such processes as a function of mass and age, but the results are still imprecise; however diffusion and rotation-induced mixing appear the main candidates (e.g. Sestito and Randich, 2005; Canto Martins et al., 2011; Pace et al., 2012; Castro et al., 2016; Bertelli Motta et al., 2018; Souto et al., 2018; Souto et al., 2019).

The large Li spread observed in field stars has been related to their rotational history, hence to planet formation (Bouvier, 2008). This hypothesis was considered by Gonzalez (2008) and Israelian et al. (2009) to explain the higher Li depletion found in stars with detected planets. However, these observations were better explained

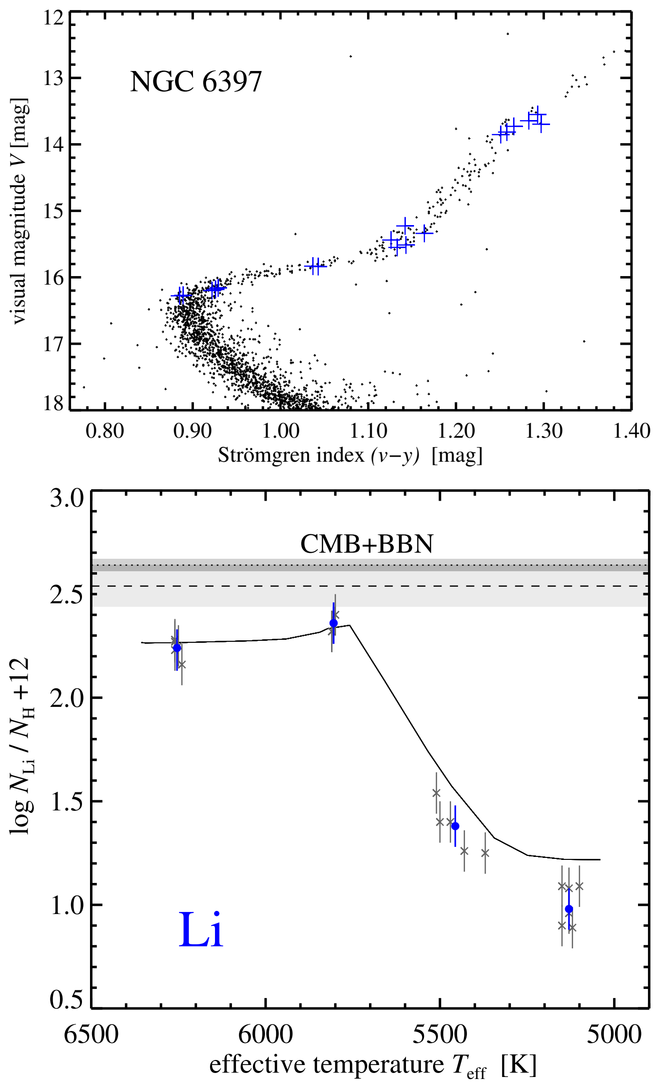

FIGURE 6.1: Adapted from Korn et al. (2006, Figs. 1 and 2). *Top panel:* Loci of the observed stars in the observational parameter space. The observed stars represented by blue crosses in the turnoff, the subgiant branch, the base red-giant branch, and the red-giant branch, from the left to the right. *Bottom panel:* Lithium as function of T_{eff} of the observed stars in the plot on the top panel. The horizontal axis locates the stars from the less evolved to the most evolved, i.e. from the turnoff to the red-giant branch. The grey crosses are the individual measurements, while the bullets are the group averages. The solid line shows the predictions of the model that considers diffusion (as described by Richard, Michaud, and Richer, 2005), with the original abundance given by the dashed horizontal line. The dotted line is the abundance calculated by the WMAP mission (Spergel et al., 2007). The shaded areas are the errors of both the WMAP measurements and the predictions of the model.

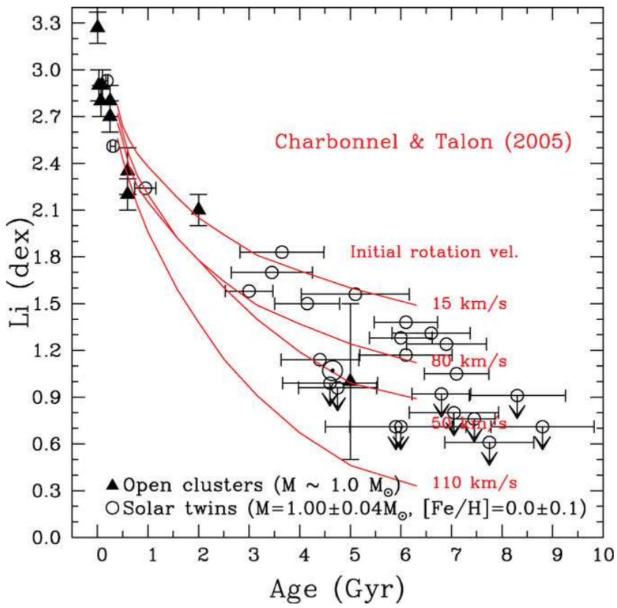

FIGURE 6.2: Adapted from Meléndez et al. (2010b). Li abundance of solar twins with 1 solar mass (±4%) and solar [Fe/H] (±0.1 dex), and for one-solar-mass stars in solar metallicity (±0.15 dex) open clusters selected from Sestito and Randich (2005) and Pasquini, Biazzo, Bonifacio, et al. (2008). Field stars are shown as circles while open clusters as triangles. Relations from Charbonnel and Talon (2005) are plotted in red.

by analysis performed with stars with more restricted parameters. Namely, the segmentation of Li abundances found by the authors above are compatible with a time-progressive depletion increased by rotation-induced mixing, in other words Li depletion as a function of the age rather than due to planetary presence (Meléndez et al., 2010b; Ghezzi et al., 2010a; Baumann, Ramírez, Meléndez, et al., 2010); see Fig. 6.2.

The Li spread observed in OC in early studies, for example in the Pleiades (Duncan and Jones, 1983; Soderblom et al., 1993a), Praesepe (Soderblom et al., 1993b), and M67 (Spite et al., 1987; Pasquini, Randich, and Pallavicini, 1997; Garcia Lopez, Rebolo, and Beckman, 1988), was revised. The revision on the Pleiades showed that the Li dispersion can be attributed to an uneven reddening distribution over the cluster stars, stellar surface activity, and the presence of spots (King, Krishnamurthi, and Pinsonneault, 2000; Xiong and Deng, 2005; Xiong and Deng, 2006). The low Li dispersion, or its absence, observed in old and moderately old OC (thus with stars with less activity) seems to support this hypothesis, for example: Hyades (0.8 Gyr) (Thorburn et al., 1993), M 34 (0.2 Gyr) (Jones et al., 1997), NGC 188 (4.3 Gyr) (Randich, Sestito, and Pallavicini, 2003), NGC 752 (1.1 Gyr) (Sestito, Randich, and Pallavicini, 2004), and Berkeley32 (3.3 Gyr) (Randich et al., 2009). On the other hand, there are other old clusters for which the scatter is still debatable, for example NGC 3680 (1.8 Gyr), and M67 (4 Gyr).

NGC 3680 was analysed by Anthony-Twarog et al. (2009), who based their abundance measurements on $T_{\rm eff}$ scales from two $T_{\rm eff}$–color relations: one (Deliyannis, Steinhauer, and Jeffries, 2002) is suited for stars in the main sequence and turnoff, which represent the majority of the their sample, and the other (Ramírez and Meléndez, 2005) was used for giants. The former relation is, in turn, based on a $T_{\rm eff}$–$(B-V)$

relation calibrated comparing spectrophotometry with synthetic flux distributions; (see Deliyannis et al., 1994; Carney, 1983). The latter relation was carefully examined by Casagrande et al. (2010), who showed its serious biases and scatter. The use of the $T_{\rm eff}$–$(B-V)$ color relations above results, in my opinion, are at least suspicious for part of the Li abundance scatter reported, and a revision of this work based on precise $T_{\rm eff}$ scales should be performed.

M67 is a very interesting OC, not only for the understanding of mixing processes and the context of lithium, but also because it has characteristics extremely similar to those of the Sun, allowing us to delve into fundamental questions regarding to the formation of the Solar System and Earth-like planets. These are, a nearly solar age (4 Gyr, Castro et al., 2011; Yadav et al., 2008b), and solar metallicity (Randich, Sestito, Primas, et al., 2006; Pace, Pasquini, and François, 2008; Pasquini, Biazzo, Bonifacio, et al., 2008; Önehag, Korn, Gustafsson, et al., 2011). Hence, several solar twins have been identified in it (Pasquini, Biazzo, Bonifacio, et al., 2008; Önehag, Gustafsson, and Korn, 2014), and even some stars with planetary companions (Brucalassi et al., 2014; Brucalassi et al., 2017). A reddening average value for the cluster was determined, $E(B-V) = 0.041$ (Taylor, 2007), and its distance modulus as well, $\mu = 9.56$-9.72, or $D = 800$-860 pc. Several recent studies indicate the evidence for atomic diffusion as the main mixing mechanism responsible for the small chemical inhomogeneity observed along the evolutionary path (Blanco-Cuaresma et al., 2015; Bertelli Motta et al., 2018; Souto et al., 2018; Souto et al., 2019).

Using HARPS spectra collected in the past 10 years, together with GAIA information (Gaia Collaboration et al., 2016b; Gaia Collaboration et al., 2018), I determined $T_{\rm eff}$ and mass of a sample of 52 single M67 stars with unprecedented accuracy. The stars are listed in Table 2.3. The HARPS-based Li abundances will allow the accurate description of the behavior of Li with stellar mass at 4 Gyrs; see for example (Pace et al., 2012; Castro et al., 2016). This is by far the largest sample of stars with systematic parameter determination performed in this cluster.

6.1 Suitability of HARPS

The first mandatory task prior to applying the Hα profile fitting to the spectra of the M67 stars, is to prove the absence of residual instrumental features in their spectra. Most of the search for planetary companions in M67 has been performed with HARPS; see Brucalassi et al. (2017, Table A.1) to check details such as instrument, number of observations, mean stellar RV determined, average RV error, RV dispersion, and binary candidates. Having shown the ability of the normalization-fitting method to recover reliable Hα profiles using the blaze-free coudé spectra as template (Sect. 3.1), I apply it to HARPS (Mayor et al., 2003). Thus, the presence of residual blaze in HARPS should be revealed empirically by systematic different temperatures.

HARPS, in order to achieve high radial-velocity precision, has a very stable field and pupil injection. It is also thermally stable and in vacuum. In addition, the HARPS archive contains plenty of observations of solar-type stars, including a rich set of solar spectra taken by observing solar system bodies for many years. All these characteristics make HARPS the ideal instrument to investigate the precision of the normalization method that I have developed. The fact that the solar-sibling observations have been repeated for several years allows to also investigate the stability of this instrument in time, and to determine to what extent the HARPS Hα profile has remained constant in time.

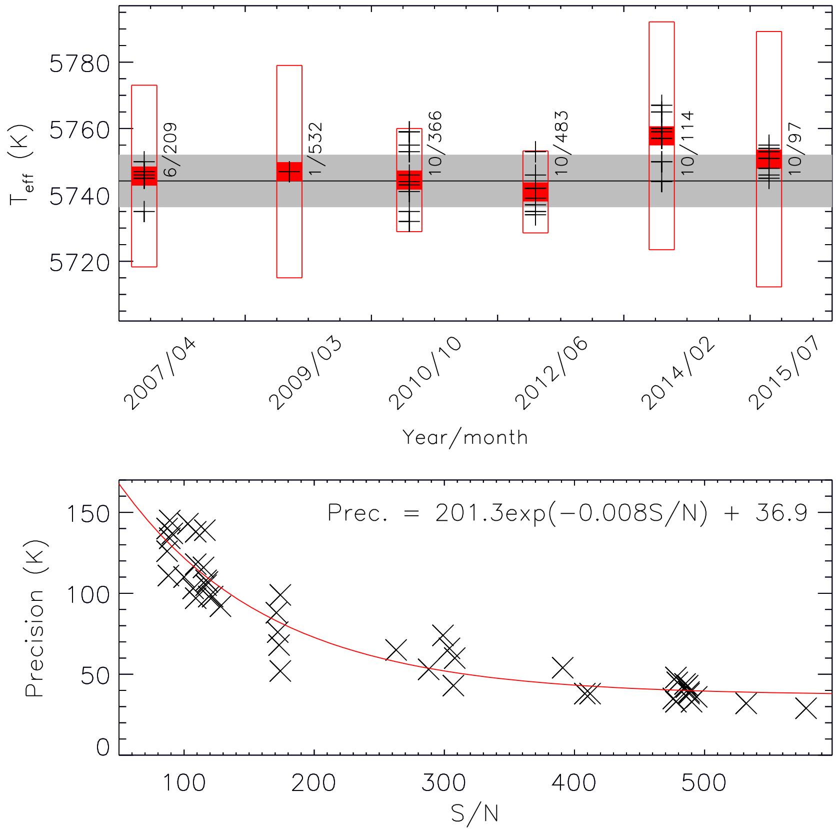

FIGURE 6.3: *Top panel:* Temperatures of the HARPS solar proxies in Table 2.2 vs. the date upon which spectra were acquired. Daily values are represented by plus symbols and weighted means and errors for each month are drawn in red. The weighted mean and error of all the measurements are represented by the continuous line and the shade on 5744 ±10 K. Next to the bars, the number of spectra analysed and the mean S/N are noted. *Bottom panel:* Errors of individual measurements in the top panel are plotted vs. S/N. The exponential curve given by the equation in the plot is the best fit to the points.

The first test is performed with all solar spectra set out in Table 2.2, for which $T_{\rm eff}^{\rm H\alpha}$(1D LTE) values were derived. The plot in the top panel of Fig. 6.3 visually summarises the results displayed in the table. For each date, $T_{\rm eff}^{\rm H\alpha}$(1D LTE) values are represented by plus symbols. Their weighted mean and corresponding spread values are drawn with bars. Next to them, the number of spectra used and their average S/N ratio are noted to show the precision reached when measurements from several spectra are combined. The weighted mean and spread of all measurements are represented by the horizontal line and the shade at 5744 ± 10 K. Evidently, there is no trend with time and the scatter is very low, which confirms the blaze stability of HARPS. This value is in perfect agreement with that of the coudé data (see values in Table 4.1), which implies that not only is the blaze stable but it is also fully removed through the flat-field procedure. In the bottom panel of Fig. 6.3 I plot the precision obtained from individual spectra as a function of S/N. It is observed that ∼40 K can be obtained from spectra of S/N = 400-500, which is close to saturation. Precision values for S/N below 100 are analysed in the next section.

In the second test I compare the temperatures derived from HARPS with those derived from coudé spectra for the stars in common in both samples; check stars

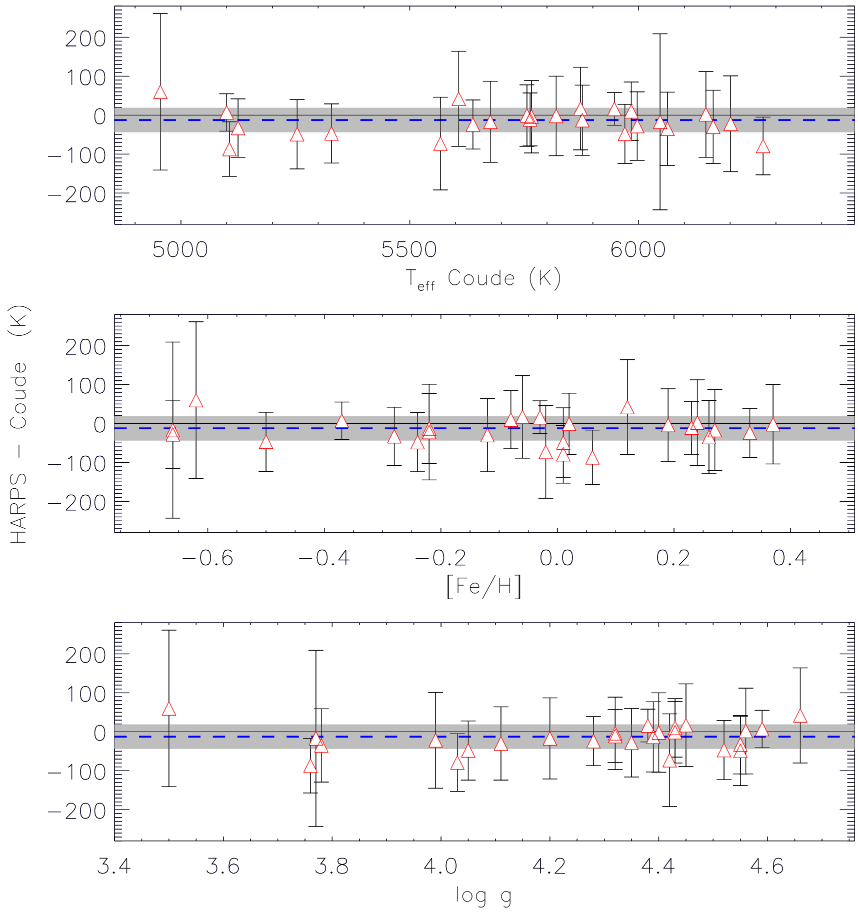

FIGURE 6.4: Temperature diagnostics from HARPS with respect to those of coudé vs. atmospheric parameters; related fits for both kind of spectra are presented in Appendices A and B. [Fe/H] and $\log g$ values from Table 2.1 were used here. The -13 K offset and its 34 K scatter are represented by the dashed lines and the shades, respectively.

in common in Table 2.1. The collection, reduction, and normalization-fitting of this set of HARPS spectra were performed by Maria Ubaldo-Melo from Observatório do Valongo; the fits of these spectra are presented in Appendix B. The application of the normalization-fitting procedure (Sect. 3.1) by two different people for each sample allows to account for biases related to subjective criteria of users of the procedure. The comparison is shown in Fig. 6.4 vs. $T_{\rm eff}$, [Fe/H], and $\log g$. It shows an excellent agreement with a negligible offset between the two samples of -13 ± 34 K with no trends. The temperatures of all stars agree within 1σ errors, with the exception of two (δ Eri and HD 184985) that agree within 2σ.

The results of the two tests are consistent with a null presence of remaining blaze features in HARPS spectra along time. Therefore, HARPS is fully suitable for applying the Hα profile fitting. The very small offset and scatter resulting from the comparison of the stars in common with the coudé sample confirms that the normalization–fitting integrated method (Sect. 3.1) minimises random and systematic errors related to the custom normalization procedure by polynomial interpolation. Hence, when this method is applied, the internal errors of the Hα profile fitting are entirely due to the spectral noise. Further, as the plot in Fig. 6.3 shows, there is no bias of temperature as a function S/N for the range analysed. For example, the data of last date 2015/07, which have S/N as low as $\sim$90, present temperature values very close to the average.

6.2 Hα profile fitting of M67 HARPS spectra

The S/N of the M67 HARPS spectra are very low compared with those used in the previous section. Their S/N are in between 7 and 33 (see histogram in Fig. 6.7), while the solar spectra have at least S/N = 87, and the Hα-test-sample have at least S/N = 100 (Sect. 2.1). It is therefore required to check if spectra with S/N as low as those of M67 produce systematic errors in the temperature determinations when the fitting procedure described in Sect. 3.1.2 is applied.

To test this, I used one of the solar normalized spectra from Table 2.2: the spectrum reflected on Moon observed in 2009/03. From it, I created various noise-increased spectra and performed fittings with the 1D LTE synthetic models (Barklem et al., 2002). I observe that the temperature determined by the fitting procedure decrease progressively as the noise increases; the corresponding fits are shown in Fig. 6.5. I also observe that the precision of the determinations deteriorates rapidly with the noise, reaching more than 600 K for S/N = 15, which is a typical S/N for the M67 spectra. Obviously, these systematics and very low precisions make the technique not competitive as long as the spectra are used in their original state.

A second test is then performed with resolution-degraded spectra, the S/N of which is naturally increased by the degradation process. The spectra in Fig. 6.5, and several other noised spectra, were degraded to the same resolution as coudé (R = 45 000), and were subsequently fitted. The related fits are presented in Fig. 6.6, the order of which goes from high to low S/N, as in Fig. 6.5. Their retrieved temperatures and corresponding errors are plotted in Fig. 6.7, to which I refer the reader for the discussion below. The temperatures follow a similar pattern with S/N observed for the non-degraded spectra: cooler values for lower S/N. Notice however that the temperatures derived from degraded spectra are not as cool as those from the original ones, for example: the temperature related to the spectrum with S/N = 15 is 5560 K (Fig. 6.5), while the temperature of its corresponding degraded spectrum is 5690 K (Fig. 6.6). The plot in the figure shows that the temperature decreases significantly for S/N < 25 (S/N values corresponding to the original spectra), reaching $\sim$5600 K for S/N = 5. The histogram in the bottom plot in the figure shows that most of the M67 spectra have S/N between 6 and 18. Considering this, I computed the weighted average temperature for the degraded solar spectra with S/N < 18, resulting 5640 $\pm$ 51 K. The difference between this value and the temperature obtained with coudé/HARPS/MUSICOS spectra (5774 $\pm$ 1 K, represented by the dashed line in the plot) is therefore the estimate of the most probable bias that the analysis of the M67 spectra will involve. This is a rough correction of +100 K that was applied to all retrieved temperatures to obtain $T_{\rm eff}^{\rm H\alpha}$(1D LTE). Notice also that by averaging several low S/N spectra, including two spectra with S/N > 10, the precision obtained is $\pm$50 K. This is the maximum expected for the available data. For stars with spectra with S/N < 10, a precision of 100 K is expected.

Besides the +100 K correction, other changes were applied to 'adapt' the Hα normalization-fitting method described in Sect. 3.1 to spectra with very low S/N: *i)* The check of the presence of telluric features is avoided, given that their contribution is negligible in spectra of such low quality. *ii)* No checking of compatibility in the transition regions is performed, but an even distribution of the noise around the continuum. With excessive noise, checking the compatibility in the transition regions makes no sense. However, as shown in the central panels of Fig. 6.6, the peaks

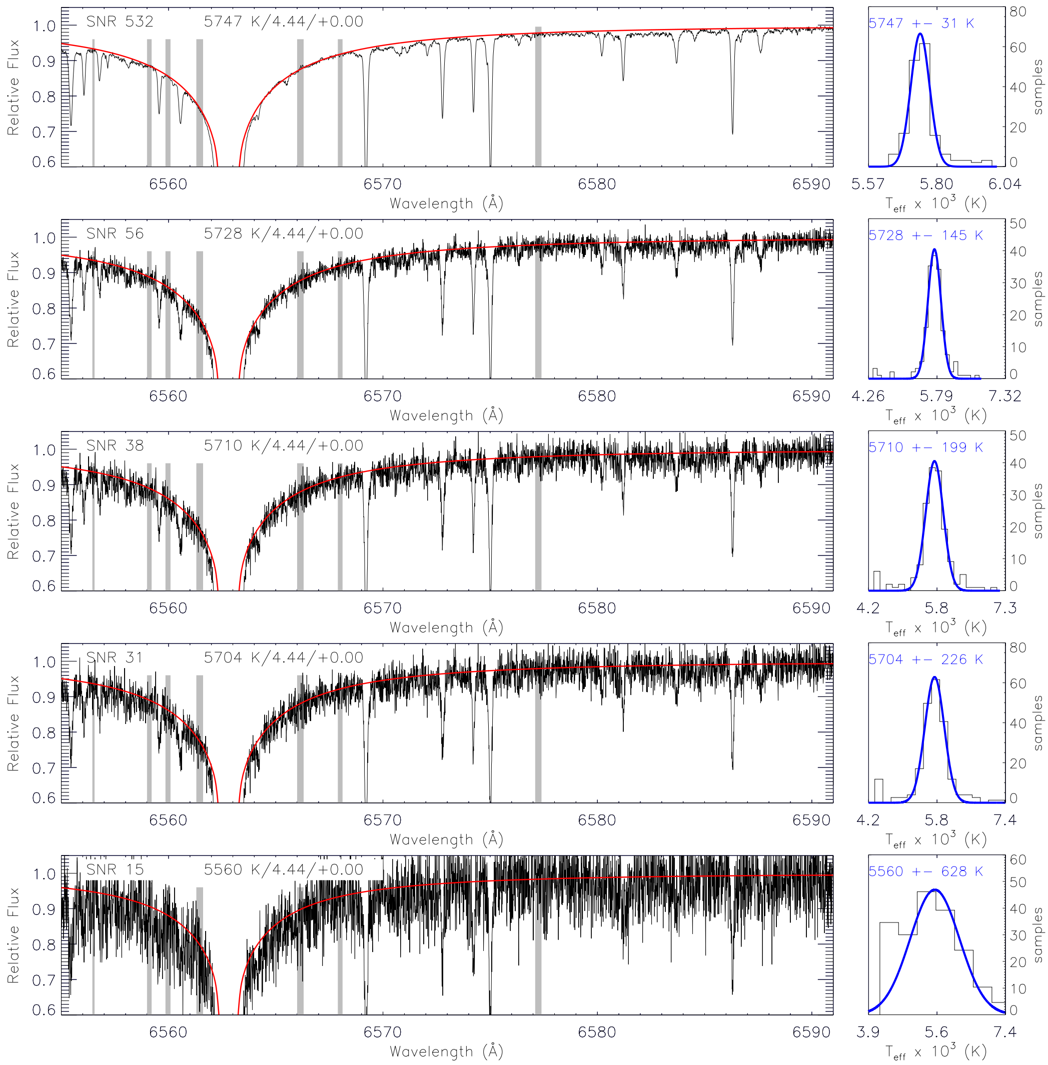

FIGURE 6.5: Fits of noise-increased solar Hα profiles. The plot on the top is the fit of the original profile as observed. The S/N of each spectra are shown in the plots. The retrieved temperatures are also shown in the plots. The right panels are the temperature distributions of the wavelength bins inside the windows of fits displayed by the shades in the plots on the left; as shown in Figs. 3.3 and 3.4. No further normalization was applied to any profile.

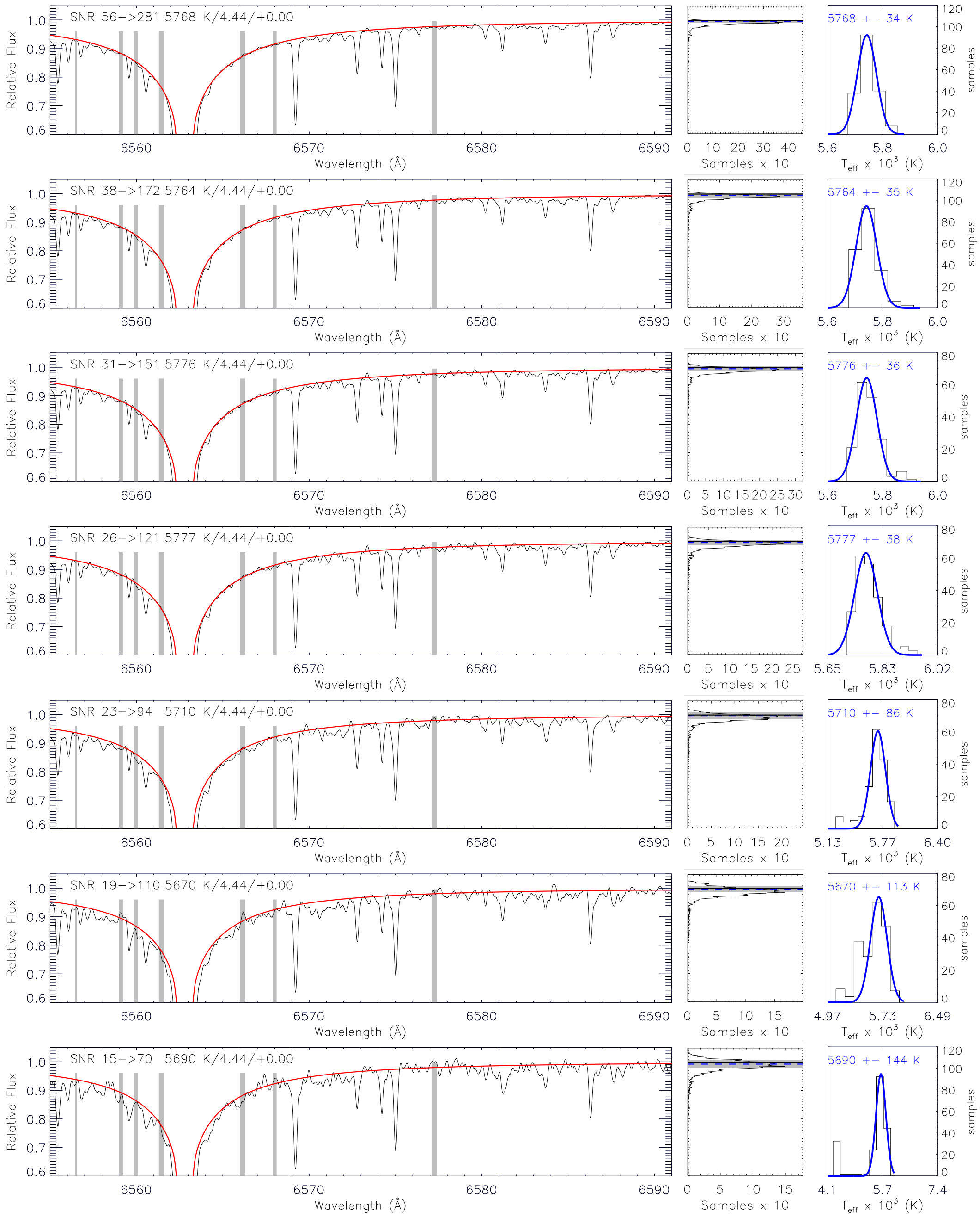

FIGURE 6.6: Same as in Fig. 6.5 but with spectra degraded to R = 45 000. The S/N of the spectra (both degraded and non-degraded) are shown in the plots. *Central panels :* Similar to Fig. 3.6, flux histograms of the spectra on the left panels with the same flux scale; wavelength ranges out of Hα only were considered. The black horizontal line points the continuum, the dashed line is the average flux of the 5 continuum windows of Fig. 3.3 and the shades are the spread. The figure continues next page.

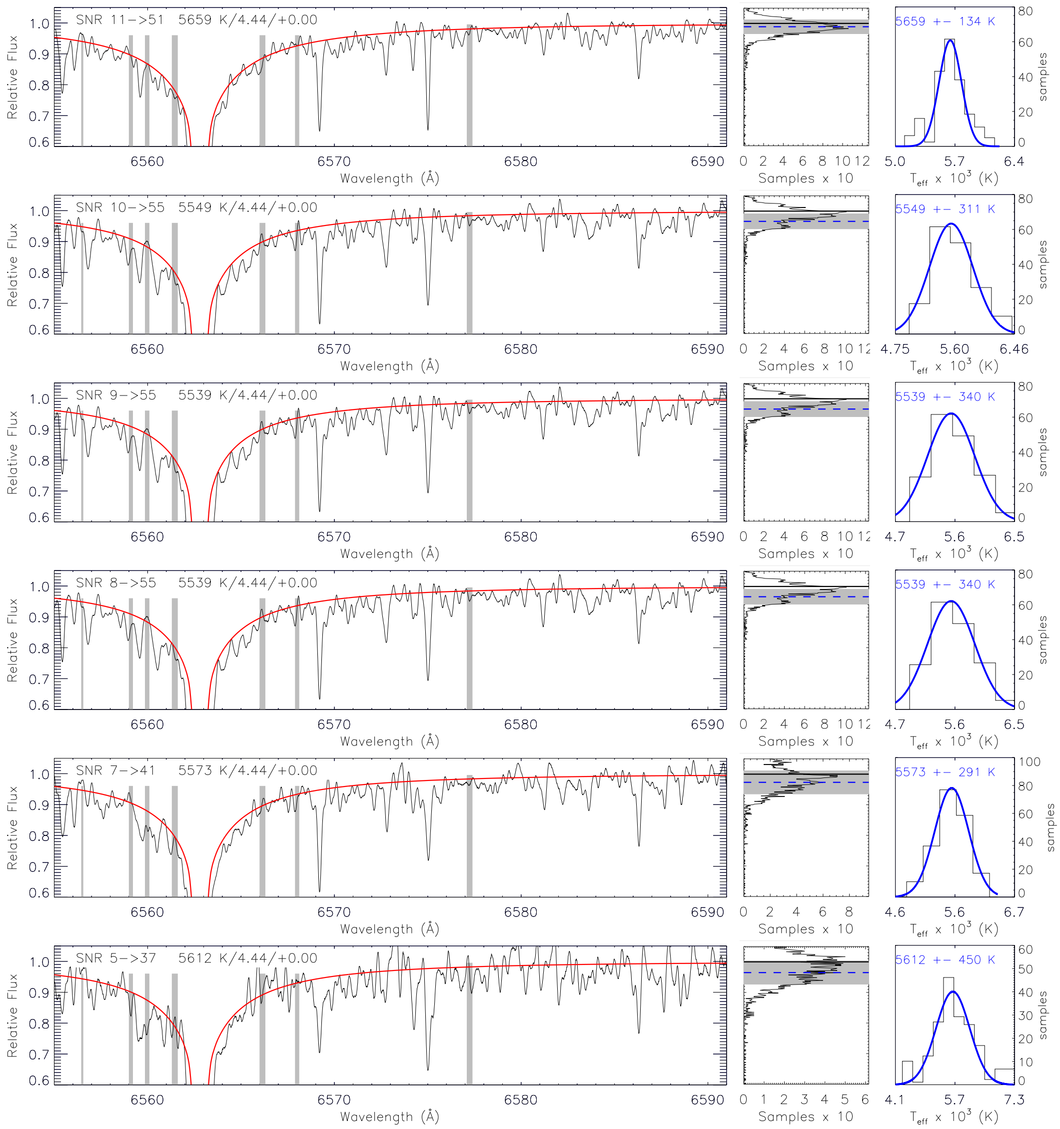

FIGURE 6.6: Same as in Fig. 6.5 but with degraded spectra to R = 45 000. The S/N of the spectra (both degraded and non-degraded) are shown in the plots. *Central panels :* Similar to Fig. 3.6, flux histograms of the spectra on the left panels with the same flux scale; wavelength ranges out of Hα only were considered. The black horizontal line points the continuum, the dashed line is the average flux of the 5 continuum windows in Table 3.2, and the shades are the spread. First plots of the figure are in the previous page.

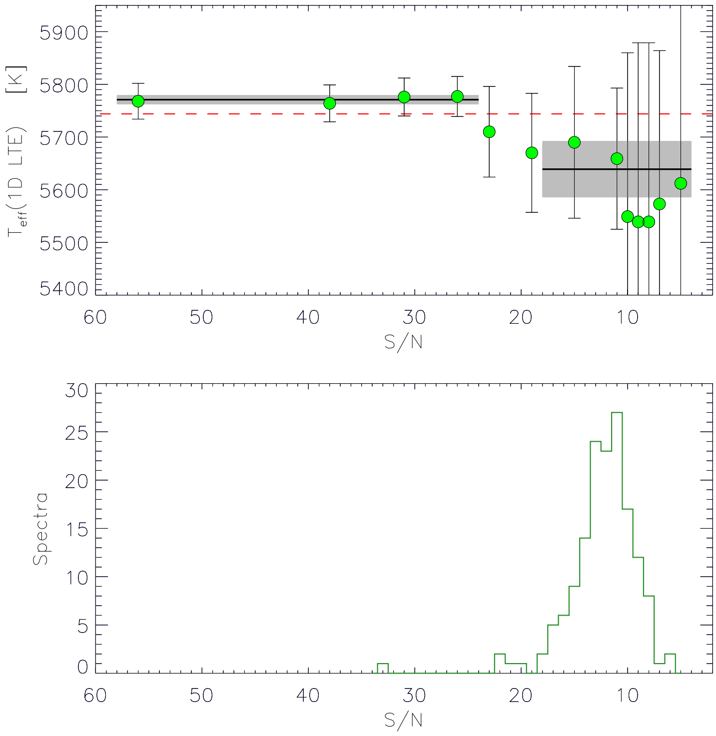

FIGURE 6.7: *Top panel:* Temperatures derived with the profiles in Fig. 6.6. The continuous lines and their shades indicate the weighted means and errors of the temperatures they cover along the horizontal axis. The dashed line represents the zero point of the Hα scale determined with coudé/HARPS/MUSICOS spectra. *Bottom panel:* Histogram of the S/N of the spectra for M67 stars analysed in this work. The axis of the plot has the same scale as the plot on the top to help the reader visualize the expected bias and errors that the fitting method produces when applied to the M67 spectra.

of the flux histograms of the spectral ranges not affected by Hα reasonably match the continuum. Therefore, the same pattern is expected for the other spectra.

I validate the adapted method with the solar twin YBP 1194, for which Önehag, Gustafsson, and Korn (2014) obtain 5780 K with high S/N spectra. Fig. 6.8 shows all fitted spectra of YBP 1194. The figure shows that the peaks of the flux histograms roughly match the unity and also that the mean flux of the continuum windows (Table 3.2) are close to one within 1σ error. The temperatures shown in the plots correspond to the values retrieved by the fitting procedure without applying any correction. Thus, the final temperature is given by the weighted average plus the correction of +100 K, plus the correction of +28 K determined to correct the offset of the model (Eq. 4.2) for the metallicity of the cluster. This results in 5800 ± 102 K, in total agreement with the determination of the authors above.

The adapted normalization-fitting is applied to the M67 spectra listed in Table 2.4, after these were degraded. The table lists the S/N of the original spectra, their related $T_{\rm eff}^{\rm H\alpha}$(1D LTE), and their weighted average with their corresponding errors. I remark that by $T_{\rm eff}^{\rm H\alpha}$(1D LTE), I refer to the retrieved temperatures corrected by +100 K only. For the fittings, it was required to introduce [Fe/H] and log g beforehand. [Fe/H] was fixed to solar, considering that its possible evolutionary variations are too small to impact the temperature. Gross preliminary log g were derived by Diego Lorenzo-Oliveira from Instituto de Astronomia, Geofísica e Ciências

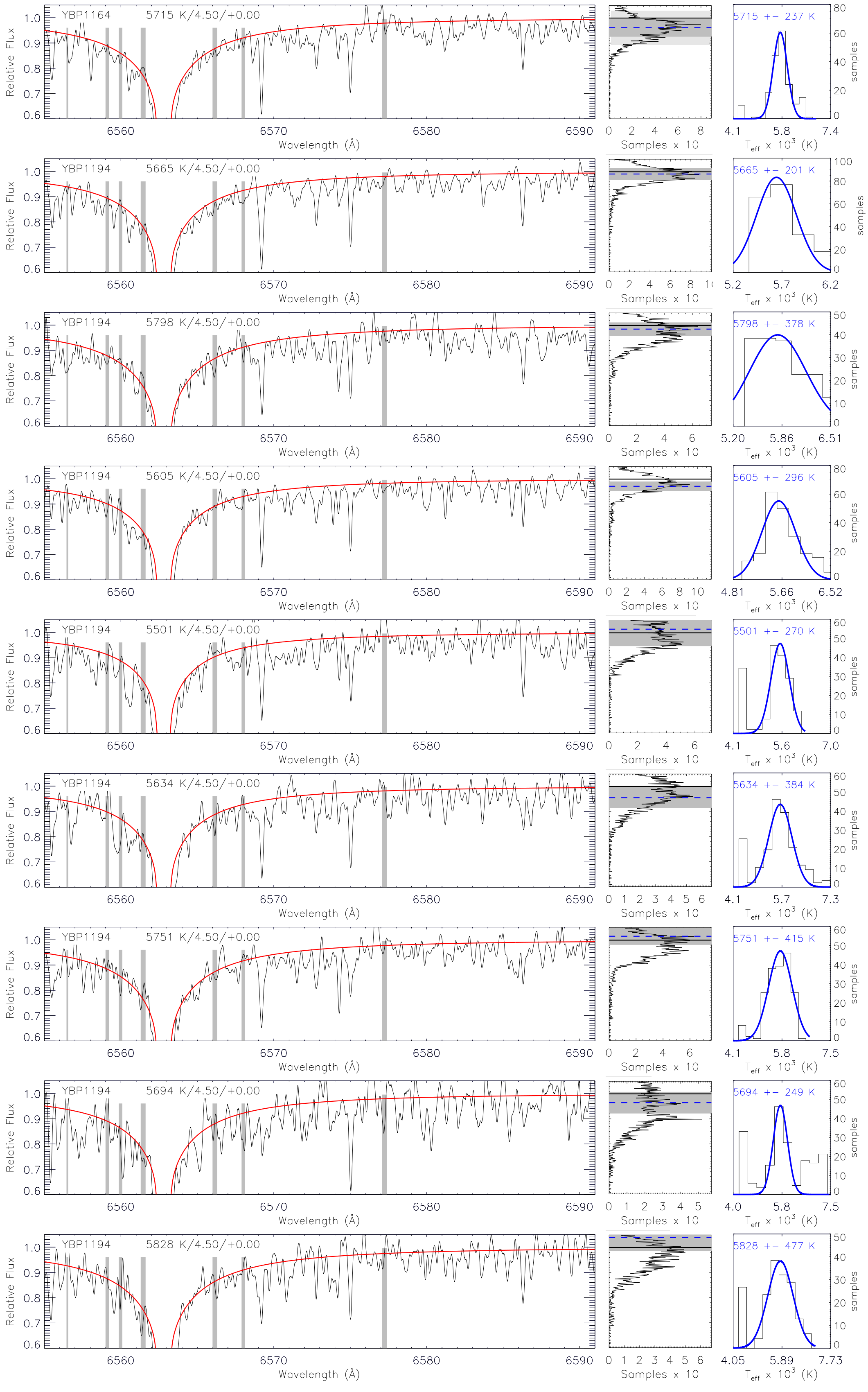

FIGURE 6.8: Similar to Fig. 6.6, but for the degraded spectra of YBP 1194. The retrieved temperatures and their errors are shown in the legends of the plots. Notice in the right hand panels that the mean flux of the continuum windows (Table 3.2) represented by the dashed line clusters around unity for all panels.) The figure continues next page.

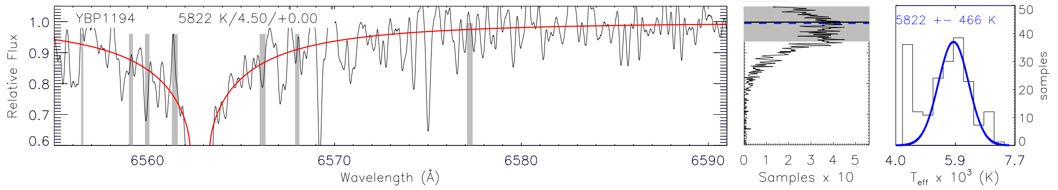

FIGURE 6.8: Similar to Fig. 6.6, but for the degraded spectra of YBP 1194. The retrieved temperatures and their errors are shown in the plots. First plots of the figure are in the previous page.

Atmosféricas (IAG/USP) by fitting evolutionary tracks, and were used for the Hα fittings only. The method applied by Diego Lorenzo-Oliveira follows the procedure described in Grieves et al. (2018). It employs the evolutionary tracks of Kim et al. (2002), and Yi, Kim, and Demarque (2003), metallicity, effective temperature, and luminosity. IRFM $T_{\rm eff}$ was used as effective temperature, which was computed using the $(B-V)$–$T_{\rm eff}$ relation of Casagrande et al. (2010), with colors derredened by 0.041 mag (Taylor, 2007). Luminosity was estimated from IRFM $T_{\rm eff}$, the bolometric calibrations of Torres (2010), and Gaia parallaxes. Table 2.3 lists the compiled Gaia parallaxes, IRFM $T_{\rm eff}$, and $T_{\rm eff}$; plus Gaia, Johnson-Cousins, and 2MASS photometry that will be used in the future to improve IRFM $T_{\rm eff}$, and thus improve the temperature comparison below as well. $T_{\rm eff}$ was derived from $T_{\rm eff}^{\rm H\alpha}$(1D LTE) by applying the correction of +28 K for the cluster metallicity (Eq. 4.2). Surface gravity, mass, radius and age will be derived as described above once the temperatures from all photometric colors are derived.

Figure 6.9 shows a comparison between both sets of temperatures, the scales of which are compatible according to the analysis done in Sect. 5.1.1, as demonstrated by the right plot in Fig. 5.2. It is observed that the temperatures agree for all stars within 1σ errors except for YBP 689 which is pointed with the green symbol. A more meaningful comparison is given by the offset between both scales, which is found to be 20 K favoring hotter values for Hα. This offset can be attributed to several reasons. The first one is a possible systematic error involved in the normalization of Hα profiles. A systematic error of +20 K would imply an average shift of the continuum of only 0.2% towards lower fluxes, which is still a good result for the quality of the analysed spectra. Assuming no systematics from normalization, systematics on the photometric colors measurements may be considered, and/or an underestimation of reddening. In the latter cases, the temperature offset would be caused by an excess of $\sim$0.005 mag in $(B-V)$, which I highlight, is nearly the third of the average error of $(B-V)$ of the M67 stars; see values in Table 2.3. The main culprit for this offset can be determined by including the 2MASS colors when computing IRFM $T_{\rm eff}$, which would improve the precision from an average value of 100 K to $\sim$30 K. To the date of this thesis, IRMF $T_{\rm eff}$ cannot be improved by using Gaia colors because there are no IRFM calibrations available yet, however I am already working on empirical Gaia color–$T_{\rm eff}$ calibrations based on the accurate temperatures of the stars in the Hα-test sample. In the near future, IRFM $T_{\rm eff}$ and Hα $T_{\rm eff}$ will be used in combination to derive mass and Li abundances for this large sample of M67 stars; more details are given in the next chapter.

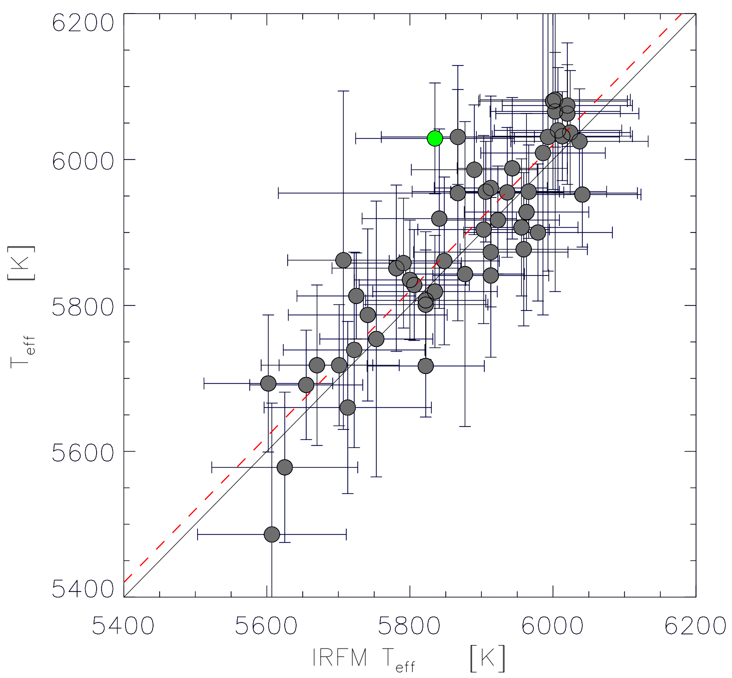

FIGURE 6.9: Comparison of IRFM T_{eff} with T_{eff} derived fitting Hα profiles (whose scale was corrected by Eq. 4.2). IRFM T_{eff} was computed using $(B - V)$ colors of Yadav et al. (2008b) only, dereddened by 0.041 mag (Taylor, 2007). The dashed line represents the constant offset of 20 K between the two temperature scales. The green point represents the only star for which discrepant temperatures were obtained.

Chapter 7

Summary, conclusions, and perspectives

I made an overview of the most often used techniques for deriving effective temperature (T_{eff}) in F-,G-, and K-type stars. These are Interferometry, InfraRed Flux Method (IRFM), excitation & ionization equilibrium of Fe lines (spectroscopy), and Hα profile fitting. All without exception deppend on model atmospheres, although the degree of dependence is marginal for the; the two former techniques.

I made a diagnostic of accuracy of the techniques above, based on Interferometry as the standard T_{eff} scale. For this purpose, I chose to work with the stars with interferometric T_{eff} selected by Heiter et al. (2015, Gaia Benchmark stars), given that several of them are supported by the most sophisticated observations, and are proven to be free from major model-induced biases. The diagnostics of accuracy do not consist simply on comparing the interferometric T_{eff} of the Gaia benchmarks with their corresponding determinations in catalogs that used other techniques because of the following reasons. First, the catalogs do not have enough stars in common and well spread in the parameter space to allow unbiased diagnostics. Second, a comparison with one catalog does not necessarily shows the offset between the two techniques because their temperature values also include systematic errors (although small in the best cases) related to the particular procedures implemented. For example, the selected line-list, and the use of either equivalent widths or spectral fitting in the case of the excitation & ionization equilibrium of Fe lines, or the fitting criterion in the case of the Hα profile fitting. Therefore, comparisons with several catalogs from the same technique have been done, and the comparisons were not direct, but through a selected sample of stars well spread in T_{eff}–[Fe/H]–$\log g$ as displayed in Fig. 2.1, the T_{eff} of which were not derived by interferometry but remain on the same base as I explain below.

The Hα profile fitting is a very powerful technique to derive accurate T_{eff}. Unlike interferometry, it is not limited to nearby stars only, which permits to explore far regions of the Galaxy. Unlike IRFM, its accuracy is not compromised by the absence of reddening or the accuracy of reddening maps. And unlike the metal line diagnostics, its temperatures are almost non-degenerate with metallicity, surface gravity, or any other parameter. Nevertheless, the profile fitting is often avoided because the accuracy of theoretical models were not clearly established to this date, and because it is very difficult to normalize broad line profiles, as ambiguous diagnostics of accuracy for the same model in the literature have shown. Therefore, if the normalization problem were solved, the accuracy of Hα models could be properly determined and used as empirical corrections to derive accurate T_{eff}. In such a case, if the diagnostic of accuracy of the Hα model is based on interferometry, its corrected temperatures would remain on the interferometric scale.

Under this premise, the main work of this thesis was focused on the Hα profile fitting. More in detail, in recovering observational normalized Hα profiles free from artificial signatures such as those related to the instruments of acquisition, namely the blaze of echelle spectrographs, and those introduced by normalization procedures. I eliminated the blaze using the single-order coudé instrument at Pico dos Dias Observatory, the signature of which imprinted on the spectra is almost perfectly approximated by low order polynomials. For eliminating, or at least minimizing the normalization errors, I developed a new method that integrates normalization and fitting iteratively. This procedure additionally uses synthetic spectra of telluric features of precipitable water vapor (PWV) to optimise the continuum location. PWV features may be very small and nearly omnipresent around Hα, so they can be easily confused with spectral noise and shift the continuum to lower flux values. I tested this method extensively in the spectra of a sample of 43 F-,G-, and K-type stars, which also includes the Sun. The normalization-fitting method applied to coudé spectra was validated empirically with a sample of stars with both spectra, coudé and MUSICOS, by recovering equivalent temperatures. MUSICOS spectra are echelle, and they were normalized by the 2D-normalization, which is an independent method.

I used the Hα model of Barklem et al. (2002), which considers interactions of hydrogen atoms in 1D model atmospheres under LTE conditions, to fit the observed profiles of the 43 stars above, and thus derive their associated temperatures $T_{\rm eff}^{\rm H\alpha}$(1D LTE). I determined that the accuracy of the model follows the relation $T_{\rm eff} = T_{\rm eff}^{\rm H\alpha}(\rm 1D\,LTE) - 159(\pm 80)[Fe/H] + 28(\pm 1)$ K (Eq. 4.2) within the metallicity range -0.65 to $+0.4$ dex. This relation was first computed by comparing $T_{\rm eff}^{\rm H\alpha}$(1D LTE) of ten Gaia Benchmark stars with their interferometric $T_{\rm eff}$, and subsequently improved for solar parameters by taking the average difference of $T_{\rm eff}^{\rm H\alpha}$(1D LTE) from 57 coudé/HARPS/MUSICOS spectra (Table 2.2) with the direct solar $T_{\rm eff}$ = 5772 K (Prša et al., 2016; Heiter et al., 2015). The relation above applied to $T_{\rm eff}^{\rm H\alpha}$(1D LTE) therefore converts the Hα scale into the interferometric scale. Thus, a 'large' sample of 43 stars with accurate $T_{\rm eff}$ were used to determine the accuracy of other techniques.

The accuracy of IRFM was determined using the temperatures of the catalog of Ramírez, Allende Prieto, and Lambert (2013), who used the Johnson-Cousins, 2MASS, Tycho, and Strömgren color–$T_{\rm eff}$ relations of Casagrande et al. (2010), which was confirmed to be consistent with interferometry within 15 to 30 K by Casagrande et al. (2014). I find this scale to be indeed consistent with interferometry, as no trends were found with respect to $T_{\rm eff}$, [Fe/H], and log g. No other IRFM scales were analyzed because previous ones have shown significant divergent results due to errors in their absolute photometric calibrations.

The accuracy of the excitation & ionization equilibrium of Fe lines from 1D atmosphere models was determined analyzing six scales in the literature. All of them show similar trends with metallicity, implying that the scale of this technique, in general, underestimates/overestimates $T_{\rm eff}$ by 100 K at [Fe/H] = -0.6/+0.4 dex. These trends are systematic although the line-lists and the model atmospheres are different. One of the catalogs analysed (Bensby, Feltzing, and Oey, 2014) considers also non-LTE corrections.

I investigated how large the contribution of 1D atmosphere models is on the trend with metallicity presented by the Hα 1D LTE scale (Eq. 4.2). For that I tested Hα profiles from 3D LTE models specially synthesized for this work. I found that they slightly improve the diagnostics for solar parameters (the offset of -28 K turns into ~ -15 K), and in the the metal poor range, [Fe/H] = -0.5 dex, they almost fully correct 1D model underestimates. It therefore follows that the trend with metallicity is largely due to the use of 1D models. The correction provided by Eq. 4.2 however is quite robust and confidently brings the Hα 1D LTE scale to the same base of Interferometry.

I further investigated the accuracy of other Hα models. I found that ambiguous zero points – that is, the temperature that the model predicts at solar parameters – determined for the same model in the literature arise from normalization errors of the different versions of the Kitt Peak National Observatory solar atlases (Kurucz, 2005; Wallace et al., 2011), which are often used as templates. I quantified the impact of these errors, and I provide them as corrections in Table 4.1. These corrections applied on predictions from 3D models in the literature (Pereira et al., 2013; Amarsi et al., 2018) support my results on the slight improvement of the accuracy for solar parameters. Remarkably, the correction applied to Hα from 3D non-LTE models (Amarsi et al., 2018) exactly reproduces the solar $T_{\rm eff}$. This result corrects the diagnostic of accuracy reported for these new Hα models, the only failure of which was thought for the Sun.

I present an application of the Hα profile fitting to the M67 open cluster, with the purpose of studying the lithium evolution at the solar age. Hundreds of HARPS spectra of 52 main sequence and turnoff cluster stars were analysed. The results presented show that $T_{\rm eff}$ from Hα agree with IRFM $T_{\rm eff}$ from dereddened colors (within 20 K), which asserts the homogeneous extinction spread on the cluster and its accurate estimate. It therefore allows to combine $T_{\rm eff}$ from Hα with IRFM $T_{\rm eff}$ from Johnson-Cousins and 2MASS colors to obtain final $T_{\rm eff}$ values with $\sim$30 K precision and a very high degree of accuracy. These temperatures will allow to trace the path that Li abundances follow with mass, which will be accurately determined by Gaia DR2 measurements. A byproduct of this research is the confirmation of the complete removal of the instrumental signature of HARPS along time. The extensive tests performed with the Sun and other field stars show that equivalent temperatures can be retrieved from HARPS as from coudé spectra which is not affected by the strong blaze characteristic of echelle spectra.

7.1 Perspectives

This PhD project has been formulated as the very first steep of a long research scheme with the aim at making available an effective tool to solve current problems in stellar evolution, and star-exoplanet connection. The projects below will be performed with the products of this thesis; some of them are in progress.

7.1.1 Metal-poor and very metal-poor benchmark stars

The immediate extension of this thesis is the diagnostic of the accuracy of the examined techniques for metal-poor stars ([Fe/H] from -2.5 to -0.5 dex). Since it is proven that the 2D-normalization recovers equally normalized profiles as the non-echelle coudé spectrograph, UVES raw data can be retrieved from ESO archives to derive Hα temperatures of stars with the characteristics above. Determining the accuracy of the techniques for very metal-poor stars ([Fe/H] from -4.0 to -2.5 dex) is a more serious problem because there are no interferometric benchmarks for this [Fe/H] range, as these are distant halo stars. Some months before the bulk of this thesis was submitted in a paper (Giribaldi et al., 2019), Amarsi et al. (2018) published the first grid of Hα profiles synthesized using 3D non-LTE model atmospheres. In that work, the Hα grids fitted with observed profiles of four metal-poor stars precisely recovered their interferometric $T_{\rm eff}$; see Fig. 4.3 and related discussion in Sect. 4.3. Further, I showed in Sect. 4.1.1 that the failure of the grids to recover the solar $T_{\rm eff}$ is not due to deficiencies of the model, but due to normalization errors in the solar template they used. Hence, these Hα grids are indeed accurate across the whole parameter space tested, which gives solid arguments to rely on them for characterizing stars in the parameter space that the Gaia benchmarks do not fill or fill scarcely. The proposal is then to extend and evenly fill the parameter space of the Gaia benchmark stars. This is already done for solar-type stars with the sample stars with accurate parameters published in Table 4.2; see parameter space in Fig. 2.1. Many metal-poor and very metal-poor candidates are listed in the catalog of Casagrande et al. (2010), whose scale is proven to be accurate as long as reddening is irrelevant. Examples of available very metal-poor stars in the ESO UVES archive are: HE 1148-0037 ([Fe/H] = −3.46 dex), BPS CS 31065-0008 ([Fe/H] = −3.36 dex), CD-24 17504 ([Fe/H] = −3.29 dex), etc. Good quality spectra of metal-poor cluster stars are, for example, those of 47 Tuc, M4, and NGC 6752. The new benchmarks should join those already characterised by Amarsi et al. (2018): HD 103095, HD 84937, HD 140283, HD 122563.

7.1.2 Abundance signatures of planet-host stars in Praesepe

This is currently being performed by the PhD student Maria Ubaldo-Melo in Observatório do Valongo. Praesepe is an old and metal-rich cluster with bright stars in the main sequence (V $\sim$ 11), and some of these stars were identified as planet-hosts. The chemical analysis of cluster stars with identical colors with and without planets may give clues in regards to why main-sequence stars hosting planets tend to be more metal-rich than those with no detection (e.g. Gonzalez, 1997; Sousa et al., 2008). Praesepe is also particular because studies on its structure found that it can be formed by two clusters merged (Holland et al., 2000; Franciosini, Randich, and Pallavicini, 2003). The spread of its iron abundance estimates in the literature (+0.11 to +0.27 dex) seem to support this idea, but the most metal-rich estimate (Pace, Pasquini, and François, 2008) is probably product of the temperature scale adopted (Ramírez and Meléndez, 2005), the bias of which ($\sim$+100 K) was proven by Casagrande et al. (2010). To clarify the problems above, Maria Ubaldo-Melo will derive Fe and other element abundances of two group of stars from new UVES spectra (resolution R = 40 000 and S/N $\sim$ 300). The abundance scales will be based in $T_{\rm eff}$ from Hα and log g from evolutionary tracks and Gaia parallaxes, as done for M67 (Chap. 6), but the technique to normalize Hα will be 2D-normalization (Sect. 3.3). The first group of stars consists on four stars with the same colours: KW 418 (hosting-planet), KW 162, KW 49, KW 10, which should present nearly the same abundances considering an homogeneous chemical abundance pattern, and no chemical enrichment due to the presence of planets. The second group of stars are six dwarfs and three giants for which variations of element abundances will be checked along the evolutionary path.

7.1.3 Stellar structure in turnoff stars

Latest models of stellar structure have warned of possible significant inaccuracies ($\sim$2%) in radius measurements by the *Kepler* and PLATO missions (Deal et al., 2018). These models predict structure modifications by atomic diffusion due to local accumulation of elements; see references about this physical process in Chap. 6. It is not clear how diffusion behaves as function of the stellar parameters $T_{\rm eff}$, metallicity, mass, and age. Namely, at which rates its main component processes "gravitational settling" (that tend to accumulate the element in deeper layers), and "radiative acceleration" (that push the element up towards the surface) work. The models of Deal et al. predict that diffusion can increase the stellar radius of stars of solar metallicity with ages around 1 Gyr in the turnoff ($T_{\rm eff} \sim 6800$ K), and that its effects should be detectable by the rise of the atmospheric iron abundance (up to 0.35 dex). However, observations in several clusters with stars of the same characteristics (e.g. IC 4651, IC 4756, NGC 2447, and NGC 3680 by Blanco-Cuaresma et al., 2015) show too little increments (up to 0.1 dex). These observational [Fe/H] measurements were derived simultaneously with other parameters by fitting synthetic spectra from 1D LTE models using the method described by Blanco-Cuaresma et al. (2014). However [Fe/H] derived by this method for the stars with the characteristics described above (solar [Fe/H] and $T_{\rm eff} > 6400$ K) seem to be underestimated by ~ 0.1 dex when compared with the determinations of the Gaia Benchmark stars (Jofré et al., 2015), which would account in favor of the rise of [Fe/H] predicted by Deal. et al. to $\sim$0.2 dex; see Fig 7.1. This [Fe/H] bias may probably be caused by $T_{\rm eff}$–[Fe/H] degeneracies involved in the spectral fitting of metal lines because LTE effects are not expected to be large for stars of solar metallicity (e.g. Bergemann et al., 2012). The approach to solve this problem is similar to that used for M67 in Chap. 6: $T_{\rm eff}$ must be derived from Hα, $\log g$ by evolutionary tracks using trigonometric distances of Gaia, and [Fe/H] by spectroscopy; all procedures performed iteratively until the self-consistency is reached.

The spectra that will be used are, in principle, the same as in Blanco-Cuaresma et al. (2015). They are free available and have the quality required for applying the procedures described above. The data of the cluster IC 4651 used in Pasquini et al. (2004) are also available, and their individual spectra are of better S/N than those of Blanco-Cuaresma et al. In case observations are needed to improve the precision of the parameter measurements, the research will be concentrated on the cluster IC 4756, whose stars are much brighter than those of the other clusters. Observations of this cluster with the ESO-VLT can be requested by means of a collaboration with Luca Pasquini.

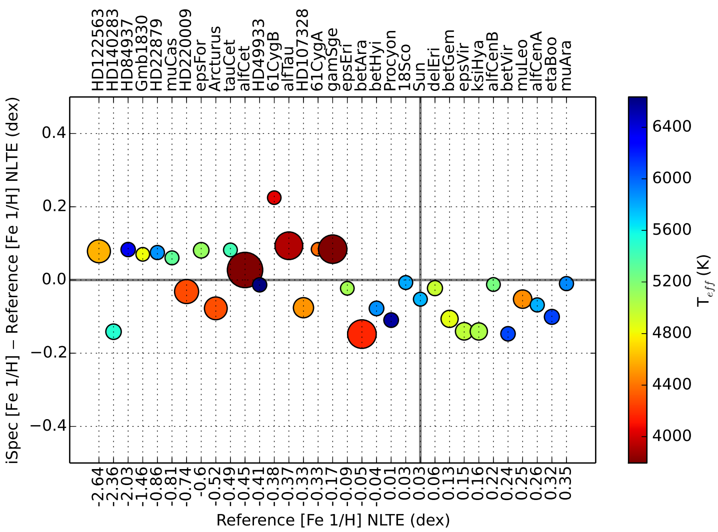

FIGURE 7.1: Adapted from Blanco-Cuaresma et al. (2014, Fig. 5). Differences in neutral iron abundances between the reference (Gaia FGK benchmark stars Jofré et al., 2015) and the derived value by iSpec using the synthetic spectral fitting method.

Appendix A

Fits of Coudé spectra

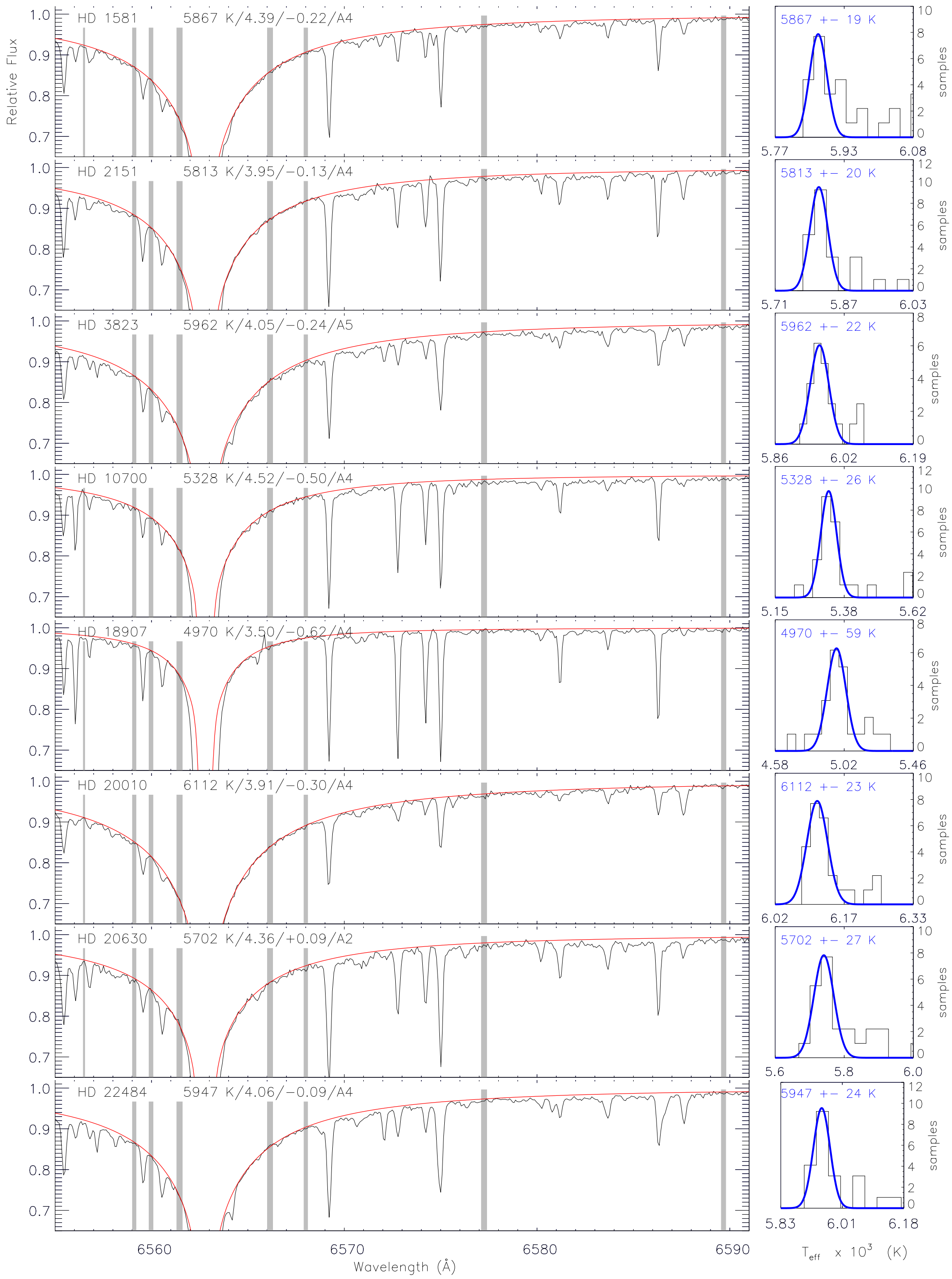

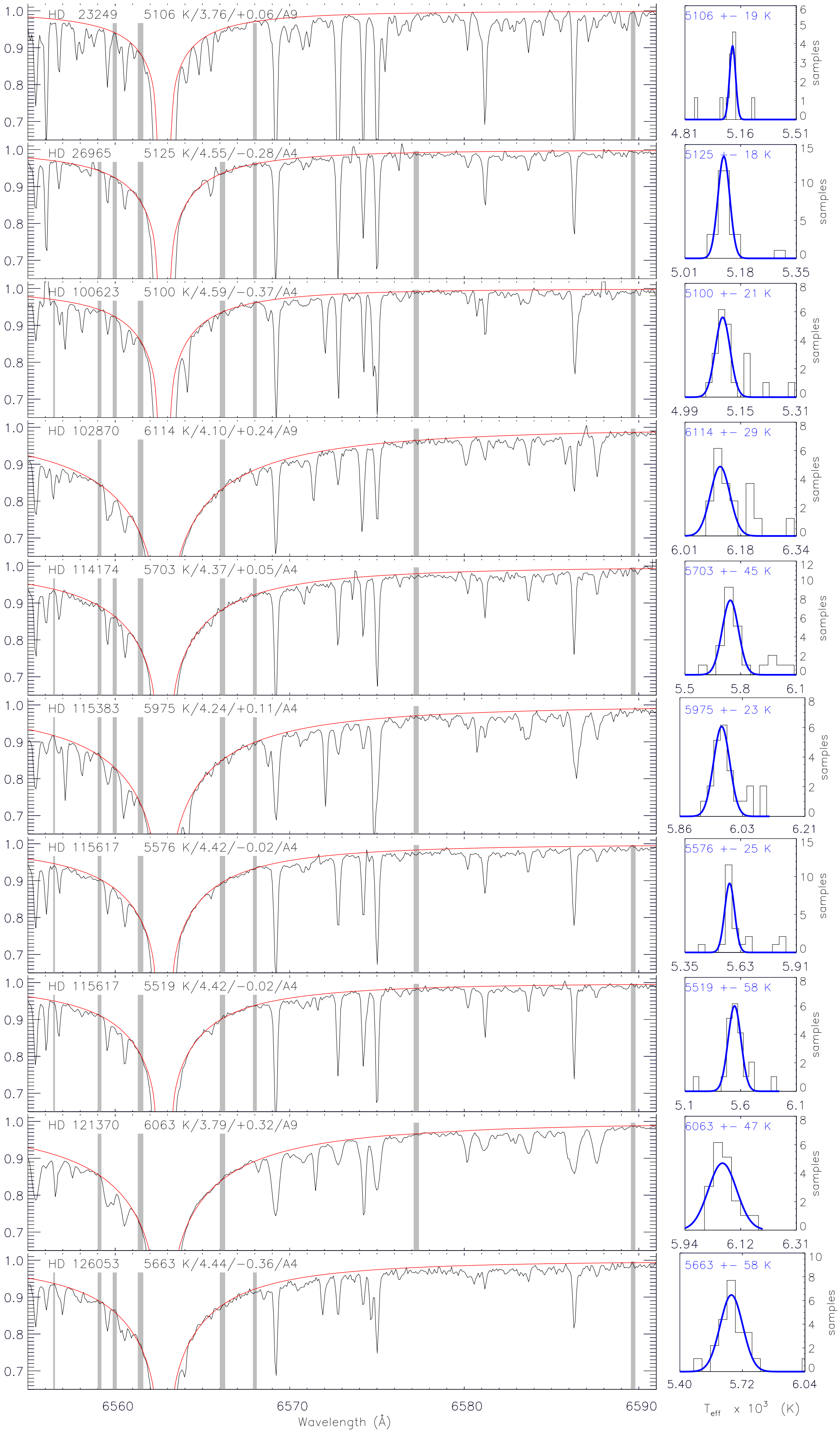

HD 23249 5106 K/3.76/+0.06/A9
5106 +− 19 K
HD 26965 5125 K/4.55/−0.28/A4
5125 +− 18 K
HD 100623 5100 K/4.59/−0.37/A4
5100 +− 21 K
HD 102870 6114 K/4.10/+0.24/A9
6114 +− 29 K
HD 114174 5703 K/4.37/+0.05/A4
5703 +− 45 K
HD 115383 5975 K/4.24/+0.11/A4
5975 +− 23 K
HD 115617 5576 K/4.42/−0.02/A4
5576 +− 25 K
HD 115617 5519 K/4.42/−0.02/A4
5519 +− 58 K
HD 121370 6063 K/3.79/+0.32/A9
6063 +− 47 K
HD 126053 5663 K/4.44/−0.36/A4
5663 +− 58 K
Wavelength (Å)
T_{eff} x 10^3 (K)
samples

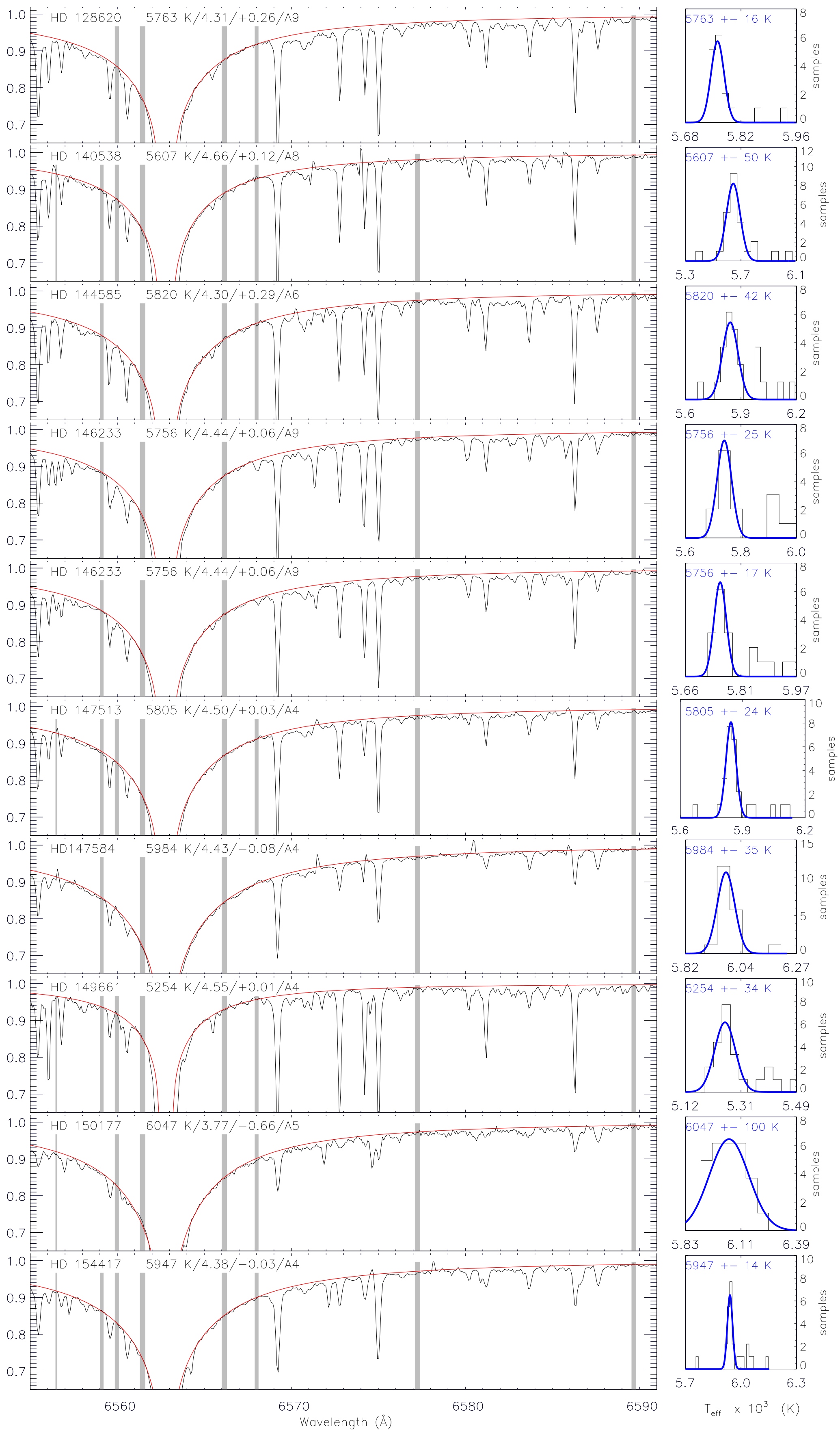
HD 128620 5763 K/4.31/+0.26/A9
5763 +− 16 K
HD 140538 5607 K/4.66/+0.12/A8
5607 +− 50 K
HD 144585 5820 K/4.30/+0.29/A6
5820 +− 42 K
HD 146233 5756 K/4.44/+0.06/A9
5756 +− 25 K
HD 146233 5756 K/4.44/+0.06/A9
5756 +− 17 K
HD 147513 5805 K/4.50/+0.03/A4
5805 +− 24 K
HD147584 5984 K/4.43/−0.08/A4
5984 +− 35 K
HD 149661 5254 K/4.55/+0.01/A4
5254 +− 34 K
HD 150177 6047 K/3.77/−0.66/A5
6047 +− 100 K
HD 154417 5947 K/4.38/−0.03/A4
5947 +− 14 K
Wavelength (Å)
samples
T_{eff} x 10^3 (K)

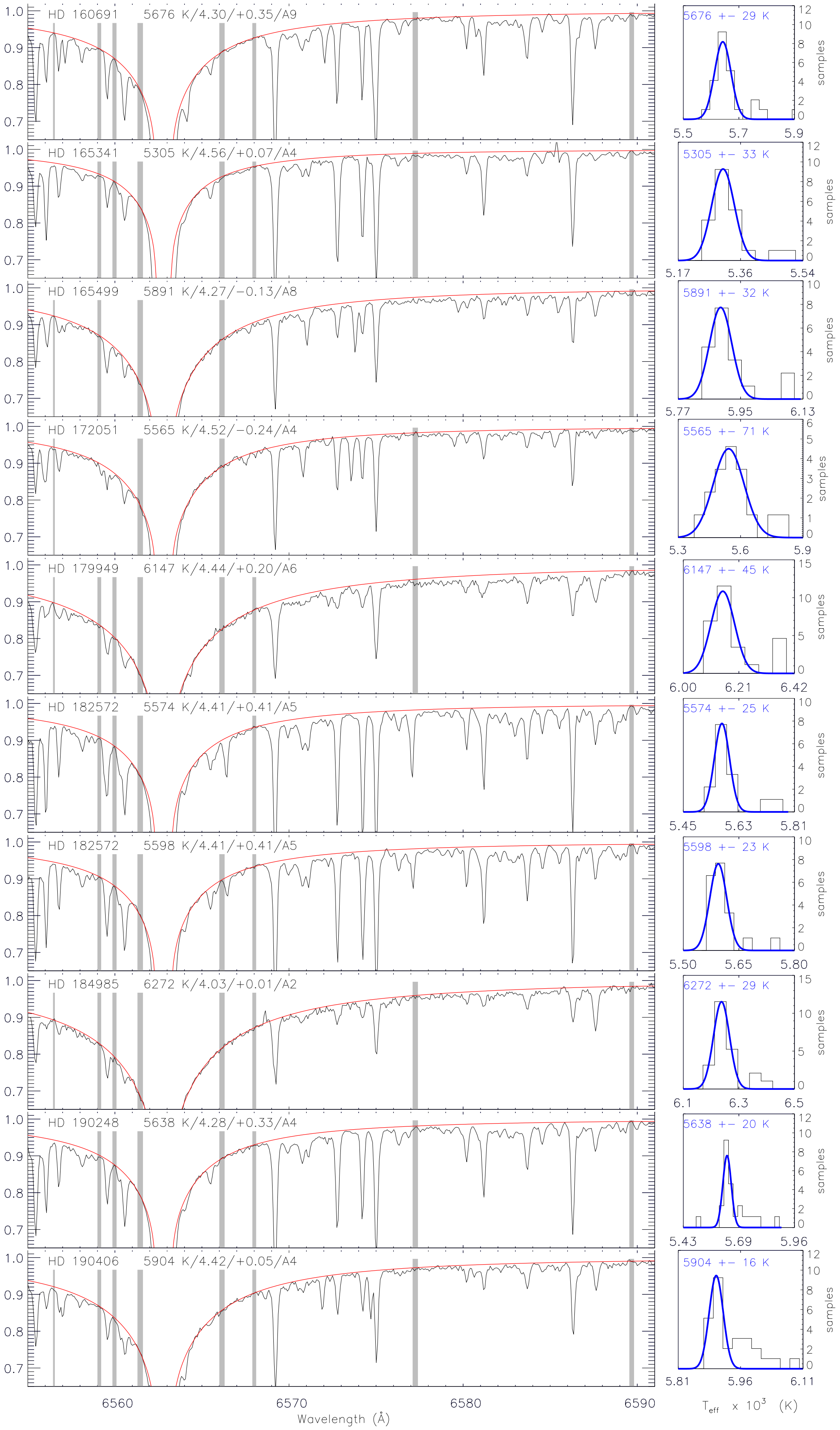
HD 160691 5676 K/4.30/+0.35/A9
5676 +- 29 K
HD 165341 5305 K/4.56/+0.07/A4
5305 +- 33 K
HD 165499 5891 K/4.27/−0.13/A8
5891 +- 32 K
HD 172051 5565 K/4.52/−0.24/A4
5565 +- 71 K
HD 179949 6147 K/4.44/+0.20/A6
6147 +- 45 K
HD 182572 5574 K/4.41/+0.41/A5
5574 +- 25 K
HD 182572 5598 K/4.41/+0.41/A5
5598 +- 23 K
HD 184985 6272 K/4.03/+0.01/A2
6272 +- 29 K
HD 190248 5638 K/4.28/+0.33/A4
5638 +- 20 K
HD 190406 5904 K/4.42/+0.05/A4
5904 +- 16 K
Wavelength (Å)
samples
T_{eff} x 10^3 (K)

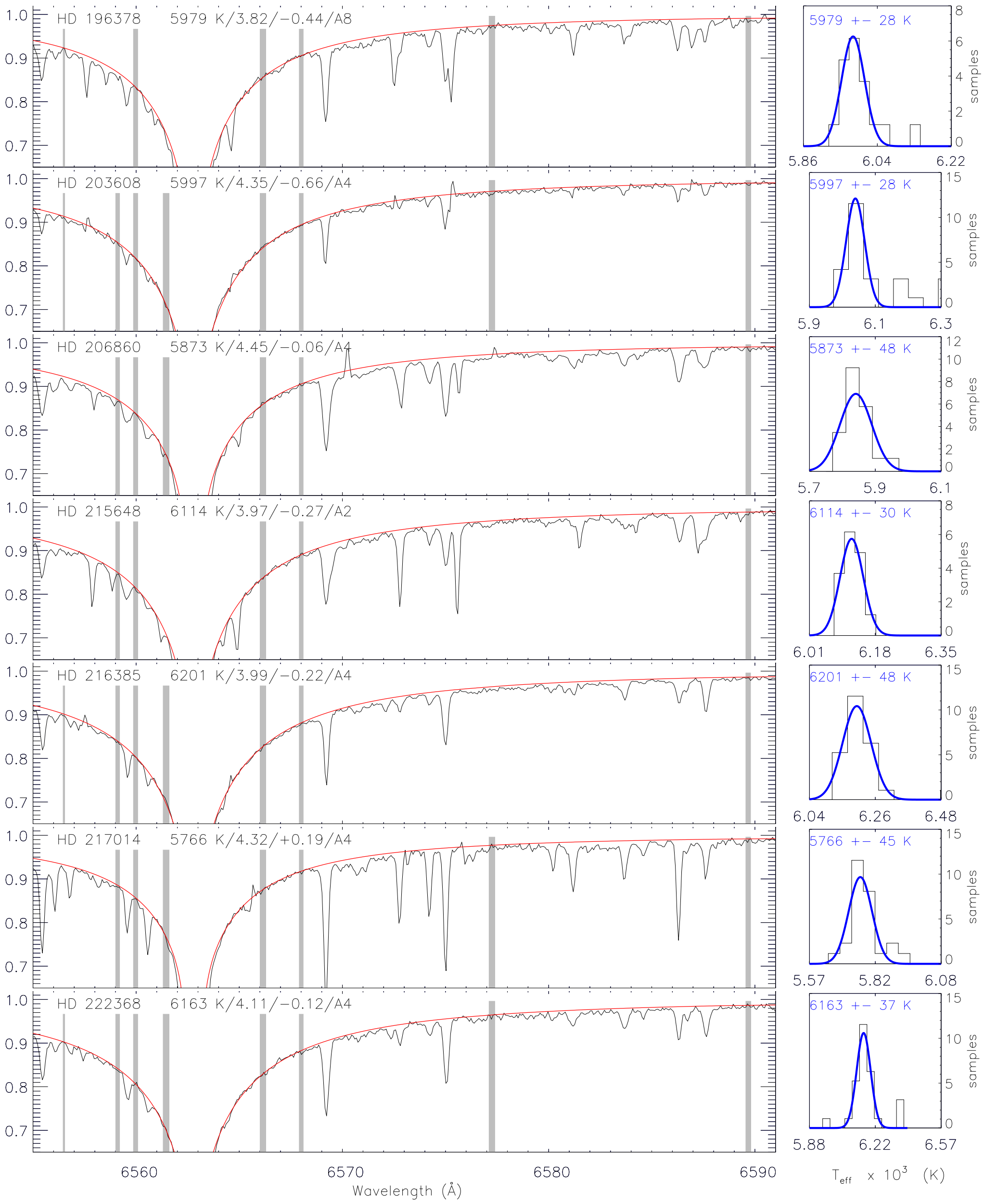
HD 196378 5979 K/3.82/−0.44/A8
5979 +− 28 K
HD 203608 5997 K/4.35/−0.66/A4
5997 +− 28 K
HD 206860 5873 K/4.45/−0.06/A4
5873 +− 48 K
HD 215648 6114 K/3.97/−0.27/A2
6114 +− 30 K
HD 216385 6201 K/3.99/−0.22/A4
6201 +− 48 K
HD 217014 5766 K/4.32/+0.19/A4
5766 +− 45 K
HD 222368 6163 K/4.11/−0.12/A4
6163 +− 37 K
samples
Wavelength (Å)
T_{eff} x 10^3 (K)

Appendix B

Fits of HARPS spectra

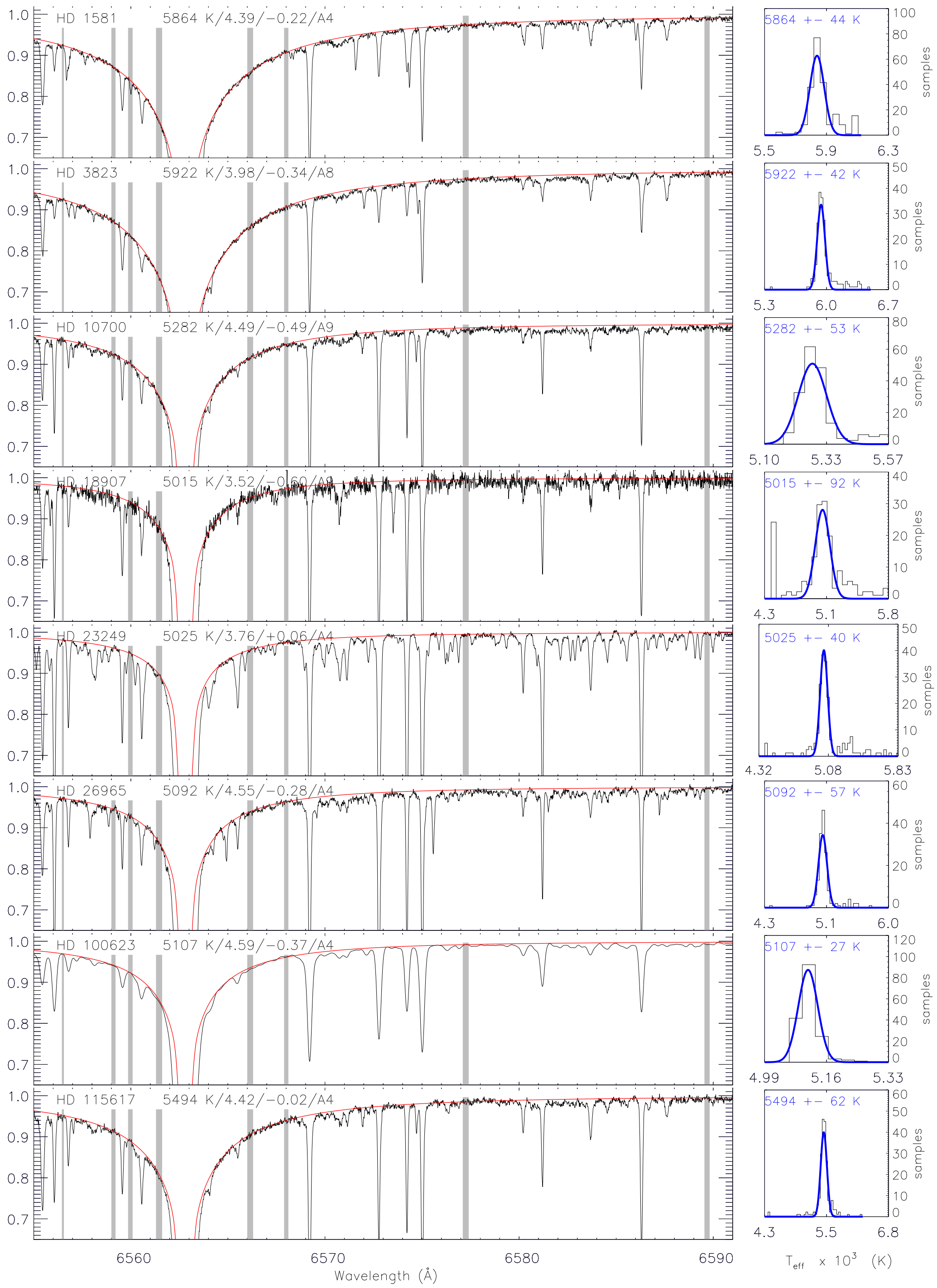

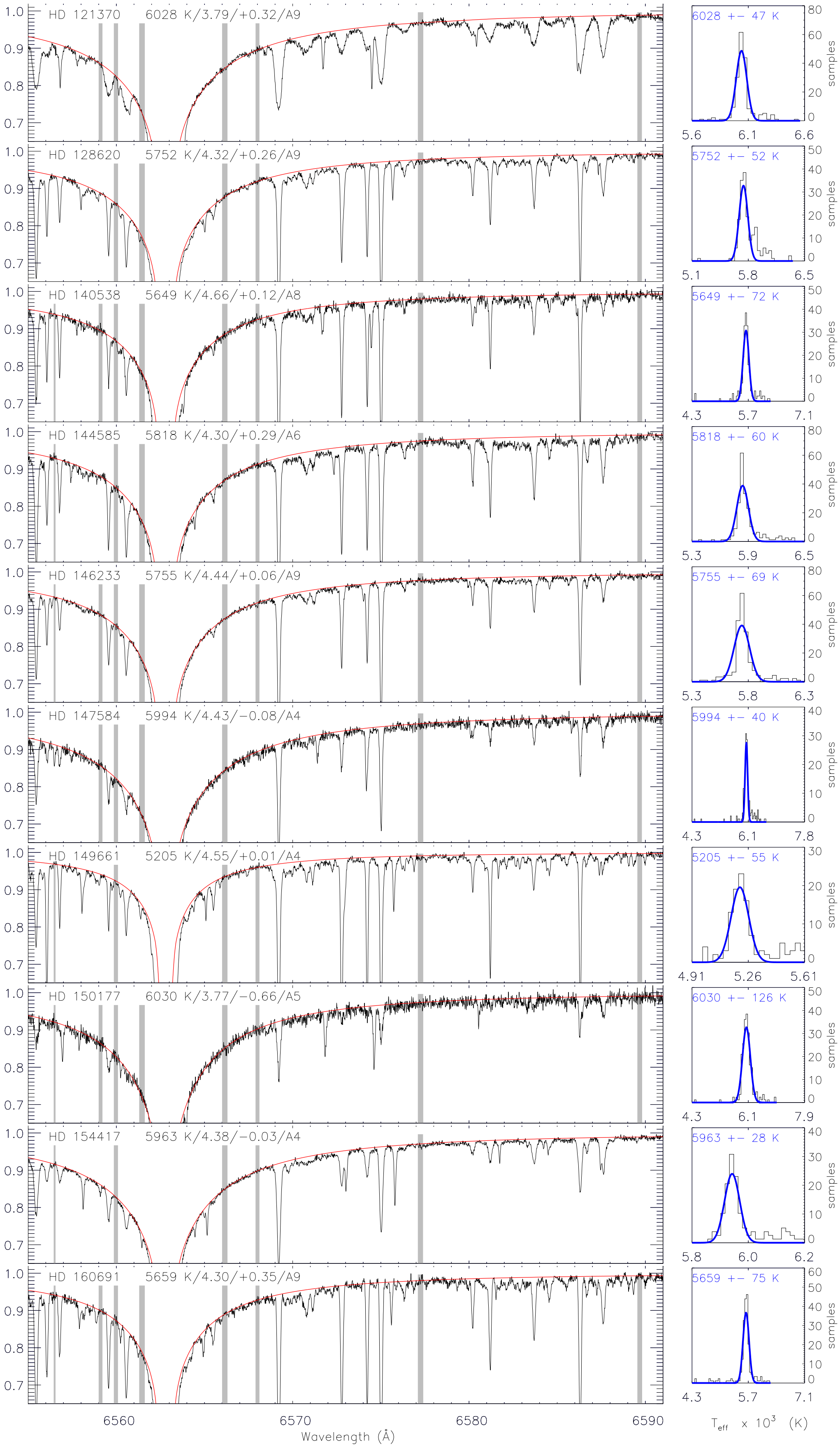
HD 121370 6028 K/3.79/+0.32/A9
6028 +− 47 K
HD 128620 5752 K/4.32/+0.26/A9
5752 +− 52 K
HD 140538 5649 K/4.66/+0.12/A8
5649 +− 72 K
HD 144585 5818 K/4.30/+0.29/A6
5818 +− 60 K
HD 146233 5755 K/4.44/+0.06/A9
5755 +− 69 K
HD 147584 5994 K/4.43/−0.08/A4
5994 +− 40 K
HD 149661 5205 K/4.55/+0.01/A4
5205 +− 55 K
HD 150177 6030 K/3.77/−0.66/A5
6030 +− 126 K
HD 154417 5963 K/4.38/−0.03/A4
5963 +− 28 K
HD 160691 5659 K/4.30/+0.35/A9
5659 +− 75 K
samples
Wavelength (Å)
T_{eff} x 10^3 (K)

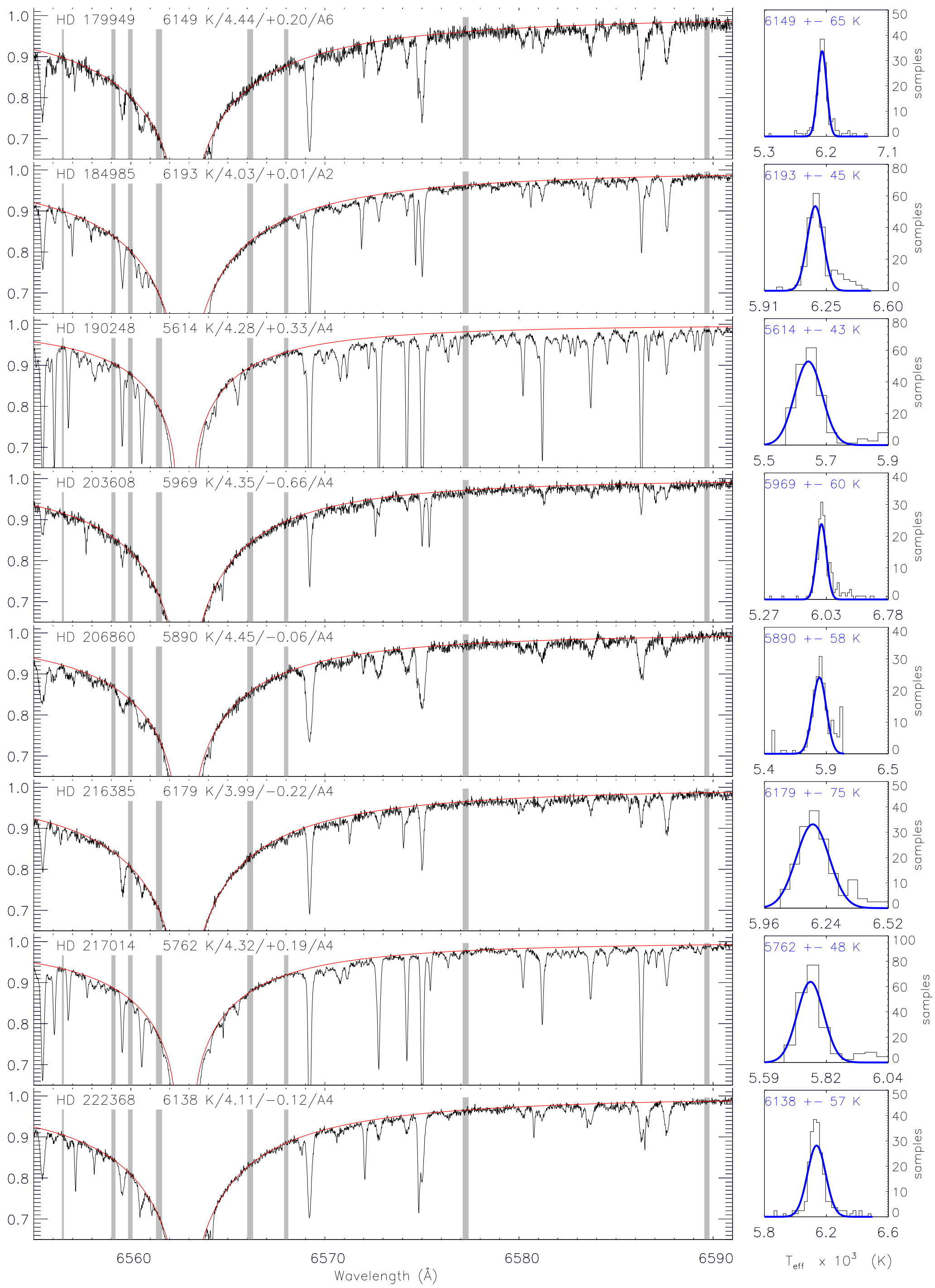

HD 179949 6149 K/4.44/+0.20/A6
6149 +− 65 K
HD 184985 6193 K/4.03/+0.01/A2
6193 +− 45 K
HD 190248 5614 K/4.28/+0.33/A4
5614 +− 43 K
HD 203608 5969 K/4.35/−0.66/A4
5969 +− 60 K
HD 206860 5890 K/4.45/−0.06/A4
5890 +− 58 K
HD 216385 6179 K/3.99/−0.22/A4
6179 +− 75 K
HD 217014 5762 K/4.32/+0.19/A4
5762 +− 48 K
HD 222368 6138 K/4.11/−0.12/A4
6138 +− 57 K
samples
Wavelength (Å)
T_{eff} x 10^3 (K)

Appendix C

Fits of MUSICOS spectra

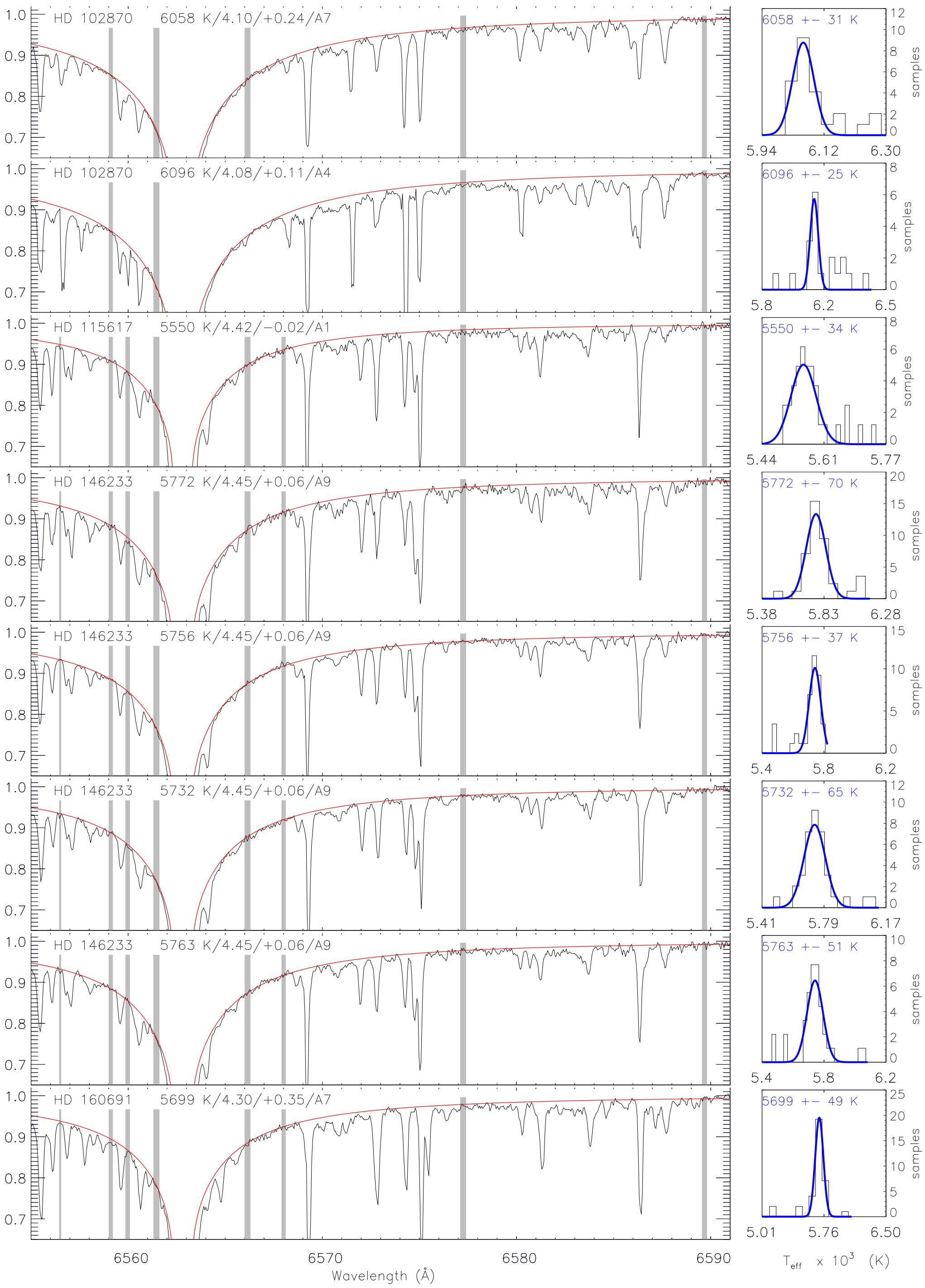

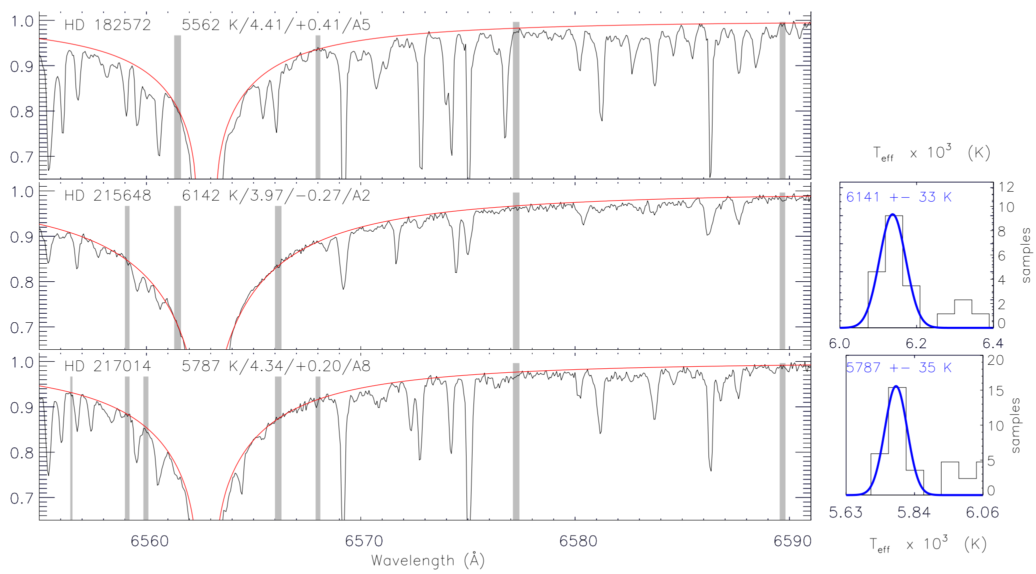
HD 182572 5562 K/4.41/+0.41/A5
HD 215648 6142 K/3.97/−0.27/A2
HD 217014 5787 K/4.34/+0.20/A8
Wavelength (Å)
6141 +− 33 K
5787 +− 35 K
samples
T_{eff} x 10^3 (K)

References

Absil, O. et al. (2006). "Circumstellar material in the <ASTROBJ>Vega</ASTROBJ> inner system revealed by CHARA/FLUOR". In: *Astronomy & Astrophysics* 452, pp. 237–244. DOI: 10.1051/0004-6361:20054522. eprint: astro-ph/0604260.

Ali, A. W. and H. R. Griem (1966). "Theory of Resonance Broadening of Spectral Lines by Atom-Atom Impacts". In: *Physical Review* 144, pp. 366–366. DOI: 10.1103/PhysRev.144.366.

Allard, N. F. et al. (2008). "Self-broadening of the hydrogen Balmer α line". In: *Astronomy & Astrophysics* 480, pp. 581–587. DOI: 10.1051/0004-6361:20078437.

Allende Prieto, C. et al. (2002). "Signatures of Convection in the Spectrum of Procyon: Fundamental Parameters and Iron Abundance". In: *The Astrophysical Journal* 567, pp. 544–565. DOI: 10.1086/338248. eprint: astro-ph/0111055.

Allende Prieto, C. et al. (2004). "S^4N: A spectroscopic survey of stars in the solar neighborhood. The Nearest 15 pc". In: *Astronomy & Astrophysics* 420, pp. 183–205. DOI: 10.1051/0004-6361:20035801. eprint: astro-ph/0403108.

Alonso, A., S. Arribas, and C. Martinez-Roger (1994). "A semi-empirical absolute flux calibration in the near infrared: Direct stellar diameters vs. IRFM determinations". In: *Astronomy & Astrophysics* 282, pp. 684–698.

— (1996). "Determination of effective temperatures for an extended sample of dwarfs and subdwarfs (F0-K5)." In: *Astronomy & Astrophysicss* 117, pp. 227–254.

Alonso, A., S. Arribas, and C. Martínez-Roger (1999a). "The effective temperature scale of giant stars (F0-K5). I. The effective temperature determination by means of the IRFM". In: *Astronomy & Astrophysicss* 139, pp. 335–358. DOI: 10.1051/aas:1999506.

— (1999b). "The effective temperature scale of giant stars (F0-K5). II. Empirical calibration of T_{eff} versus colours and [Fe/H]". In: *Astronomy & Astrophysicss* 140, pp. 261–277. DOI: 10.1051/aas:1999521.

Amarsi, A. M. et al. (2018). "Effective temperature determinations of late-type stars based on 3D non-LTE Balmer line formation". In: *Astronomy & Astrophysics* 615, A139, A139. DOI: 10.1051/0004-6361/201732546. arXiv: 1804.02305 [astro-ph.SR].

Andersen, J. (1991). "Accurate masses and radii of normal stars". In: *Astronomy & Astrophysics* 3, pp. 91–126. DOI: 10.1007/BF00873538.

Anthony-Twarog, Barbara J. et al. (2009). "Lithium in the Intermediate-Age Open Cluster, NGC 3680". In: *The Astronomical Journal* 138, pp. 1171–1191. DOI: 10.1088/0004-6256/138/4/1171. arXiv: 0908.2136 [astro-ph.SR].

Asplund, M. (2005). "New Light on Stellar Abundance Analyses: Departures from LTE and Homogeneity". In: *Annual Review of Astronomy & Astrophysics* 43, pp. 481–530. DOI: 10.1146/annurev.astro.42.053102.134001.

Asplund, M. and A. E. García Pérez (2001). "On OH line formation and oxygen abundances in metal-poor stars". In: *Astronomy & Astrophysics* 372, pp. 601–615. DOI: 10.1051/0004-6361:20010483. eprint: astro-ph/0104071.

Asplund, M. et al. (1997). "Line-blanketed model atmospheres for R Coronae Borealis stars and hydrogen-deficient carbon stars." In: *Astronomy & Astrophysics* 318, pp. 521–534.

Aufdenberg, J. P., H.-G. Ludwig, and P. Kervella (2005). "On the Limb Darkening, Spectral Energy Distribution, and Temperature Structure of Procyon". In: *The Astrophysical Journal* 633, pp. 424–439. DOI: 10.1086/452622. eprint: astro-ph/0507336.

Aufdenberg, J. P. et al. (2006). "First Results from the CHARA Array. VII. Long-Baseline Interferometric Measurements of Vega Consistent with a Pole-On, Rapidly Rotating Star". In: *The Astrophysical Journal* 645, pp. 664–675. DOI: 10.1086/504149. eprint: astro-ph/0603327.

Aumann, H. H. et al. (1984). "Discovery of a shell around Alpha Lyrae". In: *The Astrophysical Journall* 278, pp. L23–L27. DOI: 10.1086/184214.

Barklem, P. S. (2007). "Non-LTE Balmer line formation in late-type spectra: effects of atomic processes involving hydrogen atoms". In: *Astronomy & Astrophysics* 466, pp. 327–337. DOI: 10.1051/0004-6361:20066686. eprint: astro-ph/0702222.

Barklem, P. S., N. Piskunov, and B. J. O'Mara (2000). "Self-broadening in Balmer line wing formation in stellar atmospheres". In: *Astronomy & Astrophysics* 363, pp. 1091–1105. eprint: astro-ph/0010022.

Barklem, P. S. et al. (2002). "Detailed analysis of Balmer lines in cool dwarf stars". In: *Astronomy & Astrophysics* 385, pp. 951–967. DOI: 10.1051/0004-6361:20020163. eprint: astro-ph/0201537.

Baudrand, J. and T. Bohm (1992). "MUSICOS - A fiber-fed spectrograph for multi-site observations". In: *Astronomy & Astrophysics* 259, pp. 711–719.

Baumann, P., I. Ramírez, J. Meléndez, et al. (2010). "Lithium depletion in solar-like stars: no planet connection". In: *Astronomy & Astrophysics* 519, A87, A87. DOI: 10.1051/0004-6361. arXiv: 1008.0575 [astro-ph.SR].

Bazot, M. et al. (2011). "The radius and mass of the close solar twin 18 Scorpii derived from asteroseismology and interferometry". In: *Astronomy & Astrophysics* 526, L4, p. L4. DOI: 10.1051/0004-6361/201015679. arXiv: 1209.0217 [astro-ph.SR].

Bell, R. A. and B. Gustafsson (1989). "The effective temperatures and colours of G and K stars". In: *Monthly Notice of the Royal Astronomical Society* 236, pp. 653–707. DOI: 10.1093/mnras/236.3.653.

Bell, R. A. et al. (1976). "A grid of model atmospheres for metal-deficient giant stars. II". In: *Astronomy & Astrophysicss* 23, pp. 37–95.

Bensby, T., S. Feltzing, and M. S. Oey (2014). "Exploring the Milky Way stellar disk. A detailed elemental abundance study of 714 F and G dwarf stars in the solar neighbourhood". In: *Astronomy & Astrophysics* 562, A71, A71. DOI: 10.1051/0004-6361/201322631. arXiv: 1309.2631.

Bergemann, M. et al. (2012). "Non-LTE line formation of Fe in late-type stars - I. Standard stars with 1D and 3D model atmospheres". In: *Monthly Notice of the Royal Astronomical Society* 427, pp. 27–49. DOI: 10.1111/j.1365-2966.2012.21687.x. arXiv: 1207.2455 [astro-ph.SR].

Bertelli Motta, C. et al. (2018). "The Gaia-ESO Survey: evidence of atomic diffusion in M67?" In: *Monthly Notice of the Royal Astronomical Society* 478, pp. 425–438. DOI: 10.1093/mnras/sty1011. arXiv: 1804.06293 [astro-ph.SR].

Bessel, M. S. (1990). "BVRI photometry of the Gliese catalogue stars." In: *Astronomy and Astrophysics Supplement Series* 83, pp. 357–378.

Bessell, Michael S. (2000). "The Hipparcos and Tycho Photometric System Passbands". In: *Publications of the Astronomical Society of the Pacific* 112, pp. 961–965. DOI: 10.1086/316598.

Bigot, L. et al. (2006). "The limb darkening of α Centauri B. Matching 3D hydrodynamical models with interferometric measurements". In: *Astronomy & Astrophysics* 446, pp. 635–641. DOI: 10.1051/0004-6361:20053187.

Blackwell, D. E. and A. D. Petford (1991). “Derivation of stellar integrated flux from photometric indexes”. In: *Astronomy & Astrophysics* 250, pp. 459–462.

Blackwell, D. E., A. D. Petford, and M. J. Shallis (1980). “Use of the infra-red flux method for determining stellar effective temperatures and angular diameters - The stellar temperature scale”. In: *Astronomy & Astrophysics* 82, pp. 249–252.

Blackwell, D. E. and M. J. Shallis (1977). “Stellar angular diameters from infrared photometry - Application to Arcturus and other stars; with effective temperatures”. In: *Monthly Notice of the Royal Astronomical Society* 180, pp. 177–191. DOI: 10.1093/mnras/180.2.177.

Blackwell, D. E., M. J. Shallis, and M. J. Selby (1979). “The infrared flux method for determining stellar angular diameters and effective temperatures”. In: *Monthly Notice of the Royal Astronomical Society* 188, pp. 847–862. DOI: 10.1093/mnras/188.4.847.

Blackwell, D. E. et al. (1990). “Determination of temperatures and angular diameters of 114 F-M stars using the infrared flux method (IRFM)”. In: *Astronomy & Astrophysics* 232, pp. 396–410.

Blanco-Cuaresma, S. et al. (2014). “Determining stellar atmospheric parameters and chemical abundances of FGK stars with iSpec”. In: *Astronomy & Astrophysics* 569, A111, A111. DOI: 10.1051/0004-6361/201423945. arXiv: 1407.2608 [astro-ph.IM].

Blanco-Cuaresma, S. et al. (2015). “Testing the chemical tagging technique with open clusters”. In: *Astronomy & Astrophysics* 577, A47, A47. DOI: 10.1051/0004-6361/201425232. arXiv: 1503.02082 [astro-ph.SR].

Bohlin, R. C. (2007). “HST Stellar Standards with 1% Accuracy in Absolute Flux”. In: *The Future of Photometric, Spectrophotometric and Polarimetric Standardization*. Ed. by C. Sterken. Vol. 364. Astronomical Society of the Pacific Conference Series, p. 315. eprint: astro-ph/0608715.

Bohlin, R. C. and R. L. Gilliland (2004). “Hubble Space Telescope Absolute Spectrophotometry of Vega from the Far-Ultraviolet to the Infrared”. In: *The Astronomical Journal* 127, pp. 3508–3515. DOI: 10.1086/420715.

Böhm-Vitense, E. (1958). “Über die Wasserstoffkonvektionszone in Sternen verschiedener Effektivtemperaturen und Leuchtkräfte. Mit 5 Textabbildungen”. In: *Zeitschrift fuer Astrophysik* 46, p. 108.

Bonifacio, P. et al. (2007). “First stars VII - Lithium in extremely metal poor dwarfs”. In: *Astronomy & Astrophysics* 462, pp. 851–864. DOI: 10.1051/0004-6361:20064834. eprint: astro-ph/0610245.

Bonneau, D. and A. Labeyrie (1973). “Speckle Interferometry: Color-Dependent Limb Darkening Evidenced on Alpha Orionis and Omicron Ceti”. In: *The Astrophysical Journall* 181, p. L1. DOI: 10.1086/181171.

Bouvier, J. (2008). “Lithium depletion and the rotational history of exoplanet host stars”. In: *Astronomy & Astrophysics* 489, pp. L53–L56. DOI: 10.1051/0004-6361:200810574. arXiv: 0808.3917 [astro-ph].

Boyajian, T. S. et al. (2012a). “Stellar Diameters and Temperatures. I. Main-sequence A, F, and G Stars”. In: *The Astrophysical Journal* 746, 101, p. 101. DOI: 10.1088/0004-637X/746/1/101. arXiv: 1112.3316 [astro-ph.SR].

Boyajian, T. S. et al. (2012b). “Stellar Diameters and Temperatures. II. Main-sequence K- and M-stars”. In: *The Astrophysical Journal* 757, 112, p. 112. DOI: 10.1088/0004-637X/757/2/112. arXiv: 1208.2431 [astro-ph.SR].

Brucalassi, A. et al. (2014). “Three planetary companions around M 67 stars”. In: *Astronomy & Astrophysics* 561, L9, p. L9. DOI: 10.1051/0004-6361/201322584. arXiv: 1401.4905 [astro-ph.SR].

Brucalassi, A. et al. (2017). “Search for giant planets in M 67. IV. Survey results”. In: *Astronomy & Astrophysics* 603, A85, A85. DOI: 10.1051/0004-6361/201527562. arXiv: 1703.04296 [astro-ph.EP].

Burles, Scott, Kenneth M. Nollett, and Michael S. Turner (2001). “Big Bang Nucleosynthesis Predictions for Precision Cosmology”. In: *The Astrophysical Journal* 552, pp. L1–L5. DOI: 10.1086/320251. arXiv: astro-ph/0010171 [astro-ph].

Canto Martins, B. L. et al. (2011). “Lithium abundances and extra mixing processes in evolved stars of M 67”. In: *Astronomy & Astrophysics* 527, A94, A94. DOI: 10.1051/0004-6361/201015015. arXiv: 1101.3757 [astro-ph.SR].

Carney, B. W. (1983). “A photometric search for halo binaries. II. Results.” In: *The Astronomical Journal* 88, pp. 623–641. DOI: 10.1086/113351.

Casagrande, L., L. Portinari, and C. Flynn (2006). “Accurate fundamental parameters for lower main-sequence stars”. In: *Monthly Notice of the Royal Astronomical Society* 373, pp. 13–44. DOI: 10.1111/j.1365-2966.2006.10999.x. eprint: astro-ph/0608504.

Casagrande, L. et al. (2010). “An absolutely calibrated T_{eff} scale from the infrared flux method. Dwarfs and subgiants”. In: *Astronomy & Astrophysics* 512, A54, A54. DOI: 10.1051/0004-6361/200913204. arXiv: 1001.3142 [astro-ph.SR].

Casagrande, L. et al. (2011). “New constraints on the chemical evolution of the solar neighbourhood and Galactic disc(s). Improved astrophysical parameters for the Geneva-Copenhagen Survey”. In: *Astronomy & Astrophysics* 530, A138, A138. DOI: 10.1051/0004-6361/201016276. arXiv: 1103.4651 [astro-ph.GA].

Casagrande, L. et al. (2014). “Towards stellar effective temperatures and diameters at 1 per cent accuracy for future surveys”. In: *Monthly Notice of the Royal Astronomical Society* 439, pp. 2060–2073. DOI: 10.1093/mnras/stu089. arXiv: 1401.3754 [astro-ph.SR].

Castelli, F. and R. L. Kurucz (2004). “New Grids of ATLAS9 Model Atmospheres”. In: *ArXiv Astrophysics e-prints*. eprint: astro-ph/0405087.

Castro, M. et al. (2011). “Solar twins in M 67: evolutionary status and lithium abundance”. In: *Astronomy & Astrophysics* 526, A17, A17. DOI: 10.1051/0004-6361/201015034. arXiv: 1011.1276 [astro-ph.SR].

Castro, M. et al. (2016). “Mass effect on the lithium abundance evolution of open clusters: Hyades, NGC 752, and M 67”. In: *Astronomy & Astrophysics* 590, A94, A94. DOI: 10.1051/0004-6361/201527583. arXiv: 1603.08809 [astro-ph.SR].

Cayrel, R., G. Cayrel de Strobel, and B. Campbell (1985). “Steps towards the abundance scale. I - The abundance of heavy elements in the Hyades cluster”. In: *Astronomy & Astrophysics* 146, pp. 249–259.

Cayrel, R. and G. Traving (1960). “Zur Frage der Druckverbreiterung der solaren Balmerlinien. Mit 4 Textabbildungen”. In: *Zeitschrift fur Astrophysik* 50, p. 239.

Cayrel, R. et al. (2011). “The Hα Balmer line as an effective temperature criterion. I. Calibration using 1D model stellar atmospheres”. In: *Astronomy & Astrophysics* 531, A83, A83. DOI: 10.1051/0004-6361/201116911.

Cayrel de Strobel, G. (1985). “How precise are spectroscopic abundance determinations today?” In: *Calibration of Fundamental Stellar Quantities*. Ed. by D. S. Hayes, L. E. Pasinetti, and A. G. D. Philip. Vol. 111. IAU Symposium, pp. 137–158.

— (1992). “The contribution of detailed analyses of F, G and K stars to the knowledge of the stellar populations of the galactic disk.” In: *The Messenger* 70, pp. 37–42.

Cayrel de Strobel, G. and C. Bentolila (1989a). “In search of real solar twins. II”. In: *Astronomy & Astrophysics* 211, pp. 324–340.

— (1989b). “In search of real solar twins. II”. In: *Astronomy & Astrophysics* 211, pp. 324–340.

Cayrel de Strobel, G., C. Soubiran, and N. Ralite (2001). “Catalogue of [Fe/H] determinations for FGK stars: 2001 edition”. In: *Astronomy & Astrophysics* 373, pp. 159–163. DOI: 10.1051/0004-6361:20010525. arXiv: astro-ph/0106438 [astro-ph].

Cayrel de Strobel, G. et al. (1981). “In search of real solar twins”. In: *Astronomy & Astrophysics* 94, pp. 1–11.

Cayrel de Strobel, G. et al. (1997). “A catalogue of [Fe/H] determinations: 1996 edition”. In: *Astronomy and Astrophysics Supplement Series* 124, pp. 299–305. DOI: 10.1051/aas:1997194. arXiv: astro-ph/9705206 [astro-ph].

Charbonnel, Corinne and Suzanne Talon (2005). “Influence of Gravity Waves on the Internal Rotation and Li Abundance of Solar-Type Stars”. In: *Science* 309, pp. 2189–2191. DOI: 10.1126/science.1116849. arXiv: astro-ph/0511265 [astro-ph].

Chiavassa, A. et al. (2010). “Three-dimensional hydrodynamical simulations of red giant stars: semi-global models for interpreting interferometric observations”. In: *Astronomy & Astrophysics* 524, A93, A93. DOI: 10.1051/0004-6361/201015507. arXiv: 1009.1745 [astro-ph.SR].

Chiavassa, A. et al. (2012). “Three-dimensional interferometric, spectrometric, and planetary views of Procyon”. In: *Astronomy & Astrophysics* 540, A5, A5. DOI: 10.1051/0004-6361/201118652. arXiv: 1201.3264 [astro-ph.SR].

Ciardi, D. R. et al. (2001). “On the Near-Infrared Size of Vega”. In: *The Astrophysical Journal* 559, pp. 1147–1154. DOI: 10.1086/322345. eprint: astro-ph/0105561.

Claret, A. (2000). “A new non-linear limb-darkening law for LTE stellar atmosphere models. Calculations for -5.0 = log[M/H] = +1, 2000 K = T_{eff} = 50000 K at several surface gravities”. In: *Astronomy & Astrophysics* 363, pp. 1081–1190.

Claret, A., J. Diaz-Cordoves, and A. Gimenez (1995). “Linear and non-linear limb-darkening coefficients for the photometric bands R I J H K.” In: *Astronomy & Astrophysicss* 114, p. 247.

Clough, S. A. et al. (2005). “Atmospheric Radiative Transfer Modeling: A Summary of the AER Codes”. In: *Journal of Quantitative Spectroscopy and Radiative Transfer* 91.2, pp. 233–244. ISSN: 0022-4073. DOI: 10.1016/j.jqsrt.2004.05.058.

Coc, Alain, Jean-Philippe Uzan, and Elisabeth Vangioni (2014). “Standard big bang nucleosynthesis and primordial CNO abundances after Planck”. In: *Journal of Cosmology and Astro-Particle Physics* 2014, 050, p. 050. DOI: 10.1088/1475-7516/2014/10/050. arXiv: 1403.6694 [astro-ph.CO].

Cohen, M., W. A. Wheaton, and S. T. Megeath (2003). “Spectral Irradiance Calibration in the Infrared. XIV. The Absolute Calibration of 2MASS”. In: *The Astronomical Journal* 126, pp. 1090–1096. DOI: 10.1086/376474. eprint: astro-ph/0304350.

Cohen, M. et al. (1992). “Spectral irradiance calibration in the infrared. I - Ground-based and IRAS broadband calibrations”. In: *The Astronomical Journal* 104, pp. 1650–1657. DOI: 10.1086/116349.

Colavita, M. M. et al. (1999). “The Palomar Testbed Interferometer”. In: *The Astrophysical Journal* 510, pp. 505–521. DOI: 10.1086/306579. eprint: astro-ph/9810262.

Cornejo, D., I. Ramirez, and P. S. Barklem (2012). “Precise Effective Temperatures of Solar Analog Stars”. In: *ArXiv e-prints*. arXiv: 1206.0750 [astro-ph.SR].

Currie, D. G., S. L. Knapp, and K. M. Liewer (1974). “Four stellar-diameter measurements by a new technique: amplitude interferometry.” In: *The Astrophysical Journal* 187, pp. 131–134. DOI: 10.1086/152598.

Curtis, J. L. (2017). “No Maunder Minimum Candidates in M67: Mitigating Interstellar Contamination of Chromospheric Emission Lines”. In: *The Astronomical Journal* 153, 275, p. 275. DOI: 10.3847/1538-3881/aa72e9. arXiv: 1705.04711 [astro-ph.SR].

Cutri, R. M. et al. (2003). *2MASS All Sky Catalog of point sources.*

Deal, M. et al. (2018). “Impacts of radiative accelerations on solar-like oscillating main-sequence stars”. In: *Astronomy & Astrophysics* 618, A10, A10. DOI: 10.1051/0004-6361/201833361. arXiv: 1806.10533 [astro-ph.SR].

Deliyannis, C. P., D. Barrado y Navascues, and J. R. Stauffer (2000). “WIYN Open Cluster Study: A New Lithium Sample in Cool Dwarfs of M35”. In: *American Astronomical Society Meeting Abstracts*. Vol. 197, p. 41.08.

Deliyannis, Constantine P., Aaron Steinhauer, and R. D. Jeffries (2002). “Discovery of the Most Lithium-rich Dwarf: Diffusion in Action”. In: *The Astrophysical Journal* 577, pp. L39–L43. DOI: 10.1086/344046.

Deliyannis, Constantine P. et al. (1994). “Lithium in a Short-Period Tidally Locked Binary of M67: Implications for Stellar Evolution, Galactic Lithium Evolution, and Cosmology”. In: *The Astrophysical Journal* 434, p. L71. DOI: 10.1086/187577.

Duncan, D. K. and B. F. Jones (1983). “Lithium abundance and age spread in the Pleiades.” In: *The Astrophysical Journal* 271, pp. 663–671. DOI: 10.1086/161233.

Edmonds Frank N., Jr., Hans Schluter, and Donald C. Wells (1967). “Hydrogen-line Stark broadening functions”. In: *Memoirs of the Royal Astronomical Society* 71, p. 271.

Fischer, D. A. and J. Valenti (2005). “The Planet-Metallicity Correlation”. In: *The Astrophysical Journal* 622, pp. 1102–1117. DOI: 10.1086/428383.

Flores, M. et al. (2016). “Discovery of an activity cycle in the solar analog HD 45184. Exploring Balmer and metallic lines as activity proxy candidates”. In: *Astronomy & Astrophysics* 589, A135, A135. DOI: 10.1051/0004-6361/201628145. arXiv: 1604.01307 [astro-ph.SR].

Franciosini, E., S. Randich, and R. Pallavicini (2003). “Is Praesepe really different from the coeval Hyades cluster? The XMM-Newton view”. In: *Astronomy & Astrophysics* 405, pp. 551–561. DOI: 10.1051/0004-6361:20030623. eprint: astro-ph/0304519.

Frasca, A. et al. (2003). “Further identification of ROSAT all-sky survey sources in Orion”. In: *Astronomy & Astrophysics* 405, pp. 149–163. DOI: 10.1051/0004-6361:20030644.

Freytag, B. et al. (2012). “Simulations of stellar convection with CO5BOLD”. In: *Journal of Computational Physics* 231, pp. 919–959. DOI: 10.1016/j.jcp.2011.09.026. arXiv: 1110.6844 [astro-ph.SR].

Fuhrmann, K., M. Axer, and T. Gehren (1993). “Balmer lines in cool dwarf stars. 1. Basic influence of atmospheric models”. In: *Astronomy & Astrophysics* 271, p. 451.

— (1994). “Balmer lines in cool dwarf stars II. Effective temperatures and calibration of colour indices”. In: *Astronomy & Astrophysics* 285, pp. 585–594.

Fuhrmann, K. et al. (1997). “The surface gravities of cool dwarf stars revisited.” In: *Astronomy & Astrophysics* 323, pp. 909–922.

Fuhrmann, Klaus (1998). “Nearby stars of the Galactic disk and halo”. In: *Astronomy & Astrophysics* 338, pp. 161–183.

Gaia Collaboration et al. (2016a). “Gaia Data Release 1. Summary of the astrometric, photometric, and survey properties”. In: *Astronomy & Astrophysics* 595, A2, A2. DOI: 10.1051/0004-6361/201629512. arXiv: 1609.04172 [astro-ph.IM].

Gaia Collaboration et al. (2016b). “The Gaia mission”. In: *Astronomy & Astrophysics* 595, A1, A1. DOI: 10.1051/0004-6361/201629272. arXiv: 1609.04153 [astro-ph.IM].

Gaia Collaboration et al. (2018). "Gaia Data Release 2. Summary of the contents and survey properties". In: *Astronomy & Astrophysics* 616, A1, A1. DOI: 10.1051/0004-6361/201833051. arXiv: 1804.09365.

Garcia Lopez, R. J., R. Rebolo, and J. E. Beckman (1988). "Lithium Abundances and Metallicities in Stars near the Main Sequence Turnoff and a Giant in M67". In: *Publications of the Astronomical Society of the Pacific* 100, p. 1489. DOI: 10.1086/132354.

Gardiner, R. B., F. Kupka, and B. Smalley (1999). "Testing convection theories using Balmer line profiles of A, F, and G stars". In: *Astronomy & Astrophysics* 347, pp. 876–890.

Gehren, T. (1979). "Metal abundances and microturbulence in seven solar-type stars. II - Model atmosphere analyses". In: *Astronomy & Astrophysics* 75, pp. 73–82.

— (1981). "The temperature scale of solar-type stars." In: *Astronomy & Astrophysics* 100, pp. 97–106.

Gehren, T. et al. (1985). "Abundance gradients in the galactic disk from young B-type stars in clusters - First results". In: *European Southern Observatory Conference and Workshop Proceedings*. Ed. by I. J. Danziger, F. Matteucci, and K. Kjar. Vol. 21. European Southern Observatory Conference and Workshop Proceedings, pp. 171–185.

Gezari, D. Y., A. Labeyrie, and R. V. Stachnik (1972). "Speckle Interferometry: Diffraction-Limited Measurements of Nine Stars with the 200-INCH Telescope". In: *The Astrophysical Journall* 173, p. L1. DOI: 10.1086/180906.

Ghezzi, L. et al. (2010a). "Lithium Abundances in a Sample of Planet-hosting Dwarfs". In: *The Astrophysical Journal* 724, pp. 154–164. DOI: 10.1088/0004-637X/724/1/154. arXiv: 1009.2130 [astro-ph.SR].

Ghezzi, L. et al. (2010b). "Stellar Parameters and Metallicities of Stars Hosting Jovian and Neptunian Mass Planets: A Possible Dependence of Planetary Mass on Metallicity". In: *The Astrophysical Journal* 720, pp. 1290–1302. DOI: 10.1088/0004-637X/720/2/1290. arXiv: 1007.2681 [astro-ph.SR].

Giribaldi, R. E. et al. (2019). "Accurate effective temperature from Hα profiles". In: *Astronomy & Astrophysics* 624, A10, A10. DOI: 10.1051/0004-6361/201833763. arXiv: 1811.12274 [astro-ph.SR].

Gonzalez, G. (1997). "The stellar metallicity-giant planet connection". In: *Monthly Notice of the Royal Astronomical Society* 285, pp. 403–412.

Gonzalez, Guillermo (2008). "Parent stars of extrasolar planets - IX. Lithium abundances". In: *Monthly Notice of the Royal Astronomical Society* 386, pp. 928–934. DOI: 10.1111/j.1365-2966.2008.13067.x. arXiv: 0802.0434 [astro-ph].

González Hernández, J. I. and P. Bonifacio (2009a). "A new implementation of the infrared flux method using the 2MASS catalogue". In: *Astronomy & Astrophysics* 497, pp. 497–509. DOI: 10.1051/0004-6361/200810904. arXiv: 0901.3034 [astro-ph.SR].

— (2009b). "A new implementation of the infrared flux method using the 2MASS catalogue". In: *Astronomy & Astrophysics* 497, pp. 497–509. DOI: 10.1051/0004-6361/200810904. arXiv: 0901.3034 [astro-ph.SR].

Goudfrooij, P. and R. C. Bohlin (2006). *A new CTE Correction Algorithm forPoint Source Spectroscopy with theSTIS CCD:Correcting for charge trap filling by the Ôred haloÕ of theCCD Point Spread Function redward of 8000 A*. Tech. rep.

Gray, D. F. (1992). "The inferred color index of the sun". In: *Publications of the Astronomical Society of the Pacific* 104, pp. 1035–1038. DOI: 10.1086/133086.

Gray, R. O. (2007). "The Problems with Vega". In: *The Future of Photometric, Spectrophotometric and Polarimetric Standardization*. Ed. by C. Sterken. Vol. 364. Astronomical Society of the Pacific Conference Series, p. 305.

Gray, R. O. et al. (2003). "Contributions to the Nearby Stars (NStars) Project: Spectroscopy of Stars Earlier than M0 within 40 Parsecs: The Northern Sample. I." In: *The Astronomical Journal* 126, pp. 2048–2059. DOI: 10.1086/378365. eprint: astro-ph/0308182.

Grevesse, N. and A. J. Sauval (1998). "Standard Solar Composition". In: *Space Science Reviews* 85, pp. 161–174. DOI: 10.1023/A:1005161325181.

— (1999). "The solar abundance of iron and the photospheric model". In: *Astronomy & Astrophysics* 347, pp. 348–354.

Griem, Hans R. (1962). "Wing Formulae for Stark-Broadened Hydrogen and Hydrogenic Lines." In: *The Astrophysical Journal* 136, p. 422. DOI: 10.1086/147394.

— (1967). "Corrections to the Asymptotic Holtsmark Formula for Hydrogen Lines Broadened by Electrons Electronics and Ions in a Plasma". In: *The Astrophysical Journal* 147, p. 1092. DOI: 10.1086/149097.

Grieves, N. et al. (2018). "Chemo-kinematics of the Milky Way from the SDSS-III MARVELS survey". In: *Monthly Notice of the Royal Astronomical Society* 481, pp. 3244–3265. DOI: 10.1093/mnras/sty2431. arXiv: 1803.11538 [astro-ph.SR].

Guenther, D. B. (1989). "Age of the sun". In: *The Astrophysical Journal* 339, pp. 1156–1159. DOI: 10.1086/167370.

Gustafsson, B. et al. (2008). "A grid of MARCS model atmospheres for late-type stars. I. Methods and general properties". In: *Astronomy & Astrophysics* 486, pp. 951–970. DOI: 10.1051/0004-6361:200809724. arXiv: 0805.0554.

Hanbury Brown, R., J. Davis, and L. R. Allen (1974). "The Angular Diameters of 32 Stars". In: *Monthly Notice of the Royal Astronomical Society* 167, pp. 121–136. DOI: 10.1093/mnras/167.1.121.

Hanbury Brown, R. et al. (1974). "The effects of limb darkening on measurements of angular size with an intensity interferometer". In: *Monthly Notice of the Royal Astronomical Society* 167, pp. 475–484. DOI: 10.1093/mnras/167.3.475.

Hanke, M. et al. (2018). "ATHOS: On-the-fly stellar parameter determination of FGK stars based on flux ratios from optical spectra⋆". In: *Astronomy & Astrophysics* 619, A134, A134. DOI: 10.1051/0004-6361/201833351. arXiv: 1809.01655 [astro-ph.SR].

Hardorp, J. (1978). "The sun among the stars. I - A search for solar spectral analogs". In: *Astronomy & Astrophysics* 63, pp. 383–390.

— (1980a). "The sun among the stars. II - Solar color, Hyades metal content, and distance". In: *Astronomy & Astrophysics* 88, pp. 334–344.

— (1980b). "The sun among the stars. III - Energy distributions of 16 northern G-type stars and the solar flux calibration". In: *Astronomy & Astrophysics* 91, pp. 221–232.

Hauschildt, P. H., F. Allard, and E. Baron (1999). "The NextGen Model Atmosphere Grid for 3000=T_{eff}=10,000 K". In: *The Astrophysical Journal* 512, pp. 377–385. DOI: 10.1086/306745. eprint: astro-ph/9807286.

Heiter, U. et al. (2015). "Gaia FGK benchmark stars: Effective temperatures and surface gravities". In: *Astronomy & Astrophysics* 582, A49, A49. DOI: 10.1051/0004-6361/201526319. arXiv: 1506.06095 [astro-ph.SR].

Holland, K. et al. (2000). "Praesepe - two merging clusters?" In: *Monthly Notice of the Royal Astronomical Society* 319, pp. 956–962. DOI: 10.1046/j.1365-8711.2000.03949.x.

Holmberg, J., C. Flynn, and L. Portinari (2006). "The colours of the Sun". In: *Monthly Notice of the Royal Astronomical Society* 367, pp. 449–453. DOI: 10.1111/j.1365-2966.2005.09832.x. eprint: astro-ph/0511158.

Holmberg, J., B. Nordström, and J. Andersen (2009). "The Geneva-Copenhagen survey of the solar neighbourhood. III. Improved distances, ages, and kinematics". In: *Astronomy & Astrophysics* 501, pp. 941–947. DOI: 10.1051/0004-6361/200811191. arXiv: 0811.3982 [astro-ph].

Holweger, H. (1979). "Abundances of the elements in the sun - Introductory report". In: *Liege International Astrophysical Colloquia*. Ed. by A. Boury, N. Grevesse, and L. Remy-Battiau. Vol. 22. Liege International Astrophysical Colloquia, pp. 117–138.

Holweger, H. and E. A. Mueller (1974). "The photospheric barium spectrum - Solar abundance and collision broadening of BA II lines by hydrogen". In: 39, pp. 19–30. DOI: 10.1007/BF00154968.

Ireland, M. J. et al. (2008). "Sensitive visible interferometry with PAVO". In: *Optical and Infrared Interferometry*. Vol. 7013. Proceedings of the SPIE, p. 701324. DOI: 10.1117/12.788386.

Israelian, G. et al. (2009). "Enhanced lithium depletion in Sun-like stars with orbiting planets". In: *Nature* 462, pp. 189–191. DOI: 10.1038/nature08483. arXiv: 0911.4198 [astro-ph.SR].

Jofré, E. et al. (2015). "Stellar parameters and chemical abundances of 223 evolved stars with and without planets". In: *Astronomy & Astrophysics* 574, A50, A50. DOI: 10.1051/0004-6361/201424474. arXiv: 1410.6422 [astro-ph.EP].

Johnson, H. L. and W. W. Morgan (1953). "Fundamental stellar photometry for standards of spectral type on the revised system of the Yerkes spectral atlas". In: *The Astrophysical Journal* 117, p. 313. DOI: 10.1086/145697.

Jones, Burton F. et al. (1997). "The Evolution of the Lithium Abundances of Solar-Type Stars.VII.M34 (NGC 1039) and the Role of Rotation in Lithium Depletion". In: *The Astronomical Journal* 114, pp. 352–362. DOI: 10.1086/118479.

Kaufer, A. et al. (1999). "Commissioning FEROS, the new high-resolution spectrograph at La-Silla." In: *The Messenger* 95, pp. 8–12.

Kausch, W. et al. (2015). "Molecfit: A General Tool for Telluric Absorption Correction: II. Quantitative Evaluation on ESO-VLT/X-Shooterspectra". In: *Astronomy & Astrophysics* 576, A78. ISSN: 0004-6361, 1432-0746. DOI: 10.1051/0004-6361/201423909.

Kervella, P. et al. (2004). "The angular sizes of dwarf stars and subgiants. Surface brightness relations calibrated by interferometry". In: *Astronomy & Astrophysics* 426, pp. 297–307. DOI: 10.1051/0004-6361:20035930. eprint: astro-ph/0404180.

Kim, Y.-C. et al. (2002). "The Y^2 Isochrones for α-Element Enhanced Mixtures". In: *The Astrophysical Journals* 143, pp. 499–511. DOI: 10.1086/343041. eprint: astro-ph/0208175.

King, Jeremy R., Anita Krishnamurthi, and Marc H. Pinsonneault (2000). "The Lithium-Rotation Correlation in the Pleiades Revisited". In: *The Astronomical Journal* 119, pp. 859–872. DOI: 10.1086/301205. arXiv: astro-ph/9911015 [astro-ph].

Korn, A. (2008). "CIAO? ADiOS!" In: *Mem. Societa Astronomica Italiana* 79, p. 495. arXiv: 0711.0683.

Korn, A. J., J. Shi, and T. Gehren (2003). "Kinetic equilibrium of iron in the atmospheres of cool stars. III. The ionization equilibrium of selected reference stars". In: *Astronomy & Astrophysics* 407, pp. 691–703. DOI: 10.1051/0004-6361:20030907. eprint: astro-ph/0306337.

Korn, A. J. et al. (2006). "A probable stellar solution to the cosmological lithium discrepancy". In: *Nature* 442, pp. 657–659. DOI: 10.1038/nature05011. eprint: astro-ph/0608201.

Korn, A. J. et al. (2007). “Atomic Diffusion and Mixing in Old Stars. I. Very Large Telescope FLAMES-UVES Observations of Stars in NGC 6397”. In: *The Astrophysical Journal* 671, pp. 402–419. DOI: 10.1086/523098. arXiv: 0709.0639.

Kurucz, R. (1993). “ATLAS9 Stellar Atmosphere Programs and 2 km/s grid.” In: *ATLAS9 Stellar Atmosphere Programs and 2 km/s grid. Kurucz CD-ROM No. 13. Cambridge, Mass.: Smithsonian Astrophysical Observatory, 1993.* 13.

Kurucz, R. L. (1979). “Model atmospheres for G, F, A, B, and O stars”. In: *The Astrophysical Journals* 40, pp. 1–340. DOI: 10.1086/190589.

— (2005). “New atlases for solar flux, irradiance, central intensity, and limb intensity”. In: *Memorie della Societa Astronomica Italiana Supplementi* 8, p. 189.

Kurucz, R. L. et al. (1984). *Solar flux atlas from 296 to 1300 nm*.

Ludwig, H.-G. et al. (2009a). “Impact of granulation effects on the use of Balmer lines as temperature indicators”. In: *Astronomy & Astrophysics* 502, pp. L1–L4. DOI: 10.1051/0004-6361/200911997. arXiv: 0906.4697 [astro-ph.SR].

Ludwig, H.-G. et al. (2009b). “The CIFIST 3D model atmosphere grid.” In: *Mem. Societa Astronomica Italiana* 80, p. 711. arXiv: 0908.4496 [astro-ph.SR].

Ludwig, Hans-Günter et al. (2010). “Solar abundances and 3D model atmospheres”. In: *Chemical Abundances in the Universe: Connecting First Stars to Planets*. Ed. by Katia Cunha, Monique Spite, and Beatriz Barbuy. Vol. 265. IAU Symposium, pp. 201–204. DOI: 10.1017/S1743921310000542. arXiv: 0911.4248 [astro-ph.SR].

Lyra, W. and G. F. Porto de Mello (2005). “Fine structure of the chromospheric activity in Solar-type stars - The Hα line”. In: *Astronomy & Astrophysics* 431, pp. 329–338. DOI: 10.1051/0004-6361:20040249. eprint: astro-ph/0410438.

Maíz Apellániz, J. (2007). “A Uniform Set of Optical/NIR Photometric Zero Points to be Used with CHORIZOS”. In: *The Future of Photometric, Spectrophotometric and Polarimetric Standardization*. Ed. by C. Sterken. Vol. 364. Astronomical Society of the Pacific Conference Series, p. 227. eprint: astro-ph/0609430.

Maldonado, J. et al. (2015). “Searching for signatures of planet formation in stars with circumstellar debris discs”. In: *Astronomy & Astrophysics* 579, A20, A20. DOI: 10.1051/0004-6361/201525764. arXiv: 1502.07100 [astro-ph.SR].

Mayor, M. et al. (2003). “Setting New Standards with HARPS”. In: *The Messenger* 114, pp. 20–24.

Megessier, C. (1995). “Accuracy of the astrophysical absolute flux calibrations: visible and near-infrared.” In: *Astronomy & Astrophysics* 296, p. 771.

Meléndez, J. and B. Barbuy (2002). “Keck NIRSPEC Infrared OH Lines: Oxygen Abundances in Metal-poor Stars down to [Fe/H] = -2.9”. In: *The Astrophysical Journal* 575, pp. 474–483. DOI: 10.1086/341142. eprint: astro-ph/0207660.

Meléndez, J., B. Barbuy, and F. Spite (2001). “Oxygen Abundances in Metal-poor Stars (-2.2[Fe/H]-1.2) from Infrared OH Lines”. In: *The Astrophysical Journal* 556, pp. 858–871. DOI: 10.1086/321624. eprint: astro-ph/0104184.

Meléndez, J., K. Dodds-Eden, and J. A. Robles (2006). “HD 98618: A Star Closely Resembling Our Sun”. In: *The Astrophysical Journall* 641, pp. L133–L136. DOI: 10.1086/503898. eprint: astro-ph/0603219.

Meléndez, J. et al. (2009). “The Peculiar Solar Composition and Its Possible Relation to Planet Formation”. In: *The Astrophysical Journall* 704, pp. L66–L70. DOI: 10.1088/0004-637X. arXiv: 0909.2299 [astro-ph.SR].

Meléndez, J. et al. (2010a). “uvby-β photometry of solar twins . The solar colors, model atmospheres, and the T_{eff} and metallicity scales”. In: *Astronomy & Astrophysics* 522, A98, A98. DOI: 10.1051/0004-6361/201014741. arXiv: 1007.5351 [astro-ph.SR].

Meléndez, Jorge and Iván Ramírez (2007). "HIP 56948: A Solar Twin with a Low Lithium Abundance". In: *The Astrophysical Journal* 669, pp. L89–L92. DOI: 10.1086/523942. arXiv: 0709.4290 [astro-ph].

Meléndez, Jorge et al. (2010b). "Lithium in other Suns: no connection between stars and planets". In: *Light Elements in the Universe*. Ed. by Corinne Charbonnel et al. Vol. 268. IAU Symposium, pp. 341–342. DOI: 10.1017/S1743921310004382.

Mishenina, T. V. and V. V. Kovtyukh (2001). "Analysis of neutron capture elements in metal-poor stars". In: *Astronomy & Astrophysics* 370, pp. 951–966. DOI: 10.1051/0004-6361:20010295.

Moehler, S. et al. (2014). "Flux calibration of medium-resolution spectra from 300 nm to 2500 nm: Model reference spectra and telluric correction". In: *Astronomy & Astrophysics* 568, A9, A9. DOI: 10.1051/0004-6361/201423790. arXiv: 1408.1797 [astro-ph.IM].

Molenda-Żakowicz, J. et al. (2013). "Atmospheric parameters of 169 F-, G-, K- and M-type stars in the Kepler field". In: *Monthly Notice of the Royal Astronomical Society* 434, pp. 1422–1434. DOI: 10.1093/mnras/stt1095. arXiv: 1306.6011 [astro-ph.SR].

Moore, C. E., M. G. J. Minnaert, and J. Houtgast (1966). *The solar spectrum 2935 A to 8770 A*.

Mourard, D. et al. (2011). "Spatio-spectral encoding of fringes in optical long-baseline interferometry. Example of the 3T and 4T recombining mode of VEGA/CHARA". In: *Astronomy & Astrophysics* 531, A110, A110. DOI: 10.1051/0004-6361/201116976.

Mozurkewich, D. et al. (2003). "Angular Diameters of Stars from the Mark III Optical Interferometer". In: *The Astronomical Journal* 126, pp. 2502–2520. DOI: 10.1086/378596.

Neckel, H. (1986). "The absolute energy distributions of the sun, of the 'solar analogs' 16 CYG B, Hyades VB 64, 16 CYG A, and of the standard stars Alpha LYR and 29 PSC". In: *Astronomy & Astrophysics* 159, pp. 175–188.

Neckel, Heinz and Dietrich Labs (1994). "Solar Limb Darkening 1986-1990 Lambda 303-NANOMETERS to 1099-NANOMETERS". In: 153, pp. 91–114. DOI: 10.1007/BF00712494.

Nissen, P. E. (1970). "The relative metal-to-hydrogen ratio for the sun, Hyades and 53 F5 - G2 stars." In: *Astronomy & Astrophysics* 6, pp. 138–150.

Önehag, A., B. Gustafsson, and A. Korn (2014). "Abundances and possible diffusion of elements in M 67 stars". In: *Astronomy & Astrophysics* 562, A102, A102. DOI: 10.1051/0004-6361/201322663. arXiv: 1310.6297 [astro-ph.SR].

Önehag, A., A. Korn, B. Gustafsson, et al. (2011). "M67-1194, an unusually Sun-like solar twin in M67". In: *Astronomy & Astrophysics* 528, A85, A85. DOI: 10.1051/0004-6361. arXiv: 1009.4579 [astro-ph.SR].

Pace, G., L. Pasquini, and P. François (2008). "Abundances of four open clusters from solar stars". In: *Astronomy & Astrophysics* 489, pp. 403–412. DOI: 10.1051/0004-6361:200809969. arXiv: 0806.2280.

Pace, G. et al. (2012). "Lithium in M 67: From the main sequence to the red giant branch". In: *Astronomy & Astrophysics* 541, A150, A150. DOI: 10.1051/0004-6361/201117704. arXiv: 1203.4440 [astro-ph.SR].

Parker, R. et al. (1961). "Abundances in G Dwarf Stars.IV. a Redetermination of the Abundances in G Dwarfs in the Hyades." In: *The Astrophysical Journal* 133, p. 101. DOI: 10.1086/147006.

Pasquini, L., K. Biazzo, P. Bonifacio, et al. (2008). "Solar twins in M 67". In: *Astronomy & Astrophysics* 489, pp. 677–684. DOI: 10.1051/0004-6361:200809714. arXiv: 0807.0092.

Pasquini, L. and R. Pallavicini (1991). "H-alpha absolute chromospheric fluxes in G and K dwarfs and subgiants". In: *Astronomy & Astrophysics* 251, pp. 199–209.

Pasquini, L., S. Randich, and R. Pallavicini (1997). "Lithium in M 67: evidence for spread in a solar age cluster." In: *Astronomy & Astrophysics* 325, pp. 535–541.

Pasquini, L. et al. (2004). "Detailed chemical composition of the open cluster IC 4651: The iron peak, α elements, and Li". In: *Astronomy & Astrophysics* 424, pp. 951–963. DOI: 10.1051/0004-6361:20040240. eprint: arXiv:astro-ph/0406113.

Pasquini, L. et al. (2012). "Search for giant planets in M 67. I. Overview". In: *Astronomy & Astrophysics* 545, A139, A139. DOI: 10.1051/0004-6361. arXiv: 1206.5820 [astro-ph.EP].

Pasquini, Luca (2000). "Li Abundance in Pop I Stars (Invited Paper)". In: *The Light Elements and their Evolution*. Ed. by L. da Silva, R. de Medeiros, and M. Spite. Vol. 198. IAU Symposium, p. 269.

Pease, F. G. (1931). "Interferometer Methods in Astronomy". In: *Ergebnisse der exakten Naturwissenschaften* 10, p. 84. DOI: 10.1007/BFb0111943.

Pereira, T. M. D. et al. (2013). "How realistic are solar model atmospheres?" In: *Astronomy & Astrophysics* 554, A118, A118. DOI: 10.1051/0004-6361/201321227. arXiv: 1304.4932 [astro-ph.SR].

Perryman, M. A. C. et al. (1997). "The HIPPARCOS Catalogue". In: *Astronomy & Astrophysics* 323, pp. L49–L52.

Peterson, D. M. et al. (2006). "Vega is a rapidly rotating star". In: *Nature* 440, pp. 896–899. DOI: 10.1038/nature04661. eprint: astro-ph/0603520.

Peytremann, E. (1974). "Line blanketing and model stellar atmospheres III. Tables of models and broad-band colours". In: *Astronomy & Astrophysicss* 18, p. 81.

Pfeiffer, M. J. et al. (1998). "FOCES - a fibre optics Cassegrain Echelle spectrograph". In: *Astronomy & Astrophysicss* 130, pp. 381–393. DOI: 10.1051/aas:1998231.

Porto de Mello, G. F. and L. da Silva (1997). "HR 6060: The Closest Ever Solar Twin?" In: *The Astrophysical Journall* 482, p. L89. DOI: 10.1086/310693.

Porto de Mello, G. F., W. Lyra, and G. R. Keller (2008). "The Alpha Centauri binary system. Atmospheric parameters and element abundances". In: *Astronomy & Astrophysics* 488, pp. 653–666. DOI: 10.1051/0004-6361:200810031. arXiv: 0804.3712.

Porto de Mello, G. F. et al. (2014). "A photometric and spectroscopic survey of solar twin stars within 50 parsecs of the Sun. I. Atmospheric parameters and color similarity to the Sun". In: *Astronomy & Astrophysics* 563, A52, A52. DOI: 10.1051/0004-6361/201322277. arXiv: 1312.7571 [astro-ph.SR].

Praderie, F. (1967). "Sur les raies de l'hydrogène. I. Profils quasistatiques dans les atmosphères stellaires". In: *Annales d'Astrophysique* 30, p. 31.

Prša, A. et al. (2016). "Nominal Values for Selected Solar and Planetary Quantities: IAU 2015 Resolution B3". In: *The Astronomical Journal* 152, 41, p. 41. DOI: 10.3847/0004-6256/152/2/41. arXiv: 1605.09788 [astro-ph.SR].

Przybilla, N. and K. Butler (2004). "The Solar Hydrogen Spectrum in Non-Local Thermodynamic Equilibrium". In: *The Astrophysical Journall* 610, pp. L61–L64. DOI: 10.1086/423202. eprint: astro-ph/0406459.

Ramírez, I., C. Allende Prieto, and D. L. Lambert (2013). "Oxygen Abundances in Nearby FGK Stars and the Galactic Chemical Evolution of the Local Disk and Halo". In: *The Astrophysical Journal* 764, 78, p. 78. DOI: 10.1088/0004-637X/764/1/78. arXiv: 1301.1582 [astro-ph.SR].

Ramírez, I. and J. Meléndez (2005). "The Effective Temperature Scale of FGK Stars. II. T_{eff}:Color:[Fe/H] Calibrations". In: *The Astrophysical Journal* 626, pp. 465–485. DOI: 10.1086/430102. eprint: astro-ph/0503110.

Ramírez, I., J. Meléndez, and M. Asplund (2009). "Accurate abundance patterns of solar twins and analogs. Does the anomalous solar chemical composition come from planet formation?" In: *Astronomy & Astrophysics* 508, pp. L17–L20. DOI: 10.1051/0004-6361/200913038.

— (2014). "Chemical signatures of planets: beyond solar-twins". In: *Astronomy & Astrophysics* 561, A7, A7. DOI: 10.1051/0004-6361/201322558. arXiv: 1310.8581 [astro-ph.SR].

Ramírez, I. et al. (2011). "Elemental Abundance Differences in the 16 Cygni Binary System: A Signature of Gas Giant Planet Formation?" In: *The Astrophysical Journal* 740, 76, p. 76. DOI: 10.1088/0004-637X/740/2/76. arXiv: 1107.5814 [astro-ph.SR].

Ramírez, I. et al. (2014). "The Solar Twin Planet Search. I. Fundamental parameters of the stellar sample". In: *Astronomy & Astrophysics* 572, A48, A48. DOI: 10.1051/0004-6361/201424244. arXiv: 1408.4130 [astro-ph.SR].

Ramírez, Iván and Jorge Meléndez (2005). "The Effective Temperature Scale of FGK Stars. I. Determination of Temperatures and Angular Diameters with the Infrared Flux Method". In: *The Astrophysical Journal* 626, pp. 446–464. DOI: 10.1086/430101. arXiv: astro-ph/0503108 [astro-ph].

Randich, S., P. Sestito, and R. Pallavicini (2003). "Evolution of lithium beyond the solar age: A Li survey of the old open cluster NGC 188". In: *Astronomy & Astrophysics* 399, pp. 133–140. DOI: 10.1051/0004-6361:20021780. arXiv: astro-ph/0212098 [astro-ph].

Randich, S., P. Sestito, F. Primas, et al. (2006). "Element abundances of unevolved stars in the open cluster M 67". In: *Astronomy & Astrophysics* 450, pp. 557–567. DOI: 10.1051/0004-6361:20054291. eprint: arXiv:astro-ph/0601239.

Randich, S. et al. (2009). "VizieR Online Data Catalog: Radial velocities of Berkeley 32 stars (Randich+, 2009)". In: *VizieR Online Data Catalog*, J/A+A/496/441, J/A+A/496/441.

Richard, O., G. Michaud, and J. Richer (2005). "Implications of WMAP Observations on Li Abundance and Stellar Evolution Models". In: *The Astrophysical Journal* 619, pp. 538–548. DOI: 10.1086/426470. eprint: astro-ph/0409672.

Richichi, A., I. Percheron, and M. Khristoforova (2005). "CHARM2: An updated Catalog of High Angular Resolution Measurements". In: *Astronomy & Astrophysics* 431, pp. 773–777. DOI: 10.1051/0004-6361:20042039.

Ridgway, S. T. et al. (1980). "Effective temperatures of late-type stars - The field giants from K0 to M6". In: *The Astrophysical Journal* 235, pp. 126–137. DOI: 10.1086/157617.

Rothman, L.S. et al. (2013). "The HITRAN2012 Molecular Spectroscopic Database". en. In: *Journal of Quantitative Spectroscopy and Radiative Transfer* 130, pp. 4–50. ISSN: 00224073. DOI: 10.1016/j.jqsrt.2013.07.002.

Ryabchikova, T., N. Piskunov, and D. Shulyak (2015). "On the Accuracy of Atmospheric Parameter Determination in BAFGK Stars". In: *Physics and Evolution of Magnetic and Related Stars*. Ed. by Y. Y. Balega, I. I. Romanyuk, and D. O. Kudryavtsev. Vol. 494. Astronomical Society of the Pacific Conference Series, p. 308.

Ryan, Sean G., John E. Norris, and Timothy C. Beers (1999). "The Spite Lithium Plateau: Ultrathin but Postprimordial". In: *The Astrophysical Journal* 523, pp. 654–677. DOI: 10.1086/307769. arXiv: astro-ph/9903059 [astro-ph].

Santos, N. C., G. Israelian, and M. Mayor (2004). "Spectroscopic [Fe/H] for 98 extra-solar planet-host stars. Exploring the probability of planet formation". In: *Astronomy & Astrophysics* 415, pp. 1153–1166. DOI: 10.1051/0004-6361:20034469. eprint: astro-ph/0311541.

Santos, N. C. et al. (2003). “Statistical properties of exoplanets. II. Metallicity, orbital parameters, and space velocities”. In: *Astronomy & Astrophysics* 398, pp. 363–376. DOI: 10.1051/0004-6361:20021637. eprint: astro-ph/0211211.

Santos, N. C. et al. (2005). “Spectroscopic metallicities for planet-host stars: Extending the samples”. In: *Astronomy & Astrophysics* 437, pp. 1127–1133. DOI: 10.1051/0004-6361:20052895. eprint: astro-ph/0504154.

Sarajedini, A., A. Dotter, and A. Kirkpatrick (2009). “Deep 2MASS Photometry of M67 and Calibration of the Main-Sequence J - K_S Color Difference as an Age Indicator”. In: *The Astrophysical Journal* 698, pp. 1872–1878. DOI: 10.1088/0004-637X/698/2/1872. arXiv: 0904.2907 [astro-ph.SR].

Saxner, M. and G. Hammarback (1985). “An empirical temperature calibration for F dwarfs”. In: *Astronomy & Astrophysics* 151, pp. 372–390.

Sestito, P. and S. Randich (2005). “Time scales of Li evolution: a homogeneous analysis of open clusters from ZAMS to late-MS”. In: *Astronomy & Astrophysics* 442, pp. 615–627. DOI: 10.1051/0004-6361:20053482. arXiv: astro-ph/0507537 [astro-ph].

Sestito, P., S. Randich, and R. Pallavicini (2004). “Lithium evolution in intermediate age and old open clusters: NGC 752 revisited”. In: *Astronomy & Astrophysics* 426, pp. 809–817. DOI: 10.1051/0004-6361:20041237. arXiv: astro-ph/0407305 [astro-ph].

Slechta, M. and P. Skoda (2002). “2-meter telescope devices: coudé slit spectrograph and HEROS”. In: *Publications of the Astronomical Institute of the Czechoslovak Academy of Sciences* 90, pp. 1–4.

Smette, A. et al. (2015). “Molecfit: A General Tool for Telluric Absorption Correction: I. Method and Application to ESO Instruments ⋆⋆⋆”. In: *Astronomy & Astrophysics* 576, A77. ISSN: 0004-6361, 1432-0746. DOI: 10.1051/0004-6361/201423932.

Sneden, C. A. (1973). “Carbon and Nitrogen Abundances in Metal-Poor Stars.” PhD thesis. THE UNIVERSITY OF TEXAS AT AUSTIN.

Soderblom, David R. et al. (1993a). “The Evolution of the Lithium Abundances of Solar-Type Stars. III. The Pleiades”. In: *The Astronomical Journal* 106, p. 1059. DOI: 10.1086/116704.

Soderblom, David R. et al. (1993b). “The Evolution of the Lithium Abundances of Solar-Type Stars. IV. Praesepe”. In: *The Astronomical Journal* 106, p. 1080. DOI: 10.1086/116705.

Sousa, S. G. et al. (2007). “A new code for automatic determination of equivalent widths: Automatic Routine for line Equivalent widths in stellar Spectra (ARES)”. In: *Astronomy & Astrophysics* 469, pp. 783–791. DOI: 10.1051/0004-6361:20077288. eprint: astro-ph/0703696.

Sousa, S. G. et al. (2008). “Spectroscopic parameters for 451 stars in the HARPS GTO planet search program. Stellar [Fe/H] and the frequency of exo-Neptunes”. In: *Astronomy & Astrophysics* 487, pp. 373–381. DOI: 10.1051/0004-6361:200809698. arXiv: 0805.4826.

Souto, Diogo et al. (2018). “Chemical Abundances of Main-sequence, Turnoff, Subgiant, and Red Giant Stars from APOGEE Spectra. I. Signatures of Diffusion in the Open Cluster M67”. In: *The Astrophysical Journal* 857, 14, p. 14. DOI: 10.3847/1538-4357/aab612. arXiv: 1803.04461 [astro-ph.SR].

Souto, Diogo et al. (2019). “Chemical Abundances of Main-Sequence, Turnoff, Subgiant and red giant Stars from APOGEE spectra II: Atomic Diffusion in M67 Stars”. In: *arXiv e-prints*, arXiv:1902.10199, arXiv:1902.10199. arXiv: 1902.10199 [astro-ph.SR].

Spergel, D. N. et al. (2007). "Three-Year Wilkinson Microwave Anisotropy Probe (WMAP) Observations: Implications for Cosmology". In: *The Astrophysical Journals* 170, pp. 377–408. DOI: 10.1086/513700. eprint: astro-ph/0603449.

Spite, F. et al. (1987). "Measurement of lithium abundance in dwarf stars of M 67." In: *Astronomy & Astrophysics* 171, pp. L8–L9.

Spite, M. and F. Spite (1982). "Lithium abundance at the formation of the Galaxy". In: *Nature* 297, pp. 483–485. DOI: 10.1038/297483a0.

Stehle, C. (1994). "Stark broadening of hydrogen Lyman and Balmer in the conditions of stellar envelopes". In: *Astronomy and Astrophysics Supplement Series* 104, pp. 509–527.

Stehlé, C. and R. Hutcheon (1999). "Extensive tabulations of Stark broadened hydrogen line profiles". In: *Astronomy and Astrophysics Supplement Series* 140, pp. 93–97. DOI: 10.1051/aas:1999118.

Su, K. Y. L. et al. (2005). "The Vega Debris Disk: A Surprise from Spitzer". In: *The Astrophysical Journal* 628, pp. 487–500. DOI: 10.1086/430819. eprint: astro-ph/0504086.

Takeda, Y. et al. (2005). "Spectroscopic Study on the Atmospheric Parameters of Nearby F–K Dwarfs and Subgiants". In: 57, pp. 27–43. DOI: 10.1093/pasj/57.1.27.

Talon, S. (2008). "Transport Processes in Stars: Diffusion, Rotation, Magnetic fields and Internal Waves". In: *EAS Publications Series*. Ed. by C. Charbonnel and J. P. Zahn. Vol. 32. EAS Publications Series, pp. 81–130. DOI: 10.1051/eas:0832003. arXiv: 0708.1499 [astro-ph].

Taylor, B. J. (2007). "The Benchmark Cluster Reddening Project. II. A Reddening Value for M67". In: *The Astronomical Journal* 133, pp. 370–386. DOI: 10.1086/509781.

ten Brummelaar, T. A. et al. (2005). "First Results from the CHARA Array. II. A Description of the Instrument". In: *The Astrophysical Journal* 628, pp. 453–465. DOI: 10.1086/430729. eprint: astro-ph/0504082.

Thorburn, J. A. et al. (1993). "Lithium in the Hyades. I. New Observations". In: *The Astrophysical Journal* 415, p. 150. DOI: 10.1086/173152.

Torres, G. (2010). "On the Use of Empirical Bolometric Corrections for Stars". In: *The Astronomical Journal* 140, pp. 1158–1162. DOI: 10.1088/0004-6256/140/5/1158.

Tsantaki, M. et al. (2013). "Deriving precise parameters for cool solar-type stars. Optimizing the iron line list". In: *Astronomy & Astrophysics* 555, A150, A150. DOI: 10.1051/0004-6361/201321103. arXiv: 1304.6639 [astro-ph.SR].

Tueg, H. and T. Schmidt-Kaler (1982a). "A direct UBV color measurement of the sun". In: *Astronomy & Astrophysics* 105, pp. 400–404.

— (1982b). "A direct UBV color measurement of the sun". In: *Astronomy & Astrophysics* 105, pp. 400–404.

Škoda, P., B. Šurlan, and S. Tomić (2008). "Investigation of residual blaze functions in slit-based echelle spectrograph". In: *Ground-based and Airborne Instrumentation for Astronomy II*. Vol. 7014. Proceedings of the SPIE, p. 70145X. DOI: 10.1117/12.789284. arXiv: 1112.4012 [astro-ph.IM].

Valenti, J. A. and D. A. Fischer (2005). "Spectroscopic Properties of Cool Stars (SPOCS). I. 1040 F, G, and K Dwarfs from Keck, Lick, and AAT Planet Search Programs". In: *The Astrophysical Journals* 159, pp. 141–166. DOI: 10.1086/430500.

van Belle, G. T. and K. von Braun (2009). "Directly Determined Linear Radii and Effective Temperatures of Exoplanet Host Stars". In: *The Astrophysical Journal* 694, pp. 1085–1098. DOI: 10.1088/0004-637X/694/2/1085. arXiv: 0901.1206 [astro-ph.SR].

Vidal, C. R., J. Cooper, and E. W. Smith (1970). "Hydrogen Stark broadening calculations with the unified classical path theory". In: *Journal of Quantitative Spectroscopy and Radiative Transfer* 10, pp. 1011–1063. DOI: 10.1016/0022-4073(70)90121-4.

— (1973). "Hydrogen Stark-Broadening Tables". In: *The Astrophysical Journal Supplement Series* 25, p. 37. DOI: 10.1086/190264.

Wagoner, Robert V., William A. Fowler, and F. Hoyle (1967). "On the Synthesis of Elements at Very High Temperatures". In: *The Astrophysical Journal* 148, p. 3. DOI: 10.1086/149126.

Wallace, L. et al. (2011). "An Optical and Near-infrared (2958-9250 Å) Solar Flux Atlas". In: *The Astrophysical Journals* 195, 6, p. 6. DOI: 10.1088/0067-0049/195/1/6.

White, N. M. and B. H. Feierman (1987). "A Catalog of Stellar Angular Diameters Measured by Lunar Occultation". In: *The Astronomical Journal* 94, p. 751. DOI: 10.1086/114513.

White, T. R. et al. (2013). "Interferometric radii of bright Kepler stars with the CHARA Array: Cygni and 16 Cygni A and B". In: *Monthly Notice of the Royal Astronomical Society* 433, pp. 1262–1270. DOI: 10.1093/mnras/stt802. arXiv: 1305.1934 [astro-ph.SR].

Wilner, D. J. et al. (2002). "Structure in the Dusty Debris around Vega". In: *The Astrophysical Journall* 569, pp. L115–L119. DOI: 10.1086/340691. eprint: astro-ph/0203264.

Worden, S. P. (1976). "Digital analysis of speckle photographs - The angular diameter of Arcturus". In: *Publications of the Astronomical Society of the Pacific* 88, pp. 69–72. DOI: 10.1086/129899.

Xiong, Da-run and Li-cai Deng (2005). "The effect of stellar spots on the colour and apparent lithium abundance of stars". In: *Chinese Astronomy and Astrophysics* 29, pp. 263–273. DOI: 10.1016/j.chinastron.2005.06.004.

— (2006). "A re-examination of the dispersion of lithium abundance of Pleiades member stars". In: *Chinese Astronomy and Astrophysics* 30, pp. 24–40. DOI: 10.1016/j.chinastron.2006.01.003.

Yadav, R. K. S. et al. (2008a). "BVI photometry and proper motions in M67 (Yadav+, 2008)". In: *VizieR Online Data Catalog* 348, p. 40609.

— (2008b). "Ground-based CCD astrometry with wide-field imagers. II. A star catalog for M 67: WFI@2.2 m MPG/ESO astrometry, FLAMES@VLT radial velocities". In: *Astronomy & Astrophysics* 484, pp. 609–620. DOI: 10.1051/0004-6361:20079245. arXiv: 0803.0004.

Yi, S. K., Y.-C. Kim, and P. Demarque (2003). "The Y^2 Stellar Evolutionary Tracks". In: *The Astrophysical Journals* 144, pp. 259–261. DOI: 10.1086/345101. eprint: astro-ph/0210201.